UNIVERSITÀ DEGLI STUDI
DI MODENA E REGGIO EMILIA

Dottorato di ricerca in Physics and Nano Sciences

Ciclo XXXII

Single molecule studies of folding, misfolding and aggregation of proteins and chaperone activity of HSPB8

Candidato: Dhawal Choudhary

Relatore (Tutor): Prof. Ciro Cecconi

Coordinatore del Corso di Dottorato: Prof. Marco Affronte

Dedicated to

Lisha,

my parents,

and

Sawal

Acknowledgement

"..Two roads diverged in a wood, and I—

I took the one less travelled by,

And that has made all the difference."

I recall these immortal words of Frost here not because I have traversed some less travelled road over the last 3 years of my PhD. Rather to accentuate the significance of the plethora of individuals who have made all the difference in this expedition. The road I choose never promised smooth sailing but surprisingly and delightfully it has been a pleasant one and I will be remiss in my duty to not express my gratitude to these individuals who to the best of their capacity, be it as a guide, a mentor, a companion, a friend or a well-wisher have contributed to this pleasant, unforgettable and worthwhile journey. The list is long, it will take some time and space for me to get to all of them so brace yourself for some reading and coincidently this reading exercise will also serve as good practice for you to cope with the long thesis that follows.

A colleague recently told me that doing a PhD is like putting together a puzzle without any instructions, while the pieces keep changing the shape and the room is on fire. I do find this overexerted comparison funny and understand the underlying principal of the joke but I can gladly say that I cannot relate to this joke and I attribute this completely to the excellence of my supervisor ***Prof. Ciro Cecconi***. From discussing juventus to resolving alignment issues in the tweezers set up in the middle of the night, he has been a constant source of knowledge, tranquillity and motivation. I cannot thank him enough for giving me the opportunity to pursue my PhD and for providing a nurturing, friendly, inspiring and positive atmosphere. I have grown much as a researcher and honed my skills considerably under his expert supervision. I will again like to extend my warmest gratitude to him for being not just a supervisor but also a friend.

Here I will also like to express my deep reverence and gratitude for my two perpetual security blankets in life, my ***parents***. You have inspired me always by your words and your actions and have equipped me meticulously and remarkably to traverse the many spheres of

life on my own. I will not thank but still mention (because thanking my younger brother will hurt my ego) ***Sawal***, for being my personal stand-up comedian as well as my moral compass.

Doing a PhD is also easily comparable to a sinusoidal curve with exciting highs and shattering lows and I have had a fair share of both in last three years. Luckily, through these ups and down I have always had one constant to rely on, a constant who goes by the name ***Lisha***. She is the source of my resolve, my anchor in stormy seas, my life partner and I would not even start a PhD let alone finish without her presence in my life. There is so much more that I can say but here I will recall Sam Baldwin played superbly by Tom Hanks in one of our favourite movies Sleepless in Seattle - "It was a million tiny little things that, when you added them all up…" and I will leave it at that.

PhD has also bestowed upon me many opportunities to travel, learn and meet wonderful people. I will like to extend my warmest regards to ***Prof. Alessandro Mossa*** for teaching me theoretical aspects of both optical tweezers and life. I will also like to express my gratitude towards my collaborators ***Prof Serena Carra*** and ***Prof Sander J. Tans*** for their valuable guidance, advice and trust. I will like to thank ***Prof. Daniele Dell'Orco*** for hosting me in his lab in Verona and giving me the opportunity to expand my horizons in molecular biology. I will extend my gratitude further to ***Valerio*** for being an awesome mentor both in and outside the lab, to ***Giuditta*** for being witty and hardworking lab partner and to ***Alda*** for basically being indiana jones. Verona would not have been as fun or as memorable without you guys, may the force be with us.

I will like to thank ***Prof. Borja Ibarra Urruela*** for hosting me in his lab in Madrid. Here I will like to extend a special thanks to ***Dr. Sara Lorenzo*** for being an extremely kind person and an insightful and generous teacher. You have taught me plenty about the tweezers and I hope to keep learning from you in the future. I will also like to thank ***Carlos*** for being a laughing singing matador (see you soon on the amalfi coast) and to ***Ania*** for being my most polish-ed friend.

Though I will be achieving a doctorate degree for the labours of last three years, my biggest achievement will be the friendships that I have earned in Italy. Thanks a ton to ***Ting*** for cooking the best chinese food and trying extremely hard to teach me Italian. Big thanks also to ***Sarkhan*** for being Sarkhan. Thanks for seeing the sunny and funny side always and for all the cake, never change. Also, a special thanks to ***Irène*** for brightening up everything around her by just being so french, à bientôt. Heartfelt thanks also goes to ***Laura*** for braving all my

irritating jokes and being an all-around badass. A big hug and thanks to ***Pietro*** for hosting the most amazing parties, to ***Francesco*** for being the Italian version of me (just a little taller), to ***Simone*** for being a charming and perfect gentleman and to ***Enrico*** for being as classy as anyone can be.

Thanks to ***Grigorio*** for (almost) teaching me the mystic art of swimming and introducing me to the sacred world of lego building, I might join league of legends soon too. I can possibly write a meandering and endless but yet fascinating account (which will mirror every single one of our conversations) of how much I am grateful to have a friend in ***Andre Mescola***. I would rather skip that (as I have to make sure that my acknowledgment at the very least is slightly shorter than my thesis) and just say that Andrea I am thankful for every coffee, every victory and every loss we have shared, long may it last, Forza Samp.

Coming to Modena, away from the comforts of home was never an uncomfortable experience. I give credit to ***Para***, ***Stefania***, ***Francesca*** and ***Marco*** for making the transition smooth and easy by being kind and compassionate and giving me the first hand taste of incredible Italian hospitality. In the same vein, I will like to extend my deepest thanks to ***Avinash***, for helping me altruistically and tirelessly on every step of the last 3 years. You never let me miss the richness of Indian food and cricket and I will always be grateful for your friendship.

The Italian affair have been an indelible and astounding, I will like to thank ***Francesco***, ***Lina***, ***Laura***, ***Francesca***, ***Sonal***, ***Albin***, ***Mario*** and ***Isabella*** for making it so. Not forgetting my roots, I will like to specially mention ***Gurpreet mam***, ***Lokesh sir***, ***Reema mam*** and ***Avneet sir*** for being my friends and mentors and for inspiring me to pursue a professional life of scientific research. I will also like to thank ***Krishna***, ***Saurabh***, ***Sugandh***, ***Nisha***, ***Khushboo***, ***Surbhi*** and ***Priyanka*** for their friendship and never ending support.

I thank each of you not because I have to but because I want to, and I will give rest to this want by recalling Wordsworth

"*My heart leaps up when I behold. A rainbow in the sky:*

So was it when my life began; So is it now I am a man;

So be it when I shall grow old…."

Table of Content

Page

Title Page

Dedication

Acknowledgement

Abstract 1

Chapter 1: Introduction 4

1.1 Single Molecule Force Spectroscopy Techniques 4

1.2 Optical Tweezers 5

1.3 Protein Folding 8

1.4 Chaperones 9

1.5 HSPB8 11

1.6 Contribution of Chapters 12

1.7 References 13

Chapter 2: Biological Applications of Recent Developments in Optical Tweezers 19

2.1 Introduction 21

2.2 Plasmonic Optical Tweezers 22

2.3 Photonic crystal Optical Tweezers 26

2.4 Femtosecond Optical Tweezers 28

2.5 Optical tweezers combined with fluorescence 32

2.6 Conclusions 40

2.7 References 42

Chapter 3: The Complex Conformational Dynamics of Neuronal Calcium Sensor-1: A Single Molecule Perspective 52

3.1 Introduction 54

3.1.1 NCS-1 is a multi-functional, two-domain protein 54

3.1.2 A single molecule perspective on protein folding using direct mechanical manipulation 55

3.2 Simple folding mechanism under resting conditions 58

3.3 Increasing folding complexity under calcium activating conditions 59

3.4 Pathologically high calcium concentrations open access to misfolding pathways 61

3.5 Comparison to the folding network of calmodulin 62

3.6 Conclusions and Future perspectives 63

3.7 References 65

Chapter 4: Studying heat shock proteins through single-molecule mechanical manipulation 72

4.1 Introduction 74

4.2 HSPs and small HSPs 75

4.3 Structural, Mechanical and Functional Properties of HSPs 77

4.4 Structural, Mechanical and Functional Properties of small HSPs 90

4.5 Conclusions 92

4.6 References 95

Chapter 5: Single-molecule studies of the molecular mechanisms underlying the chaperone activity of HSPB8 102

5.1 Introduction 103

5.2 Experimental approach 104

5.3 Results 106

5.3.1 Pulling on 4MBP 106

5.3.2 Pulling on 4MBP in presence of wild type HSPB8 109

5.3.3 Pulling on 4MBP in the presence of mutant HSPB8-K141E 111

5.3.4 Pulling on sMBP 111

5.3.5 Pulling on sMBP in the presence of HSPB8 113

5.3.6 Pulling on sMBP in the presence of mutant HSPB8-K141E 113

5.4 Discussion 114

5.5 Conclusions 120

5.6 References 122

Conclusion 125

Abstract

Optical tweezers have evolved as an exemplary Single Molecule Force Spectroscopy (SMFS) technique over the past three decades. A distinct and bio medically relevant application of Optical Tweezers is their ability to observe directly at single molecule level the folding, misfolding and aggregation of protein molecules. Additionally the dynamic approach of Optical Tweezer setup also allows for the isolated study of interactions between two or more biomolecules, such as chaperone-protein interactions, in real time. The medical relevance of such studies stems from the fact that misfolding and aggregation of proteins are deleterious processes and have been linked to many neurodegenerative disorders. While molecular chaperones have evolved as an evolutionarily conserved sword and shield mechanism against such deleterious processes, wherein their holdase action acts as a shield preventing further aggregation of misfolded protein species and their foldase action acts as a sword and actively assists misfolded structure to regains their natively folded state. The dysfunction of this chaperone activity is also cytotoxic and can lead to loss of proteostasis. The present thesis dwells deeper in this specific application of Optical tweezer. The thesis will elaborate upon how optical tweezers can extract the mechanistic details of the folding and misfolding of protein molecules by reviewing the experiments performed on NCS-1 (Neuronal Calcium Sensor 1). It will also discuss the experimental approach taken by SMFS techniques like Optical Tweezers and AFM (Atomic Force Microscopy) to study the structural and functional dynamics of molecular chaperones. Furthermore, the thesis will explore the recent developments in Optical Tweezers and their biological applications. Finally, I describe the results of experiments we have carried out on the maltose binding protein to elucidate the mechanism of action of the chaperone HSPB8. We have mechanically denatured homotetramers of MBP as well as single MBP molecules and analyzed their folding and aggregation processes in the presence and absence of wild-type HSPB8 and its mutant form HSPB8-K141E/N. Our results reveal a strong holdase activity of wild type HSPB8, which either prevents completely the aggregation of denatured MBP molecules or allows the substrate to form only small and mechanically weak aggregates while this holdase activity is significantly suppressed in the mutant. Moreover, and importantly, a careful analysis of the

data also discloses an unexpected foldase activity of both wild type and mutated forms of HSPB8, which guides the folding process of denatured MBP molecules into their native states. Our findings highlight new mechanisms of interaction between HSPB8 and its substrates and suggest a more complex physiological role for this chaperone than previously assumed.

Introduction

Chapter 1

Introduction

1.1 Single Molecule Force Spectroscopy Techniques

Mechanical forces play a fundamental role in every facet of biological cycle from chromosomal segregation to protein translocation. The omnipresence of these forces presents a distinct gateway to gauge and understand biomolecular processes in terms of their mechanical and physical properties such as free energy, structural rigidity, conversion efficiency etc [1]. This viewpoint has ushered a new age in the study of biomolecular processes in the past two decades specially coupled with advent of Single Molecule Force Spectroscopy (SMFS) Techniques. While it was not possible in past to observe directly the forces exerted by biomolecules on each other, SMFS techniques allow for the real-time measurement in a quasi-static equilibrium of applied forces and the structural and functional implication of these applied forces on a single cell or even better a single biomolecule at a time. SMFS techniques distinguish themselves from other ensamble based biomolecular techniques by the virtue of their approach. As SMFS techniques stipulate the study of a single biomolecule at a time in real time, hence rare or metastable events which otherwise can get blurred or completely lost in ensemble studies due to averaging effects can be observed in repetition by SMFS techniques. While the ever growing envelop of SMFS techniques engulfs a plethora of techniques such as Optical Tweezers [2], Atomic Force Microscopy (AFM) [3], Micro-needle manipulation [4], Magnetic Tweezers [5] etc, but at a very fundamental level all SMFS techniques entail two basic structural elements, a probing set up to apply and detect force and a trapping or tracking mechanism to spatially locate the biomolecule [6-8]. The aforementioned techniques have been successfully applied in past 3 decades to study various biomolecular processes underlying the folding and misfolding of proteins [9-17], DNA [18-23] and RNA [24, 25] molecules, binding interactions

between ligand-receptor pairs [26, 27], molecular motors [28-31]. The main protagonist of the present thesis will be one of the most versatile SMFS techniques, Optical Tweezers.

1.2 Optical Tweezers

Optical tweezers are SMFS assays wherein a laser beam is deployed in a dual role, as both the probing as well as the spatial detection element. Since the pioneering work of Arthur Ashkin [2, 32, 33], for which he was awarded the 2019 Nobel Prize in Physics, Optical Tweezers have evolved into a behemoth in the field of single cell and single molecule manipulation with the capacity to trap and manipulate target particles from nanometer to micrometer range in a three dimensional space with extremely high precision . The present generation of Optical Tweezer assays are capable of exerting and detecting forces at pico-newton scale with sub-millisecond time resolution.

The most important and fascination part of Optical Tweezer setups obviously is the optical trap in itself. The optical trap is generated by highly focussing a laser beam through an objective lens with large numerical aperture, as can be seen in figure 1. Consider a laser beam hitting a refractive bead (Figure 1A), which acts as a converging lens. When this bead is situated in an off axis position, the central optical rays with strong light intensity are refracted downwards while the peripheral optical rays with week light intensity are refracted in an upward direction. Due to the downward refraction the light rays suffer a change in momentum ΔP1 in downward direction and conversely ΔP2 in upward direction due to peripheral rays, where Pin is the momentum of light entering the bead and Pout is the momentum of light leaving the bead. As,

$$\Delta P1 > \Delta P2$$

The bead experiences an overall change in momentum ΔP in the downward direction. Consecutively it experiences an equal and opposite force in upward direction called gradient force which pushes the bead along the spatial gradient of light intensity, given by,

$$F_{grad} = \Delta P$$

Additionally some of the light rays are reflected back by the bead resulting in a change in momentum Δp towards the laser beam and hence experiences an equal and opposite force in the opposite direction along the optical axis called scattering force, given by,

$$F_{sct} = \Delta p$$

For the bead to trapped by the laser beam, the Gradient force needs to overcome the scattering force. This is done by introducing a lens with large numerical aperture creating a high spatial gradient as seen in Figure 1B, which focusses the laser beam in a diffraction-limited spot generating a stable three-dimensional optical trap. In order to generate a strong optical trap a dual beam system is employed by focusing two laser beams at the same spot, Figure 2. A bead trapped in this optical trap experiences force directly proportional to its displacement from the central trapping position, very similar to that experienced by a spring as given by hooks law. In Chapter 2 of this thesis, I will discuss some recent trends in Optical Tweezers and their biological applications.

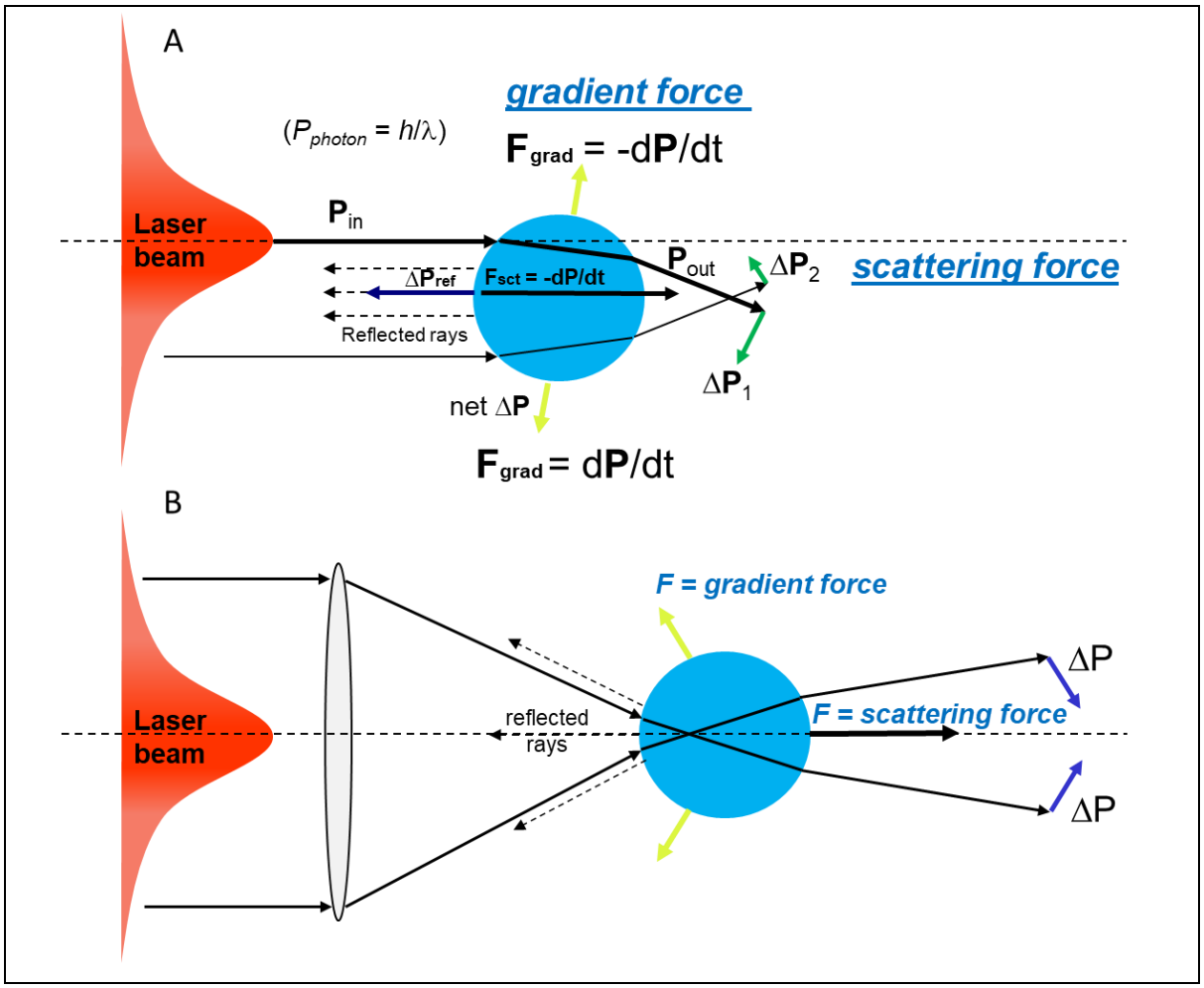

Figure 1: A) Schematic describing a polystyrene bead in the off axis position of a gaussian laser beam. Change in momentum due to reflected rays results in an equal and opposite force experienced by the bead pushing the bead forward termed scattering force. Gradient forces in the lateral direction are experienced by the bead because of change in momentum experienced from refracted rays. B) A highly focused lens is introduced in front of the gaussian shaped laser beam profile so the gradient forces can overcome the scattering force in order to generate a stable optical trap.

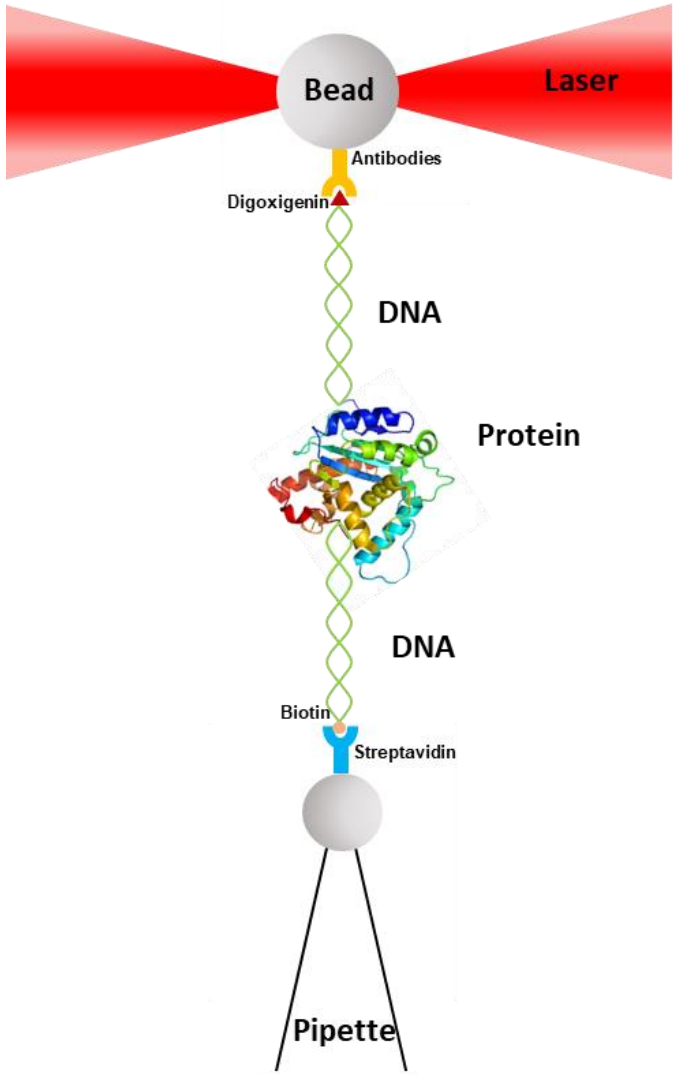

Figure 2: Schematic describing the optical tweezer experimental setup used in our lab to manipulate biomolecules. The biomolecule, in this case a protein molecule, is sandwiched between two long DNA handles. One DNA handle is tethered to an optically trapped bead via a digoxigenin-antibody connection while the other DNA handle it attached to a bead stuck on top of pipette via a biotin-strepdavidin connection.

While it is easy enough to see how optical tweezers can efficiently trap a micrometer sized polystyrene bead, the question that arises is that how can these assays manipulate a single bio-molecule? The answer lies within the capacity of optical tweezers to trap a polystyrene bead, funnily enough. The biomolecule in question is biochemically linked from one end to the trapped polystyrene bead, while the other end of the biomolecule can either be functionalized to a surface or connected to another polystyrene bead. The variability in the secondary attachment point gives us the three simple and popular types of Optical tweezer setups, (a) Biomolecule tethered between trapped bead and surface, (B) Biomolecule tethered between two beads with one in optical trap and another held by a micropipette, (c) Biomolecule tethered between two beads witch each bead in an optical trap [34]. Furthermore for small biomolecules, long DNA handles are used as spacers between the molecule and beads in order to prevent interactions between the two tethering surfaces.

1.3 Protein Folding

Among the numerous single molecule studies performed using Optical Tweezers, a noteworthy application is their ability to characterize the conformational equilibria related to protein folding [11, 35, 36]. While protein-folding problem remains a complex and medically relevant question in biological circles to this date, Optical tweezers have helped shed light on many key aspects of this issue such as identifying various conformational dynamics involved in the folding and misfolding of proteins as well as mapping the energy landscape of protein folding trajectories. In Chapter 3 of this thesis, I will discuss how optical tweezers are employed to manipulate and extract vital information related to the folding and misfolding pathways of

complex multi-domains proteins, focusing on the experimental assays performed on NCS-1 (Neuronal Calcium Senor – 1) protein in our lab recently.

The reason why protein-folding problem constitutes one of the most sought out biological questions is very easy to understand [37]. Proteins, which basically are long amino acid chains, are able to perform multitude of cellular functions only when the polypeptide chain folds in a specific three-dimensional structure, termed as the native state of a protein. A failure to form this native structure results in disruption of proteostasis due to the formation of misfolded and furthermore aggregated structures. Loss of proteostasis due to misfolding and aggregation of proteins is extremely cytotoxic and has been linked to the manifestation of many neurodegenerative disorders, such as Parkinson disease, Amyotrophic Lateral Sclerosis (ALS), Dementia etc [38-40]. This is where the so-called cellular Protein Quality Control (PQC) system enters the picture, performing the main tasks of preserving the evolutionarily conserved protein folding pathways, assisting in refolding of misfolded conformations and eradication of irreversibly misfolded species to prevent them from aggregating. As evident from Figure 3, an integral part of PQC is a specific evolutionarily conserved protein family called Molecular Chaperones.

1.4 Chaperones

Molecular chaperones can be defined as protein families that actively assist in the native folding of other proteins [41, 42]. While a more nuanced view of the role performed by molecular chaperones as well as the employment of SMFS techniques to explore the structural and functional dynamics of molecular chaperones will be discussed in chapters 4 of this thesis, at the very basic level chaperone activity can be understood in terms of two broad functions performed by molecular chaperone i.e., holdase function and foldase function. The holdase functions of molecular chaperones can be viewed as an essential damage limitation step. Once proteins start to misfold and further aggregate in the cellular environment, the cascading deleterious effects of these processes are masked by active molecular chaperones through their holdase functions, wherein they in a way quarantine such species by binding to them and hence preventing further misfolding or aggregations [43]. At this point the foldase function of

molecular chaperones comes to the fore as they assist in the refolding of the misfolded protein species, hence restoring proteostasis. The mechanisms of action involved in these two fundamental functions of molecular chaperones will be elaborated upon further in this thesis [41, 44].

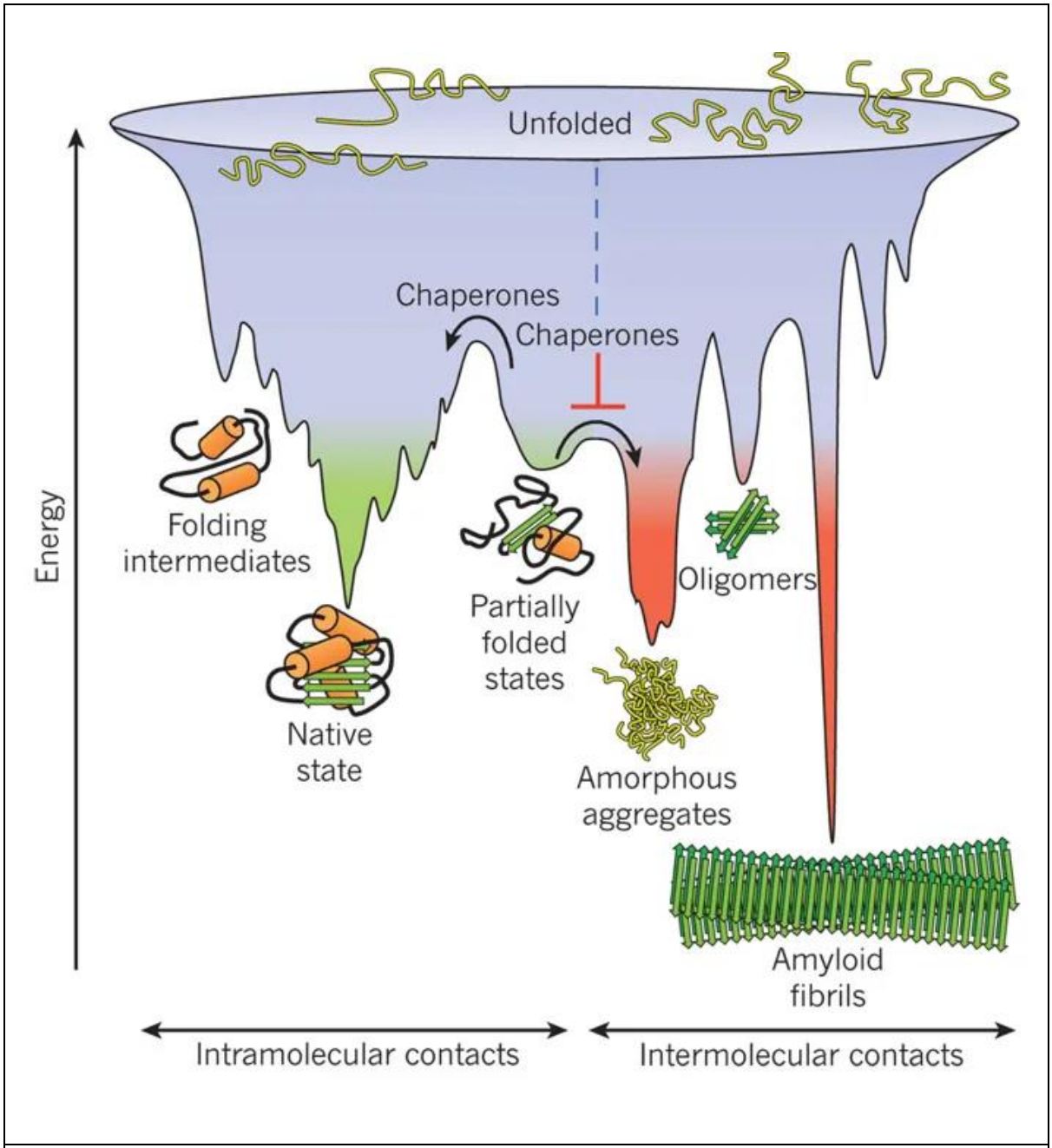

Figure 3: Funnel shaped energy landscape scheme describing the frustrated search of proteins towards a native conformation via native intramolecular interactions. Chaperones assist in accelerating the transition of kinetically trapped partially folded protein species towards favourable downhill path (green region). The red region describes the aggregated

protein structures resulting from intermolecular non-native interactions between partially folded species. Reprinted with permission from Springer Nature Customer Service Centre GmbH : Springer Nature, Nature [41] Copyright 2011.

Heat Shock Proteins (HSP) are a major class of molecular chaperones, appropriately named so as the members of this family are found to be active under stressful conditions in cellular environment to counter the upregulation of protein aggregation in such conditions [45]. HSP chaperones are further classified on the basis of their molecular weight, namely HSP100, HSP90, HSP70, small HSPs etc, with each chaperone involved in many diverse aspects of Protein Quality Control [46]. HSPb8, one of the 10 members of the mammalian small HSP family [40], will be another prominent protagonist in the narrative of this thesis and its effects on aggregation of proteins as well as protein folding will be investigated in Chapter 5.

1.5 HSPB8

HSPB8, also known as HSP22, is expressed in a wide variety of human tissues including motoneurons in the spinal cord as well as striated and smooth muscles [47, 48]. Structurally HSPB8 is characterise by its two primary domains with N domain extending from residue 1 – 85 and the C domain or the α-crystallin domain spanning from residue 86 – 176 . Additionally, unlike other small HSPs HSPB8 predominantly exists as a monomer, does not form stable complexes with other HSPs and its α-crystallin domain does not comprise of two β-sheets but rather is composed of a principally randomly coiled structure [49-51]. Rather, HSPB8 interacts actively with BCL2 associated athanogene 3 (BAG-3), which is a co chaperone of HSP70, and forms a tight complex. It can then interact with HSP70 resulting in HSPB8–BAG-3–HSP70 chaperone complex.

HSPB8 is known to provide protection against protein aggregation, for example the HSPB8–BAG-3–HSP70 complex has been shown to sort and process misfolded protein within a stress granule [52], and hence it has a perceived holdase function as a molecular chaperone. HSPB8 upregulation may also help preserve proteostasis in the case of motoneurons disease (MDs) such as amyotrophic lateral sclerosis (ALS) and spinal and bulbar muscular atrophy (SBMA) [40, 53, 54]. Expression of HSPB8 is also known to decline with age specifically in

motoneurons leaving them vulnerable to deleterious impacts of protein aggregation [53]. Additionally, two missense mutations in the α-crystallin domain of HSPB8, namely HSPB8-K141E and HSPB8-K141N, have been linked to motor neuropathies such as Charcot-Marie-Tooth neuropathy type 2L (CMT2L) and other muscular and neuronal disorders [55, 56]. Chapter 5 of this thesis will focus on the results obtained from single molecule studies of wild type HSPB8 and its mutated version HSPB8-K141E using optical tweezers to probe its functional activity in order to elaborate upon its role as a molecular chaperone and the mechanisms involved in its chaperone activity.

1.6 Contribution to Chapters

Chapter 2 titled "Biological Applications of Recent Developments in Optical Tweezers" is a review article published in biomolecules [57]. As the first author of this publication, I was heavily involved in the compilation and interpretation of the literature reviewed in the manuscript as well as writing the manuscript.

Chapter 3 titled "The Complex Conformational Dynamics of Neuronal Calcium Sensor-1: A Single Molecule Perspective", was published as a review article in the special edition of Frontiers in Molecular Neuroscience [58]. I am the first author of this publication and was heavily involved in writing and in the interpretation of the literature discussed in the publication.

Chapter 4 titled "Studying heat shock proteins through single-molecule mechanical manipulation" has been accepted for publication as a book chapter in "Second big book of small Heat Shock Proteins". I am the first author of this publication and was heavily involved in writing and in the interpretation of the literature discussed in the publication.

Chapter 5 titled "Single-molecule studies of the molecular mechanisms underlying the chaperone activity of HSPB8" which is currently a working paper. I performed, designed and analysed all the experiments discussed in the chapter.

1.7 References

1. Bustamante, C., et al., *Mechanical processes in biochemistry.* Annual review of biochemistry, 2004. **73**(1): p. 705-748.
2. Ashkin, A., et al., *Observation of a single-beam gradient force optical trap for dielectric particles.* Optics letters, 1986. **11**(5): p. 288-290.
3. Bustamante, C., et al., *Single-molecule studies of DNA mechanics.* Current Opinion in Structural Biology, 2000. **10**(3): p. 279-285.
4. Cluzel, P., et al., *DNA: An extensible molecule.* Science, 1996. **271**(5250): p. 792-794.
5. Neuman, K.C., T. Lionnet, and J.F. Allemand, *Single-molecule micromanipulation techniques.* Annual Review of Materials Research, 2007. **37**: p. 33-67.
6. Bustamante, C., J.C. Macosko, and G.J. Wuite, *Grabbing the cat by the tail: manipulating molecules one by one.* Nature Reviews Molecular Cell Biology, 2000. **1**(2): p. 130.
7. Neuman, K.C. and A. Nagy, *Single-molecule force spectroscopy: optical tweezers, magnetic tweezers and atomic force microscopy.* Nature methods, 2008. **5**(6): p. 491.
8. Greenleaf, W.J., M.T. Woodside, and S.M. Block, *High-resolution, single-molecule measurements of biomolecular motion.* Annu. Rev. Biophys. Biomol. Struct., 2007. **36**: p. 171-190.
9. Heidarsson, P.O., et al., *Direct single-molecule observation of calcium-dependent misfolding in human neuronal calcium sensor-1.* Proceedings of the National Academy of Sciences, 2014. **111**(36): p. 13069-13074.
10. Jahn, M., et al., *Folding and Domain Interactions of Three Orthologs of Hsp90 Studied by Single-Molecule Force Spectroscopy.* Structure, 2018. **26**(1): p. 96-105. e4.
11. Cecconi, C., et al., *Direct observation of the three-state folding of a single protein molecule.* Science, 2005. **309**(5743): p. 2057-2060.
12. Bechtluft, P., et al., *Direct observation of chaperone-induced changes in a protein folding pathway.* Science, 2007. **318**(5855): p. 1458-1461.
13. Gao, Y., G. Sirinakis, and Y. Zhang, *Highly anisotropic stability and folding kinetics of a single coiled coil protein under mechanical tension.* Journal of the American Chemical Society, 2011. **133**(32): p. 12749-12757.

14. Chen, H., et al., *Dynamics of equilibrium folding and unfolding transitions of titin immunoglobulin domain under constant forces.* Journal of the American Chemical Society, 2015. **137**(10): p. 3540-3546.
15. Liu, R., et al., *Mechanical characterization of protein L in the low-force regime by electromagnetic tweezers/evanescent nanometry.* Biophysical journal, 2009. **96**(9): p. 3810-3821.
16. Yao, M., et al., *Mechanical activation of vinculin binding to talin locks talin in an unfolded conformation.* Scientific reports, 2014. **4**: p. 4610.
17. Rivas-Pardo, J.A., et al., *Work done by titin protein folding assists muscle contraction.* Cell reports, 2016. **14**(6): p. 1339-1347.
18. Smith, S.B., Y. Cui, and C. Bustamante, *Overstretching B-DNA: the elastic response of individual double-stranded and single-stranded DNA molecules.* Science, 1996. **271**(5250): p. 795-799.
19. Zhang, Y., et al., *DNA translocation and loop formation mechanism of chromatin remodeling by SWI/SNF and RSC.* Molecular cell, 2006. **24**(4): p. 559-568.
20. Mossa, A., et al., *Dynamic force spectroscopy of DNA hairpins: I. Force kinetics and free energy landscapes.* Journal of Statistical Mechanics: Theory and Experiment, 2009. **2009**(02): p. P02060.
21. Manosas, M., et al., *Single molecule high-throughput footprinting of small and large DNA ligands.* Nature communications, 2017. **8**(1): p. 304.
22. Bianco, P., et al., *Transient Kinetics Measured with Force Steps Discriminate between Double Stranded DNA Elongation and Melting and Define the Reaction Energetics.* Biophysical Journal, 2014. **106**(2): p. 66a.
23. Morin, J.A., et al., *DNA synthesis determines the binding mode of the human mitochondrial single-stranded DNA-binding protein.* Nucleic acids research, 2017. **45**(12): p. 7237-7248.
24. Li, P.T., C. Bustamante, and I. Tinoco, *Real-time control of the energy landscape by force directs the folding of RNA molecules.* Proceedings of the National Academy of Sciences, 2007. **104**(17): p. 7039-7044.
25. Ritchie, D.B. and M.T. Woodside, *Probing the structural dynamics of proteins and nucleic acids with optical tweezers.* Current opinion in structural biology, 2015. **34**: p. 43-51.
26. Kim, J., et al., *A mechanically stabilized receptor–ligand flex-bond important in the vasculature.* Nature, 2010. **466**(7309): p. 992.
27. Mescola, A., et al., *Single-molecule force spectroscopy to decipher the early signalling step in membrane-bound penicillin receptors embedded into a lipid bilayer.* Nanoscale, 2019.

28. Morin, J.A., B. Ibarra, and F.J. Cao, *Kinetic modeling of molecular motors: pause model and parameter determination from single-molecule experiments.* Journal of Statistical Mechanics: Theory and Experiment, 2016. **2016**(5): p. 054031.
29. Milic, B., et al., *Intraflagellar transport velocity is governed by the number of active KIF17 and KIF3AB motors and their motility properties under load.* Proceedings of the National Academy of Sciences, 2017. **114**(33): p. E6830-E6838.
30. Brunnbauer, M., et al., *Torque generation of kinesin motors is governed by the stability of the neck domain.* Molecular cell, 2012. **46**(2): p. 147-158.
31. Naranjo, T., et al., *Dynamics of individual molecular shuttles under mechanical force.* Nature communications, 2018. **9**(1): p. 4512.
32. Ashkin, A. and J.M. Dziedzic, *Optical trapping and manipulation of viruses and bacteria.* Science, 1987. **235**(4795): p. 1517-1520.
33. Ashkin, A., J.M. Dziedzic, and T. Yamane, *Optical trapping and manipulation of single cells using infrared laser beams.* Nature, 1987. **330**(6150): p. 769.
34. Moffitt, J.R., et al., *Recent advances in optical tweezers.* Annual review of biochemistry, 2008. **77**.
35. Heidarsson, P.O., et al., *Single-molecule folding mechanism of an EF-hand neuronal calcium sensor.* Structure, 2013. **21**(10): p. 1812-1821.
36. Jahn, M., et al., *Folding and assembly of the large molecular machine Hsp90 studied in single-molecule experiments.* Proceedings of the National Academy of Sciences, 2016. **113**(5): p. 1232-1237.
37. Dill, K.A. and J.L. MacCallum, *The protein-folding problem, 50 years on.* science, 2012. **338**(6110): p. 1042-1046.
38. Morimoto, R.I., *Proteotoxic stress and inducible chaperone networks in neurodegenerative disease and aging.* Genes & development, 2008. **22**(11): p. 1427-1438.
39. Balch, W.E., et al., *Adapting proteostasis for disease intervention.* science, 2008. **319**(5865): p. 916-919.
40. Carra, S., et al., *HspB8, a small heat shock protein mutated in human neuromuscular disorders, has in vivo chaperone activity in cultured cells.* Human molecular genetics, 2005. **14**(12): p. 1659-1669.
41. Hartl, F.U., A. Bracher, and M. Hayer-Hartl, *Molecular chaperones in protein folding and proteostasis.* Nature, 2011. **475**(7356): p. 324.
42. Hendrick, J.P. and F.-U. Hartl, *Molecular chaperone functions of heat-shock proteins.* Annual review of biochemistry, 1993. **62**(1): p. 349-384.

43. Haslbeck, M., et al., *Some like it hot: the structure and function of small heat-shock proteins.* Nature structural & molecular biology, 2005. **12**(10): p. 842.

44. Kim, Y.E., et al., *Molecular chaperone functions in protein folding and proteostasis.* Annual review of biochemistry, 2013. **82**: p. 323-355.

45. Whitley, D., S.P. Goldberg, and W.D. Jordan, *Heat shock proteins: a review of the molecular chaperones.* Journal of Vascular Surgery, 1999. **29**(4): p. 748-751.

46. Lindquist, S. and E. Craig, *The heat-shock proteins.* Annual review of genetics, 1988. **22**(1): p. 631-677.

47. Rusmini, P., et al., *The role of the heat shock protein B8 (HSPB8) in motoneuron diseases.* Frontiers in molecular neuroscience, 2017. **10**: p. 176.

48. Benndorf, R., et al., *HSP22, a new member of the small heat shock protein superfamily, interacts with mimic of phosphorylated HSP27 (3DHSP27).* Journal of Biological Chemistry, 2001. **276**(29): p. 26753-26761.

49. Hu, Z., et al., *Structure, function, property, and role in neurologic diseases and other diseases of the sHsp22.* Journal of neuroscience research, 2007. **85**(10): p. 2071-2079.

50. Kim, M.V., A.S. Seit-Nebi, and N.B. Gusev, *The problem of protein kinase activity of small heat shock protein Hsp22 (H11 or HspB8).* Biochemical and biophysical research communications, 2004. **325**(3): p. 649-652.

51. Verschuure, P., et al., *Expression of small heat shock proteins HspB2, HspB8, Hsp20 and cvHsp in different tissues of the perinatal developing pig.* European journal of cell biology, 2003. **82**(10): p. 523-530.

52. Ganassi, M., et al., *A surveillance function of the HSPB8-BAG3-HSP70 chaperone complex ensures stress granule integrity and dynamism.* Molecular cell, 2016. **63**(5): p. 796-810.

53. Crippa, V., et al., *The small heat shock protein B8 (HspB8) promotes autophagic removal of misfolded proteins involved in amyotrophic lateral sclerosis (ALS).* Human molecular genetics, 2010. **19**(17): p. 3440-3456.

54. Rusmini, P., et al., *Clearance of the mutant androgen receptor in motoneuronal models of spinal and bulbar muscular atrophy.* Neurobiology of aging, 2013. **34**(11): p. 2585-2603.

55. Irobi, J., et al., *Mutant HSPB8 causes motor neuron-specific neurite degeneration.* Human molecular genetics, 2010. **19**(16): p. 3254-3265.

56. Fontaine, J.-M., et al., *Abnormal small heat shock protein interactions involving neuropathy-associated HSP22 (HSPB8) mutants.* The FASEB journal, 2006. **20**(12): p. 2168-2170.

57. Choudhary, D., et al., *Bio-molecular applications of recent developments in optical tweezers.* Biomolecules, 2019. **9**(1): p. 23.

58. Choudhary, D., et al., *The complex conformational dynamics of neuronal calcium sensor-1: a single molecule perspective.* Frontiers in molecular neuroscience, 2018. **11**.

Biological Applications of Recent Developments in Optical Tweezers

Chapter 2

Biological Applications of Recent Developments in Optical Tweezers

Abstract

In the past three decades, the ability to optically manipulate biomolecules has spurred a new era of medical and biophysical research. Optical Tweezers (OT) have enabled experimenters to trap, sort and probe cells as well as discern the structural dynamics of proteins and nucleic acids at single molecule level. The steady improvement in OT's resolving power has progressively pushed the envelope of their applications; there are, however, some inherent limitations that are prompting researchers to look for alternatives to the conventional techniques. To begin with, OT are restricted by their one-dimensional approach, which makes it difficult to conjure an exhaustive three-dimensional picture of biological systems. The high-intensity trapping laser can damage biological samples, a fact that restricts the feasibility of in vivo applications. Finally, direct manipulation of biological matter at nanometer scale remains a significant challenge for conventional OT. A conspicuous amount of literature has been dedicated in the last 10 years to address the aforementioned shortcomings. Innovations in laser technology and advances in various other spheres of applied physics have been capitalised upon to evolve the next generation OT systems. In this review we elucidate a few of these developments, with particular focus on their biological applications. The manipulation of nanoscopic objects has been achieved by means of Plasmonic Optical Tweezers (POT), which utilise localised surface plasmons to generate optical traps with enhanced trapping potential, and Photonic Crystal Optical Tweezers (PhC OT), which attain the same goal by employing different photonic crystal geometries. Femtosecond Optical Tweezers (fs OT), constructed by

replacing the Continuous Wave (cw) laser source with a femtosecond laser, promise to greatly reduce the damage to living samples. Finally, one way to transcend the one-dimensional nature of the data gained by OT is to couple them to the other large family of single molecule tools, i.e. fluorescence-based imaging techniques. We discuss the distinct advantages of the aforementioned techniques as well as the alternative experimental perspective they provide in comparison to conventional OT.

2.1 Introduction

Optical Tweezers (OT) technology has emerged as a prime tool for biological research over the last three decades, ever since the seminal works by Ashkin and co-authors [1-3]. The ability of light to exert force on matter is exploited by OT to precisely and noninvasively manipulate target molecules. Since its origins, this technique has experienced a dramatic evolution that has increasingly broadened its range of applications in biophysics. Thanks to the development of accurate manipulation techniques [4-7], advanced strategies to reduce mechanical and thermal noise [8], and increasingly sophisticated spatial and temporal detection methods [9, 10], it is nowadays possible to use optical tweezers to measure piconewton forces and up to angstrom-level displacements [11]. Parallel and in close connection to the instrumental developments, recent breakthroughs in statistical mechanics have coalesced into the field called stochastic thermodynamics [12, 13] which is now accepted as the physical framework to interpret experimental data. These technical and theoretical advances have allowed biophysicists to employ optical tweezers in the investigation of an increasing number of biological processes, including the mechanochemistry of molecular motors [14-17], the torsional and bending rigidity of biopolymers [18], the non-covalent binding interactions between ligand-receptor pairs [19], and the mechanical unfolding, refolding and misfolding [20-22] of proteins [23-26], DNA [27-31] and RNA [32, 33] molecules.

The further expansion of the already broad spectrum of OT's applications is however restricted due to certain experimental limitations. It is still very difficult, for example, with conventional optical tweezers to directly trap nanometer-sized targets. Conventional OT are also ill-equipped for providing detailed conformational and chemical change analysis about complex biomolecular systems. Moreover, cell manipulation by laser is often accompanied by photo damage which narrows the scope of such experiments. A considerable effort has been devoted to overcome the restrictions on conventional OT [34, 35], developing new instrumental setups by inventively combining optical traps with spectroscopy [36], microfluidics [37], acoustics [38], plasmonics [39, 40] and photonics [41] to name a few. The next generation versions of optical tweezers boast an expansive literature and have paved the way for new perspectives in optical manipulation and single molecule studies. This review narrows its focus down to four variations of conventional optical tweezers specifically designed to address the aforementioned limitations namely Plasmonic Optical Tweezers (POT), Photonic Crystal

Optical Tweezers (PhC OT), Femtosecond Optical Tweezers (fs OT) and Optical Tweezers combined with various fluorescence techniques. In particular, it will provide a description of the main instrumental features, biological applications and further scope of these techniques.

2.2 Plasmonic Optical Tweezers

A major limitation of conventional optical tweezers is their inability to manipulate directly minuscule biomolecules, such as DNA, RNA and proteins. This limitation can be easily understood if we consider that, when the radius r of the particle is much smaller than the wavelength of the light (Rayleigh regime), the trapping potential (U) generated by a laser beam is given by [42]:

$$U \approx -\int F_{trap} dx = -\int (|\alpha|/2) \nabla \langle E^2 \rangle dx = -(|\alpha|/2) \langle E^2 \rangle \quad (1)$$

where F_{trap} is the trapping force experienced by the particle, $\langle E^2 \rangle$ is the time averaged square of the electric field and α is the polarizability of the target particle, which depends on its volume ($V = 4/3\,\pi r^3$) according to the relation:

$$\alpha = 3V \frac{\epsilon_p - \epsilon_m}{\epsilon_p + 2\epsilon_m} \quad (2)$$

where ϵ_p and ϵ_m are the dielectric constants of the particle and the medium, respectively. In order to achieve a stable trapping, *U* must be much higher than the thermal fluctuations of the particle in the medium, that is [2, 43]:

$$|U| \gg K_B T \quad (3)$$

where K_B is the Boltzmann constant and *T* the absolute temperature. For a nanometer sized particle α becomes very small, and so does *U*. As a consequence, equation 3 does not hold true and the particle escapes the optical trap.

The observation that a larger trapping force can be achieved in regions where the electric field is rapidly varying led to the development of near-field optical microscopy [44]. In the presence of laser illumination the free electron density on the surface of a metal can undergo collective oscillations that result in standing waves called *plasmons*. Under these conditions the charge concentration due to geometrical features like tips or sharp edges creates

an evanescent field whose intensity decreases very fast with the distance from the conductor surface. The field enhancement due to localised surface plasmons has opened up new possibilities for optical trapping at the nanometre scale [44]. Based on this principle a novel technique for optical manipulation has recently been developed, which has been called Plasmonic Optical Tweezers (POT) [39, 42, 43]. Improved optical trapping is achieved in POT by subwavelength concentration of propagating laser light into plasmonic hotspots composed of evanescent field with high localised intensity. Expertly fabricated plasmonic nanostructures are used as a conduit to create such plasmonic hotspots thereby strongly enhancing the electric field of the incident laser light. The increased electric filed compensates for the low polarizability of nanometre sized particles, resulting in strong trapping potential. Thus equation *(3)* is re-established in POT allowing for the trapping and manipulation of miniscule particles.

The realization of three dimensional plasmonic optical traps was first reported by Grigorenko et al [39]. The authors used a focused 1,604 nm diode laser beam to generate plasmonic optical traps in proximity of closely spaced pairs of gold nanodots. The near-fields of the nanodot pairs produced subwavelength trapping volumes where nano-sized polystyrene beads could be stably captured. The large stiffness of the potential well of the plasmonic trap significantly quenches the Brownian motion of the captured object, dramatically improving particle positioning as compared to that normally achieved with conventional diffraction-limited optical traps. Escape-velocity measurements showed large trapping forces even with low laser powers, opening up new exciting possibilities for the nanomanipulation of biological samples with plasmonic trapping.

After the pioneering work of Grigorenko et al new experimental approaches were designed to improve POT. Thermal energy released due to ohmic losses during plasmon excitation can trigger overheating of water, generation of steam bubbles and thermal convection. To counter these overheating problems Wang et al exploited the high thermal conductive properties of copper and silicon [45]. Through simple nanofabrication techniques, the authors generated nanopillars on a gold film deposited on a cooper layer in contact with a silicon substrate. During plasmonic trapping, copper and silicon act as heat-sink conducting the heat from the nanopillar to the substrate, thus minimizing (the generated heat in) water warming. Using these nanostructures, the authors were able to stably trap 110 nm beads and rotate them upon manual rotation of the incident linear polarization (λ = 974 nm). On the other hand, when circularly polarized light was used for trapping, the captured beads could be

passively rotated clockwise or anti-clockwise by changing the handedness of the incident light, demonstrating precise control gained at nanoscale through plasmonic optical trapping.

Direct trapping of smaller and smaller particles was then achieved employing nanostructures with varying morphologies, such as nano apertures in gold film [46], double-nanoholes (DNH) [47] and nano dipole antennas [48]. Righini et al further [49] extended the work done in [39] by developing plasmonic optical traps between gold nano antennas employing laser light with three times less intensity. Significantly, not only were they able to trap polystyrene beads of variable size ranging from 1 μm to 200 nm but also successfully demonstrated the trapping of *E. Coli* bacteria for the first time. The elongated cells of *E. Coli* bacteria were immobilised in a stable horizontal geometry in the optical trap by focussing Ti:Sapahire laser with a wavelength of 800 nm on an array of gold nano antennas spaced by a distance of 30 nm. The authors also studied the growth of the optically trapped cells and these cells were shown to grow and divide on a time scale similar to the cells which were not trapped, signifying lack of significant photodamage to cells due to optical trapping. Similarly, Huang et al were able to trap yeast cells (*S.cerevisiae*) by combing plasmonic optical traps with microfluidics [50]. These results open considerable avenues for application of POT in biological matter manipulation. In 2011 POT was used to trap single protein molecules [51]. Double-nanoholes milled on thin gold films were employed by Pang et al. to generate plasmonic traps capable of stably trapping single bovine serum albumin (BSA) molecules, Figure 1. The trapping of a single protein could easily be detected by the instrument and the fate of the captured molecule could be followed with high resolution over an extended period of time. Under the action of the optical forces, a trapped BSA molecule readily denatures and then hops between its folded and unfolded states, giving rise to two distinct levels of optical power in the recorded traces (Figure 1c). The ease with which the double-nanohole (DNH) optical tweezers reveals the trapping of a single BSA molecule has prompted the authors to hypothesize a possible development of the instrument in a biosensor for single protein detection.

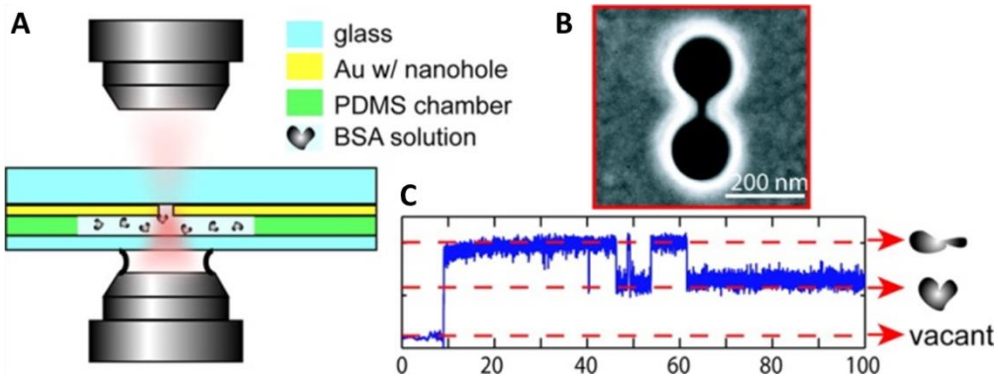

Figure 1: Double-nanohole optical tweezers. A) A 820 nm laser is focused with a 100X oil immersion microscope objective near a double-nanohole milled on a commercially available 100 nm thick Au film. The plasmonic trap is generated inside a polydimethylsiloxane (PDMS) microwell filled with a 1 % BSA solution (w/w) in PBS buffer. B) Scanning electro microscope image of the double-nanohole fabricated using a focused ion beam (FIB). The double-nanohole is characterized by two sharp tips (cusps) separated by 15 nm. C) Time trace of the optical power trasmitted through the double-nanohole. Upon trapping of a BSA molecule the optical power sharply increases and then fluctuates between two distinct levels as the molecules hops between its folded and unfolded states. Reprinted with permission from [51]. Copyright 2012 American Chemical Society.

A few years later, the same experimental group used a DNH optical tweezers to trap single 10 bp DNA hairpins and study their interaction with the tumor suppressor p53 protein [52]. The authors showed that after trapping, the optical forces of a plasmonic trap unzip a 10 bp DNA hairpin in a time scale of ~ 0.1 s. If the same experiment is performed in the presence of p53, the unzipping time becomes longer as the binding of p53 to the DNA stabilizes the hairpin, increasing its unfolding activation energy by ~ 2 x 10^{-20} J. No unzipping delay is instead observed in the presence of the p53 mutant (cys135ser), revealing the inability of this protein to suppress the denaturation of a DNA hairpin and providing a possible molecular-level explanation for the ineffectiveness of p53 in suppressing tumour growth. Although the work presented in [52] does not provide definitive results on the mechanism of interaction between DNA and p53, it certainly shows the capability of DNH optical tweezers to study directly the interaction between proteins and short DNA molecules, without the need to use molecular

handles and/or fluorescence labels as done typically in experiments performed with conventional optical tweezers.

2.3 Photonic crystal optical tweezers

The same idea of using evanescent near-fields that allow POT to trap objects well below the diffraction limit has promoted the development of slot waveguides [53] and photonic crystal traps [35, 54]. Light propagating by total internal reflection into a waveguide generates an evanescent field on the outside whose intensity decays exponentially with the distance from the waveguide surface. This near-field can be used to transport a dielectric particle along the waveguide, while a fixed-position trap can be realized by placing a photonic crystal resonator along the track, demonstrating a new class of optical trap, termed Photonic Crystal Optical Tweezers (PhC OT) [55]. Photonic crystals (PhC) [56-58] can be described as structures with a periodic pattern in the dielectric properties. In close analogy with ordinary crystals, PhC are characterized by photonic band gaps, which allow or forbid light in a certain frequency range to pass through.

The biological applications of photonic crystals are not yet plentiful but have already highlighted the advantages that this technique presents compared to traditional optical tweezers, especially with regard to the ability to trap biological material without damaging it. Chen et al. have designed special photonic crystal resonators capable of trapping nanometer-sized objects with minimal temperature increase [41], Figure 2. They fabricated a small hole in the center of the cavity and manufacture the device using silicon nitride in order to operate the photonic crystal resonator at 1064 nm [59]. At this wavelength the optical absorption of water is reduced by two orders of magnitude compared to that measured at 1550 nm, the resonant wavelength of silicon resonators, and thus local warming at the resonator cavity is reduced [41, 60]. Using these devices, Chen et al. managed to trap nanometer-sized objects with a local temperature rise of less than 0.3 K, thus minimizing the possibility of damaging biological matter. Figure 2 shows the optical trapping of a truncated version of the Wilson disease protein (MW ~46 kDa). When proteins in solution pass near the optically excited resonator they remain stably trapped. This process is reversible as the proteins returns free in

solution as the 1064 nm laser is switched off. Using the silicon nitride PhC resonators fabricated by Chen et al. it is thus possible to confine biomolecules reversibly in subwavelength trapping volumes without subjecting them to temperature increases that would compromise their functionality. This opens up new perspectives for further studies of the interactions between proteins and their targets (other proteins, DNA fragments or nano particles), and for facilitating assembly of nanometer-sized biomaterial. More recently, photonic crystals have also been employed to optically trap eukaryotic and prokaryotic cells [61]. By focusing a continuous wave (CW) 1060 nm laser on the surface of 2D photonic crystals, Jing et al. were able to create low intensity optical traps where they could stably capture living cells. By analyzing the morphology of the cells and the cellular adsorption of propidium iodide over time [62] the authors showed that trapped NIH/3T3 mammalian fibroblasts maintain their viability for more than 30 minutes, while *E. coli* cells can complete their 20-minute life cycles. Being able to extend the viability of optically trapped cells, the PhC OT described in [61] have great potential for various biomedical applications, including the characterization of the mechanical properties of cells [63] or the study of the relation between mass and cell growth.

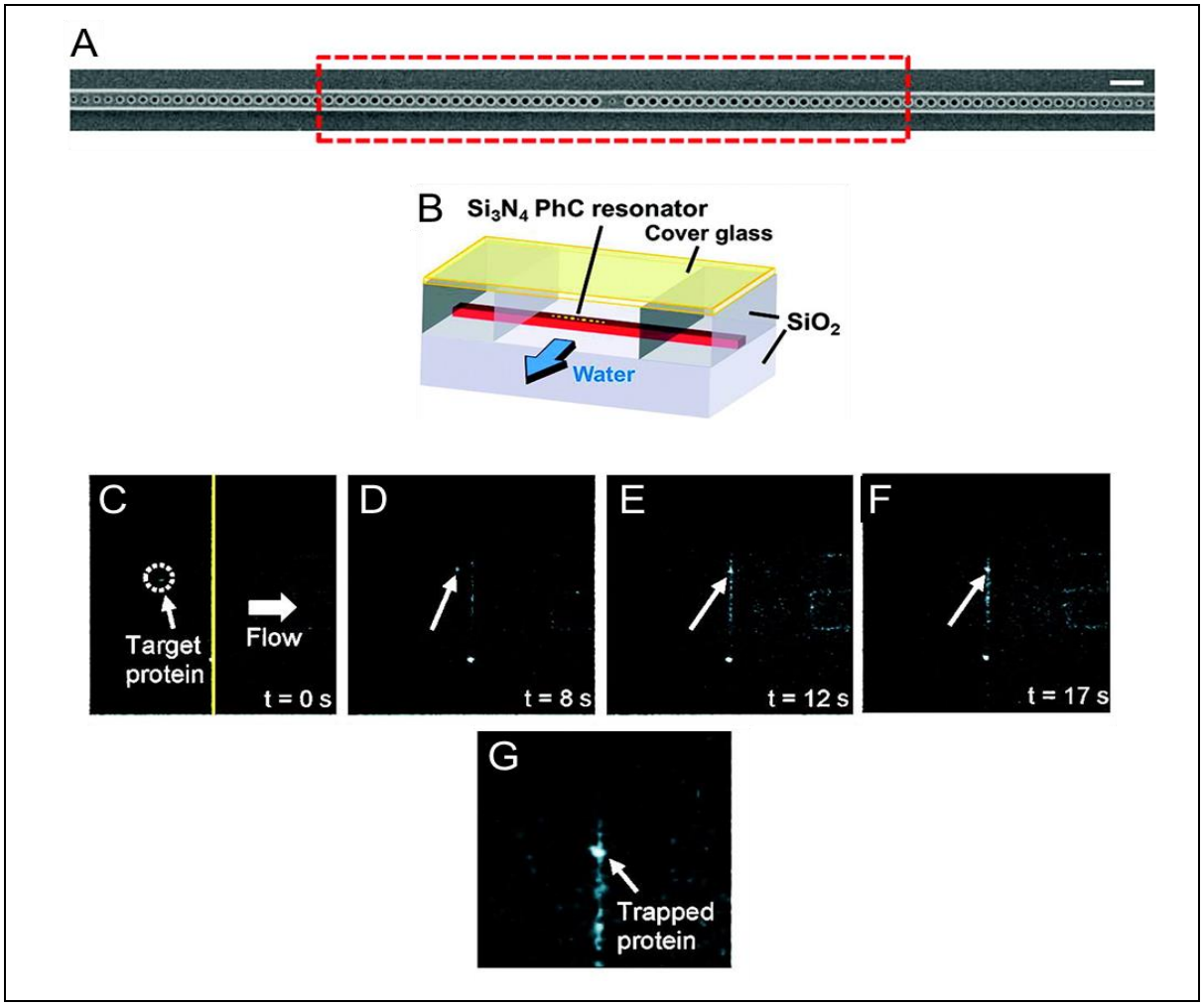

Figure 2: Trapping of individual proteins with a photonic crystal resonator. A) Scanning electron microscope image of the silicon nitrite photonic crystal resonator fabricated by Chen et al. to trap nanometer-sized objects [41]. The resonator consists of a central hole flanked by 53 holes on both sides and is operated at 1064 nm. Scale bar, 1 μm. B) Schematic of the flow chamber used to flow protein molecules near the resonator. C-F) Fluorescence microscope images of Cy5-labeled Wilson disease proteins inside the flow chamber. As the flow is activated (t = 0 s), the proteins that are conveyed near the optically excited resonator remain stably trapped. A high resolution picture of a group of trapped proteins is shown in G). Adapted with permission from [41]. Copyright 2012 American Chemical Society.

2.4 Femtosecond Optical Tweezers

A recent evolution in instrumental design for optical trapping technique has been the replacement of continuous-wave laser sources with ultrashort femtosecond lasers. Optical tweezers using continuous wave (cw) laser sources are characterized by their constant trapping force. A femtosecond (fs) laser source on the other hand allows for a different dynamics in optical trapping as the target is put through spontaneous impulsive cycles of drag and release [64]. These drag and release cycles are due to the nature of fs lasers that produce a constant stream of laser pulses with high peak power followed by brief intervals where no force is experienced by the target. During the laser pulses extremely high photon pressure is induced by fs laser sources, which is approximately 10^5 times higher than that of cw laser with same power [65]. Under these conditions, in order to achieve stable trapping, the diffusion experienced by the target during a no pulse interval due to gravitational and Brownian forces must be countered by the optical force acting on the particle during a high peak pulse [66]. As shown by Xing et al., the diffusion velocity v_1 of a spherical target particle of radius r and volume V during the no pulse interval *t* is dominated by the competition between gravity and buoyancy, so it is given by [66]:

$$v_1 = \left(\rho_p - \rho_m\right) gV/(6\pi\mu r) \tag{4}$$

where g is the acceleration due to gravity, μ is the liquid viscosity, ρ_p and ρ_m are the densities of the particles and the medium, respectively. It follows that the displacement of the particle during the no pulse interval is

$$s_1 = v_1 t. \tag{5}$$

On the other hand, during the pulse interval t_0 the optical trapping force F will drag the particle back towards the trap with a velocity v_2 given by:

$$v_2 = \left[F - \left(\rho_p - \rho_m\right) gV\right] / (6\pi\mu r) \tag{6}$$

and the displacement of the particle will be

$$s_2 = v_2 t_0. \tag{7}$$

For stable trapping with a femtosecond laser the restoring displacement s_2 must be larger than the falling displacement s_1, and thus the following equation must hold true:

$$\mathrm{F} \geq \left(\rho_p - \rho_m\right) gV[(t + t_0)/t_0] \tag{8}$$

This stability condition can be achieved both in the Rayleigh regime [67] (trapped particle much smaller than the trapping wavelength) and Lorenz-Mie regime [68] (trapping wavelength and trapped particle size are of the same order of magnitude). Malmqvist and Hertz were the first to report simultaneous optical trapping of and second-harmonic generation in 50–100-nm particles using a 1,06 um fs laser [67], while Agate et al were the first to demonstrate femtosecond Optical Tweezers (fs OT) in the Lorenz-Mie regime [68]. In [68], the authors used a titanium-sapphire NIR fs laser to stably trap ~ 1um beads and measured the lateral trapping force (Q-value) acting on the captured bead to demonstrate that the tweezing action of a fs laser can be as effective as that of a cw laser with the same average power. Moreover, and importantly, Agate et al. showed that fs laser can be used for simultaneous trapping and multiphoton absorption of a target particle. The impulsive pulses of fs laser rapidly release energy resulting in extremely high peak powers. The light intensity of such pulse is in the range of 10^5 W/cm^2 and the peak power can be as high as few megawatts. The interaction of such high intensity high peak power laser with material induces deviation from classical behavior, enabling the exploration of nonlinear processes such as multi-photon absorption [64]. Using a fs laser operating at 800 nm, Agate et al. achieved two-photon excitation of optically trapped dye-doped polymer particles absorbing at 400 nm and emitting at ~ 450 nm, and showed how the fluorescent light could be turned on and off reversibly by simply switching the laser source

between the fs and the cw regimes, with no effect on tweezing efficiency. The possibility of switching on and off the light emitted by a trapped particle is a unique feature of femtosecond OT that might have interesting developments for the manipulation and visualization of biological samples. A better theoretical understanding of the roles played in optical trapping by the various facets of femtosecond lasers, such as pulse width, pulse repetition rate, transient forces and multiphoton absorptions will help us device better fs OT systems [69, 70].

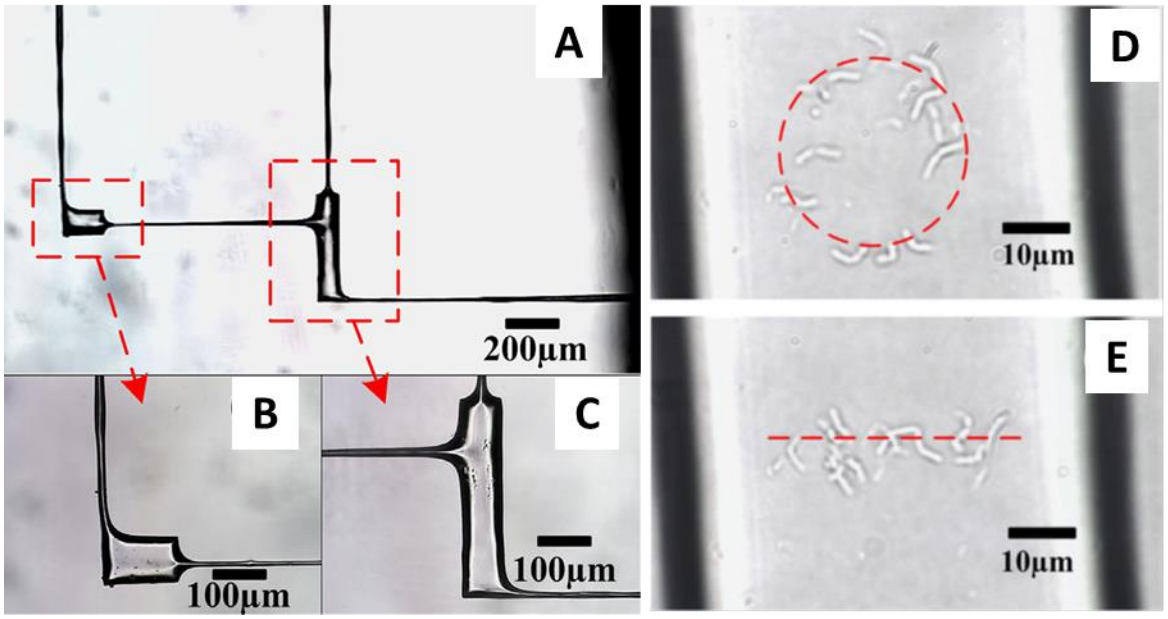

Figure 3: A) Microfluidic device made of 2 micro-pools and four microchannels. B) and C) show magnified views of the micro-pools. D) and E) show circular and linear distributions of B. subtilis manipulated inside the micro-pools with a fs laser trap. Adapted with permission from [71]. Copyright 2014 Elsevier.

The biological applications of fs lasers have been limited to date and confined mostly, although not exclusively, to the manipulation of cells. Yet, the importance of fs lasers in biology is bound to increase as some intrinsic features of these lasers make them particularly well suited for the manipulation of soft matter. Femtosecond lasers have high peak power, but their short pulse duration prevents the mode-locked laser oscillators to generate a population inversion at high energies, limiting the pulse energy to a few nano joules. As a consequence,

fs lasers operate in a weak energy regime, making them a viable tool for the manipulation of cells. In [72], Ming Zhou et al. used a 800-nm femtosecond Ti:sapphire laser to stably trap human red blood cells (hRBCs), and showed the ability to make them rotate inside the trap by modulating the laser light intensity. Stable optical trapping of hRBCs with fs lasers was also achieved by Fang-lin Mao et al. who also measured the escape velocity of these cells from the optical traps to show a tweezing efficiency comparable to that of cw lasers. No cell damage was reported in these studies as well as in the study presented in [71] by Yan Li et al., where the authors used fs lasers to trap living prokaryotic cells. Yan Li et al. first performed a water-assisted femtosecond laser ablation of the internal surface of a microfluidic device to make it less rough and thus improve its optical properties (Figure 3). Then they used the same fs laser to trap single B. subtilis cells and move them from one micro-pool to another through microchannels of 10 μm diameter. Finally, they manipulated individual B. subtilis inside the micro-pools to distribute them according to specific patterns. The results of these studies reveal the great potential that the combination microfluidic devices - fs laser OT might have for living cell sorting and manipulation.

Fs lasers have also been used in POT to trap biomolecules. Roxworthy and Toussiant [73] were the first to report on efficient trapping of nanosized objects using POT incorporated with fs lasers. They used a 100 fs Ti:Sapphire (800 nm) laser and gold bowtie nanoantenna arrays to create plasmonic traps that stably captured silver nanoparticles (80 nm), reporting a two- and five-fold increase in trap stiffness compared to cw laser plasmonic traps and conventional OT traps, respectively. Similarly, Tatsuya Shoji et al. [74] used a fs NIR laser to create plasmonic traps on gold nanopyramidal arrays for capturing λ-DNA molecules stained with YOYO-1, Figure 4. When they focused the laser on the plasmonic substrate they observed accumulation of the DNA molecules in the irradiated area that under a fluorescent microscope becomes brighter and brighter over time as more and more molecules are trapped. Upon switching off the laser light the molecules rapidly go back in solution. The authors trapped λ - DNA molecules on the same plasmonic substrate also using a cw laser, but in this case the trapping process was not reversible as the molecules remained stuck on the gold surface when the cw laser irradiation was turned off. Why reversible trapping and release of DNA is possible only with fs lasers is not clear but surely these results reveal important differences between fs and cw plasmonic traps that should be understood better to exploit them efficiently for the manipulation of other biomolecules.

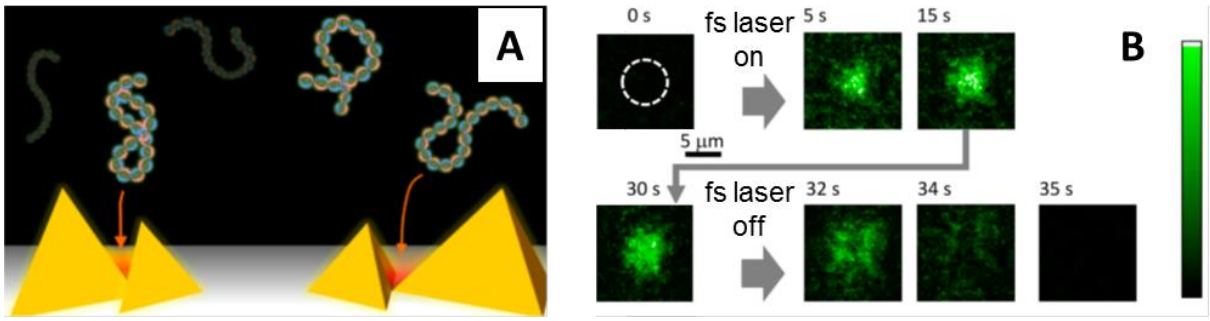

Figure 4: A) Cartoon showing gold nanopyramidal dimers and DNA molecules being trapped in plasmonic traps (red areas). B) Fluorescence micrographs showing assembly of l-DNA molecules stained with YOYO-1 in the area of the plasmonic substrate irradiated with the fs laser (dashed white circle). As the fs laser is turned on, the irradiated area becomes brighter and brighter over time as an increasing number of molecules are trapped. When the laser is turned off the molecules go back in solution. Adapted with permission from [74]. Copyright 2013 American Chemical Society.

2.5 Optical tweezers combined with fluorescence

An obvious limitation of optical tweezers is that they provide one-dimensional data: we can measure the molecular extension only along the direction of the applied force. The experimenter is therefore compelled to adopt as a reaction coordinate the end-to-end extension, a choice which could miss important details of the system under investigation [75, 76]. There are ways to circumvent this obstacle by adopting special experimental configurations that allow simultaneous manipulation along different directions: for instance, the Q-trap consisting of four independently controlled optical traps [77], or the DNA Y-structure whose trunk is anchored to a microscope coverslip while the two arms are manipulated by a dual trap [78]. The peculiar geometry severely limits the kind of systems which can be studied by these means. In a more generally applicable approach, one can resort to repeated experiments, where handles are attached to different sites of the same molecule [79, 80], but this is hardly a satisfying solution. On their own, optical tweezers remain blind to chemical and structural changes that does not

produce a measurable variation of the molecular extension in the one direction susceptible of measurement.

It is therefore quite natural to try and complement the strength of optical tweezers by marrying them with the other great family of single-molecule experimental methods: those based on fluorescence properties [81]. From the simple localization of a single fluorophore to the high-resolution detection of Förster Resonance Energy Transfer (FRET) [82], fluorescence-based methods add visualization capabilities to the mechanical manipulation skills of OT, the result being a very powerful single-molecule technique whose potential has just begun to be explored. A few recent reviews [83-85] make an excellent job of detailing the earlier successes and the state of the art of such hybrid experimental setups. Here we limit ourselves to a very concise sketch of the most promising instrumental developments and biological applications, with special attention to the latest results.

Any attempt to combine fluorescence and optical manipulation runs into two main technical challenges: 1) the weak fluorescence signal must be efficiently isolated from other light sources (bright-field illumination, background fluorescence, the same trapping laser); 2) the high-intensity laser used for the trap hastens the phenomenon of photobleaching [86]. Regarding the first issue, there are, broadly speaking, two traditional approaches to fluorescence spectroscopy, namely wide-field and confocal, and they offer a trade-off between ease of visualization and absence of background luminosity. As for the photobleaching problem, three conceptually different solutions have been successfully essayed: clever fine-tuning of the optical properties of the setup, and separation between fluorescence and trapping either in space, or in time. Finally, it is possible to add fluorescence detection to several OT setups: single trap or double (or multi-) trap, with the option of using the coverslip as an additional tethering point.

In the following we will show a selection of recent literature that covers many of the variations in the experimental setup and the biological system under study. Before that, however, it may be useful to give a quick rundown on the terminology of fluorescence techniques. We refer to *epi-illumination* when the light used for the excitation of the fluorophore goes through the same objective lens that is used for focusing the fluorescence to the observer. As all the fluorescence produced within the sample is detected, unwanted background fluorescence limits the concentration of fluorophores at which it is still possible to resolve a single emitter. The desire to reduce the background luminosity lead to the introduction of the *total internal reflection fluorescence* (TIRF): fluorophores are excited by an evanescent

field which decays exponentially with the distance from the reflecting surface, thus limiting the field of view to a narrow (no more than 200 nm) region close to the coverslip. Both epi-illumination and TIRF are *wide-field* techniques, offering direct access to a wide field of view.

A drastic solution to the background problem is to let the fluorescent light reach the detector through a pinhole that blocks most of the out-of-focus signal. This is the principle of *confocal* microscopy. One common use of the confocal setup is to detect FRET [87, 88]. The efficiency of the energy transfer between two chromophores is an extremely sensitive measure of the distance between them, providing sub-nanometer details about spatial rearrangements undergone by the molecule object of investigation. As the field of view in confocal microscopy is limited to a very small region (ideally just a spot), a complete image of the sample can be obtained only by scanning, i.e. moving the confocal point within a grid of predefined positions. This has the advantage that a 3D image can be reconstructed, albeit with reduced temporal resolution, and the disadvantage of accelerated photobleaching per detected photon [89], due to the fact that also out-of-focus portions of the sample are submitted to long exposure time while only a fraction of the fluorescence actually reaches detector. This can be avoided by switching from single-photon to *two-photon excitation* (TPE) fluorescence: two lower energy photons are simultaneously (i.e., within one attosecond) absorbed by the fluorophore, which then releases a shorter wavelength photon. The cross-section for two-photon absorption is small, so a powerful excitation laser is needed, but the illumination is efficiently concentrated (both in time and space) so there is no out-of-focus photobleaching and the lifetime of fluorophores results actually longer.

Equipped with some basic fluorescence vocabulary, we can now embark on an admittedly non-comprehensive overview of recent interesting experiments. One field where combined OT and fluorescence techniques really shine is that of molecular motors. Ishii et al. [90] used a combination of optical trapping, TIRF and epifluorescence to enrich a standard assay of motility. In Figure 5, a fluorescently labeled thin filament reconstituted from actin, tropomyosin and troponin is tethered to a fluorescent polystyrene bead and interacts with heavy meromyosin (HMM in the figure) molecules attached to the coverslip.

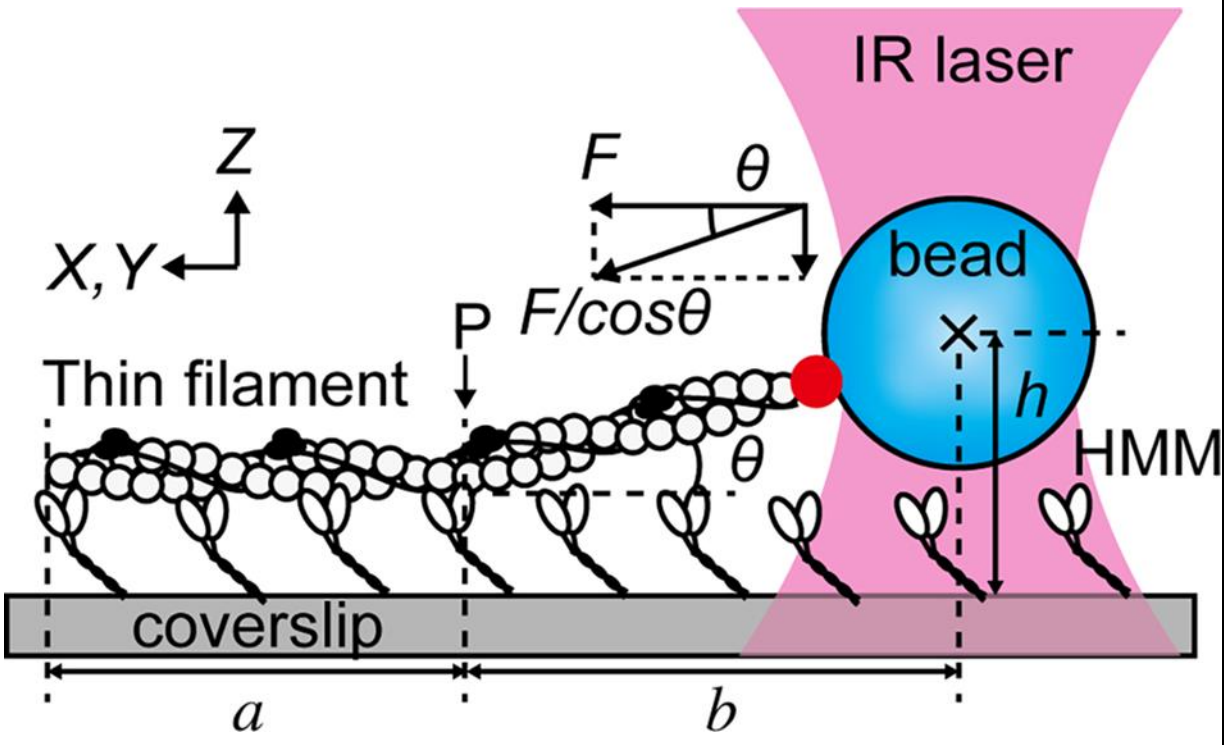

Figure 5: Experimental setup used by Ishii et al [90]. The filament made of actin, tropomyosin and troponin is attached to the coverslip by its interaction with heavy meromyosin molecules (HMM in the figure). One end is connected to an optically trapped polystyrene bead. The filament is labeled with fluorophores, and imaged by wide-field techniques. Optical tweezers measure the intensity of the force F/cos θ, while fluorescence allows to estimate both the lengths h and b; in this way, the z-component of the force can be reconstructed. Reprinted with permission from [90].

The instrument can switch between TIRF, which images only the region denoted by *a*, and epi-illumination, which allows to visualize also region *b*. The height *h* of the trapped bead with respect to the coverslip is measured from the fluorescence intensity of the bead: the angle θ can thus be estimated and the 3D nature of the force vector is properly taken into account. In a somewhat similar OT setup which also makes use of the coverslip as an anchoring point, TIRF has been recently employed to distinguish parallel from anti-parallel microtubule bundles [91]. It was therefore possible to ascertain that the mechanical action of the mitotic kinesin Kif15 treats differently the two cases, sliding apart only the anti-parallel bundles. Another aspect of mitosis which has been clarified to unprecedented detail is the attachment to

microtubules of kinetochores (the molecular machines responsible for chromosome separation). The trap-and-surface geometry OT enhanced by two-color TIRF allowed to clarify the role played by the central kinetochore component Mis12/MIND in enhancing the microtubule-binding affinity of the external Ndc80 complex [92]. Lin and Ha have published a detailed protocol [93] for building and calibrating an OT integrated with TIRF; they also guide the reader through the steps to setup an experiment about helicase translocation on single-stranded DNA.

The trap-and-surface geometry we have described so far lends itself quite naturally to be coupled with wide-field fluorescence, especially TIRF due to the role played by the surface, but it has been successfully combined with confocal methods as well. Figure 6, shows a typical setup: FRET intensity varies with the distance between the chromophores, that is the end-to-end extension of the molecule (in this case, repeats of a peptide derived from spider silk), while the optical trap is used to apply and measure force [94].

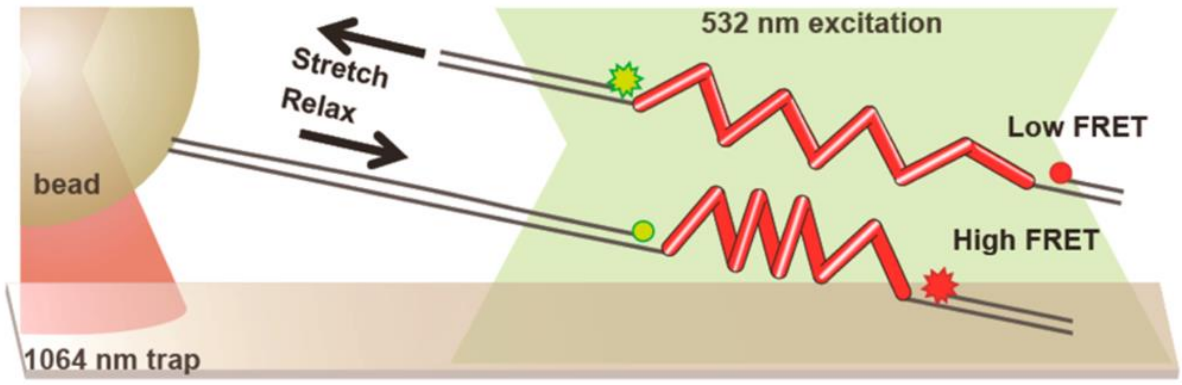

Figure 6: Combination of optical trapping and FRET in the experimental setup devised by Brenner et al. [94]. The end-to-end extension of the repeat protein made of spider silk peptides is measured by FRET, while OT are used to apply force. Trapping laser and fluorescence excitation are kept well apart by long dsDNA handles. Reprinted with permission from [94]. Copyright 2016 American Chemical Society

Observe that the focal points of the trap and the fluorescence excitation lasers are kept well separated (around 15 μm for this experiment) to avoid excessive photobleaching: the force exerted by the trap is transmitted by means of long DNA handles. The goal of this research was

to study the effect of force on FRET intensity in order to use the peptide repeats as tension sensors in live cell imaging. As regards instrumental developments, a stimulating new direction has been pioneered by Lee and Hohng [95], who managed to combine optical trapping with three-color FRET. The possibility of simultaneously measuring the mutual distances of three dyes while applying force promises to be a powerful way to address systems of increased complexity.

It is possible, by splitting the trapping laser into perpendicularly polarized beams, to generate two traps that can be independently controlled. Dispensing with a macroscopic anchoring point greatly reduces the thermal drift effects and provides higher resolution OT. The Amsterdam-based group led by Wuite and Peterman is having considerable success in studying DNA repairing molecular machines by coupling the dual trap setup with epifluorescence and a sophisticated microfluidic flow system. A very recent, paradigmatic experiment is illustrated in Figure 7 [96].

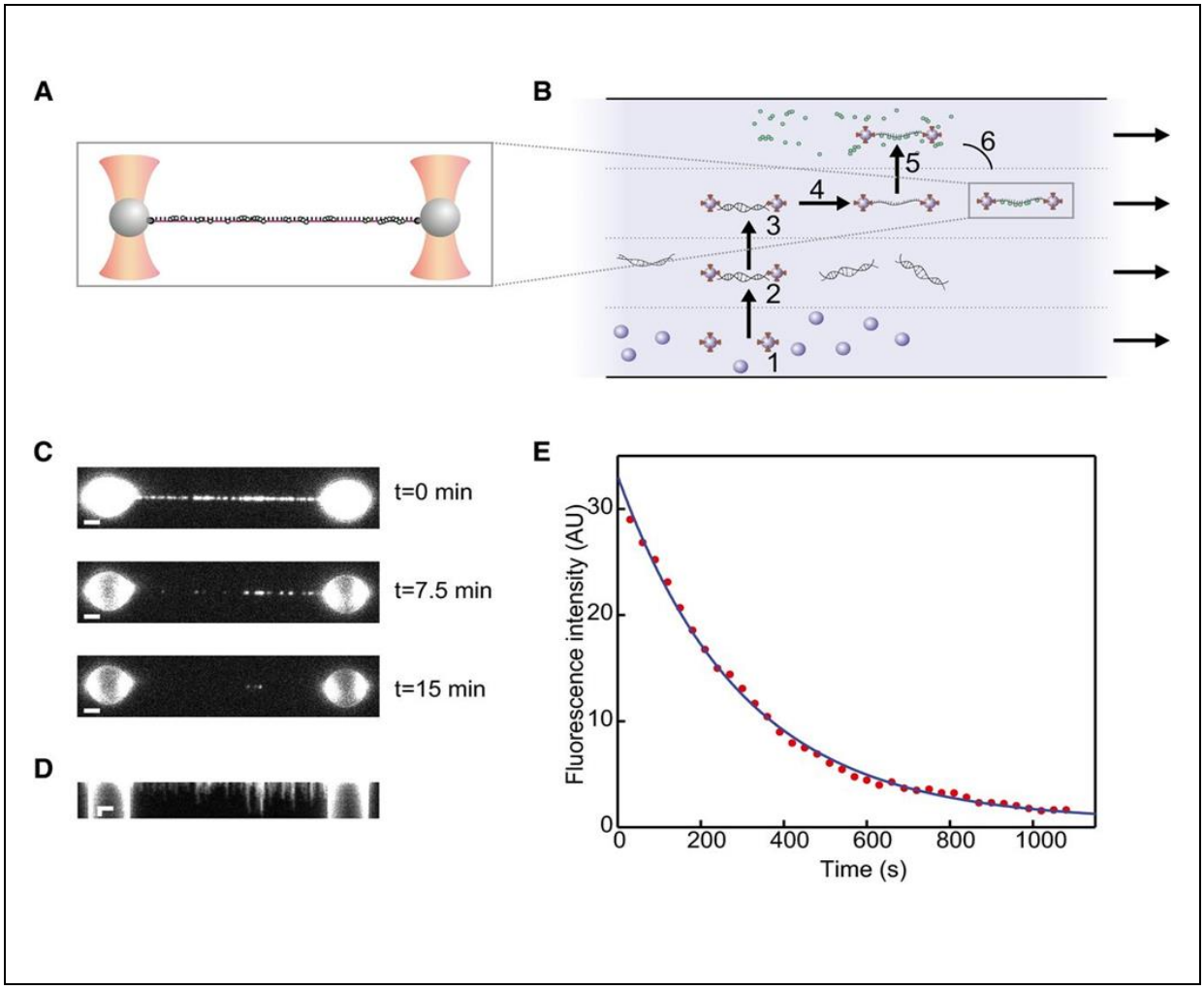

Figure 7: Experiment by Brouwer et al. [96]. A: dual-trap setup: the molecular construct under study comprises ssDNA to which fluorescently labeled RAD51 complexes (represented as green dots) are attached. B: 4-channel microfluidic system used to assemble the molecule: the traps capture two polystyrene beads from the bottom channel (1), then a dsDNA segment is attached to the beads (2), isolated (3) and stretched to form ssDNA (4); RAD51 proteins interact with ssDNA in the top channel (5); finally, the construct is moved to the free channel where measurements are performed (6). C: from these images obtained by epi-illumination the fluorescence intensity as a function of time is estimated. D: kymograph of the same dataset in figure C. E: an exponential fitted to the data yields an estimation of the disassembly rate. Reprinted with permission from [96].

The pair of traps is used to move among the four laminar channels to assemble the molecular construct, comprised of ssDNA and fluorescently labelled RAD51 complexes, which are then imaged by epi-illumination. The integrated fluorescence intensity over time in subfigure E allows to measure the disassembly rate, and the experiment can be repeated at different values of the tension, as measured by the OT. A persuasive demonstration of the power of combining manipulation and imaging in single molecule experiments! A similar dual trap plus microfluidics plus wide-field fluorescence (both TIRF and epi-illumination) has been used by another group to study RecA, another protein involved in DNA repairing [97]. The integration of high resolution OT with polarized fluorescence microscopy has been

demonstrated in a very recent study [98] of the behaviour of YOYO-intercalated dsDNA subject to forces up to 80 pN, well beyond the DNA overstretching transition. The use of linearly polarized excitation light allowed to check the orientation of the dyes, perpendicular to the axis of the DNA, and to characterize the fast dynamics that they undertake in the time between excitation and emission.

If the trapping and the excitation lasers are kept well apart, it is possible to integrate confocal fluorescence into a dual trap OT. A recent demonstration of the advantages of this approach is given by the experiment depicted in Figure 8 [99].

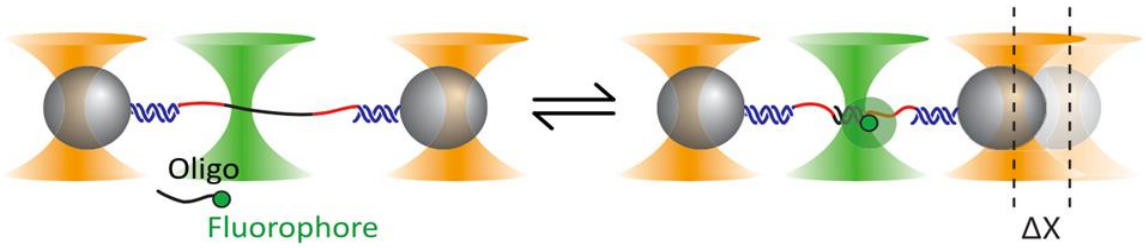

Figure 8: Experimental setup adopted by Whitley et al. [99]. The ssDNA binding site (black in the figure), is connected by means of two spacers (red) and two dsDNA handles (blue) to two trapped beads. Binding events of the tagged oligonucleotides are identified by confocal fluorescence. Reprinted with permission from [99]. Copyright 2018 American Physical Society

Here the goal is to study the elastic properties of very short (around 10 bp) fragments of dsDNA. To this end a ssDNA sequence is tethered by long dsDNA handles to two trapped polystyrene beads. Short complementary oligonucleotides are designed to hybridize with segments of the ssDNA, thus forming short fragments of dsDNA. However, the effect of the oligo binding in the low-force regime (around 5 pN) is so small as to lay at the threshold of detectability even for high resolution OT. The solution: tagging the oligo with a fluorophore and using confocal fluorescence to unambiguously identify binding events. With a similar dual trap plus confocal fluorescence setup Ganim and Rief [100] were able to study the response to tension of the green fluorescent protein, establishing that fluorescence is lost right at the outset of an unfolding event and is not recovered until complete refolding. Another confocal fluorescence technique, FRET, excels at revealing small changes in the tertiary structure, and has been profitably coupled to high resolution dual trap OT to study the thiamine pyrophosphate riboswitch [101]. The authors managed to observe details about the orientation of a certain helix-arm motif that would have been inaccessible by force or fluorescence spectroscopy alone.

In the examples we have seen so far, the spatial separation between the traps and the confocal fluorescence spot requires the adoption of long dsDNA handles, whose compliance limits the OT resolution. Stiffer, shorter handles grant a better signal to noise ratio, but then the proximity of the trapping light enhances photobleaching. A clever solution is to interlace at high frequency (typically more than 50 kHz) the trapping and the fluorescence excitation lights in such a way that the fluorophore is never simultaneously exposed to both. The sophistication

of the instrumental design is more than compensated by the increase in resolution, see for instance the very detailed reconstruction of the energy landscape of ssDNA binding protein obtained by the authors of [102]. Whitley et al. [103] have recently published a thorough description of the instrumental design of an interlaced OT/FRET setup, with a guide to alignment procedures and tutorial instructions to perform an experiment on helicase UvrD. An alternative design proposed by Sirinakis et al. [104] offers great versatility, combining in a single instrument dual trap OT with either wide-field or confocal fluorescence.

The success of the approach based on joint force spectroscopy and fluorescence imaging is not limited to *in vitro* experiments. In their study of the mechanical properties of filopodia, Leijnse et al. [105] used confocal scanning microscopy to image F-actin in living HEK293 cells, and optically trapped beads to manipulate single filopodia. This allowed them to reveal rotational motion and helical buckling of the actin shaft inside retracting filopodia, a mechanism which had previously gone unnoticed. A similar approach (scanning confocal 3D imaging accompanied by OT-induced manipulation) was applied to the study of adhesion between cells and biomaterial scaffold [106]. The remarkable observation that the cell growth during the first week of culture is strongly correlated to the adhesion forces measured within a few seconds after the first contact suggests a quick way of predicting scaffold biocompatibility, with possible impact on the field of regenerative medicine. In conclusion, we would like to mention a recent experiment in which Pang et al. [107] managed to optically trap and image (by two-photon fluorescence) single HIV-1 virions in culture fluid, a powerful new technique for virology.

2.6 Conclusions

The advent of optical trapping techniques in the sphere of medical science and biophysics has been accompanied by the exploration of new horizons in the optical tweezers technology. In this paper we illustrate and discuss some of the latest versions of OT, highlighting their instrumental features and biological applications. While these techniques are opening new avenues of optical manipulation, a salient feature common to all of them is the vast potential for further improvement, especially when dealing with biomaterials. POT have facilitated efficient optical trapping in the Rayleigh regime, making small biomolecules a fair game for

optical trapping experiments [51, 52]. Yet, controlled probing and manipulation capabilities by means of plasmonic traps are still limited. Moreover, photothermal effects observed during plasmonic trapping diminish the efficiency of this technique as they create adverse local thermophoretic gradients [45]. Integrating POT with lab-on-chip devices, like Surface Plasmon Resonance (SPR)-based biosensors [108] and Surface Acoustic Waves (SAW) resonators [109], might allow us to explore different schemes of manipulation and enhance the investigation power of this technique. Similarly, theoretical studies in the field of thermal convection [110] and employment of novel material and nanostructure geometries [45] might help us develop new strategies to curb the shortcomings due to thermal effects. Fs OT and PhC OT can be extremely effective for in vivo manipulation experiments as they cause little photothermal damage to the cells [61, 71]. Combining this optical trapping capability with the tools at the disposal of lab-on-chip devices will most likely offer a powerful method to investigate biophysical properties of living cells [61, 71]. On the other hand, hybrid systems combining optical traps with fluorescence techniques are so advanced from an instrumental viewpoint that at the moment of writing there are two readily available commercial solutions (JPK Nano Tracker™ and LUMICKS C-Trap™) that integrate optical manipulation with several kinds of fluorescent imaging. As technical problems are being ironed out, research groups are shifting their attention from the instrument to its ingenuous biological applications, making optical trapping an increasingly powerful tool in life science studies, a fitting homage to the seminal paper [1] that, more than 30 years ago, started the single-molecule revolution.

2.7 References

1. Ashkin, A. and J.M. Dziedzic, *OPTICAL TRAPPING AND MANIPULATION OF VIRUSES AND BACTERIA.* Science, 1987. **235**(4795): p. 1517-1520.
2. Ashkin, A., et al., *Observation of a single-beam gradient force optical trap for dielectric particles.* Optics letters, 1986. **11**(5): p. 288-290.
3. Ashkin, A., J.M. Dziedzic, and T. Yamane, *Optical trapping and manipulation of single cells using infrared laser beams.* Nature, 1987. **330**(6150): p. 769.
4. Svoboda, K., et al., *DIRECT OBSERVATION OF KINESIN STEPPING BY OPTICAL TRAPPING INTERFEROMETRY.* Nature, 1993. **365**(6448): p. 721-727.
5. Kishino, A. and T. Yanagida, *FORCE MEASUREMENTS BY MICROMANIPULATION OF A SINGLE ACTIN FILAMENT BY GLASS NEEDLES.* Nature, 1988. **334**(6177): p. 74-76.
6. Evans, E., K. Ritchie, and R. Merkel, *SENSITIVE FORCE TECHNIQUE TO PROBE MOLECULAR ADHESION AND STRUCTURAL LINKAGES AT BIOLOGICAL INTERFACES.* Biophysical Journal, 1995. **68**(6): p. 2580-2587.
7. Smith, S.B., L. Finzi, and C. Bustamante, *DIRECT MECHANICAL MEASUREMENTS OF THE ELASTICITY OF SINGLE DNA-MOLECULES BY USING MAGNETIC BEADS.* Science, 1992. **258**(5085): p. 1122-1126.
8. Capitanio, M. and F.S. Pavone, *Interrogating Biology with Force: Single Molecule High-Resolution Measurements with Optical Tweezers.* Biophysical Journal, 2013. **105**(6): p. 1293-1303.
9. Moffitt, J.R., et al., *Differential detection of dual traps improves the spatial resolution of optical tweezers.* Proceedings of the National Academy of Sciences of the United States of America, 2006. **103**(24): p. 9006-9011.
10. Carter, A.R., et al., *Stabilization of an optical microscope to 0.1 nm in three dimensions.* Applied Optics, 2007. **46**(3): p. 421-427.
11. Chakraborty, A., C.A. Meng, and S.M. Block, *Observing Single RNA Polymerase Molecules Down to Base-Pair Resolution*, in *Optical Tweezers: Methods and Protocols*, A. Gennerich, Editor. 2017, Springer New York: New York, NY. p. 391-409.

12. Seifert, U., *Stochastic thermodynamics, fluctuation theorems and molecular machines.* Reports on Progress in Physics, 2012. **75**(12): p. 58.
13. Ciliberto, S., *Experiments in Stochastic Thermodynamics: Short History and Perspectives.* Physical Review X, 2017. **7**(2): p. 26.
14. Milic, B., et al., *Intraflagellar transport velocity is governed by the number of active KIF17 and KIF3AB motors and their motility properties under load.* Proceedings of the National Academy of Sciences of the United States of America, 2017. **114**(33): p. E6830-E6838.
15. Brunnbauer, M., et al., *Torque Generation of Kinesin Motors Is Governed by the Stability of the Neck Domain.* Molecular Cell, 2012. **46**(2): p. 147-158.
16. Lisica, A., et al., *Mechanisms of backtrack recovery by RNA polymerases I and II.* Proceedings of the National Academy of Sciences of the United States of America, 2016. **113**(11): p. 2946-2951.
17. Naranjo, T., et al., *Dynamics of individual molecular shuttles under mechanical force.* Nature Communications, 2018. **9**(1): p. 4512.
18. Bryant, Z., et al., *Structural transitions and elasticity from torque measurements on DNA.* Nature, 2003. **424**(6946): p. 338-341.
19. Kim, J., et al., *A mechanically stabilized receptor-ligand flex-bond important in the vasculature.* Nature, 2010. **466**(7309): p. 992-U123.
20. Heidarsson, P.O., et al., *Direct single-molecule observation of calcium-dependent misfolding in human neuronal calcium sensor-1.* Proceedings of the National Academy of Sciences, 2014. **111**(36): p. 13069-13074.
21. Alemany, A., et al., *Experimental free-energy measurements of kinetic molecular states using fluctuation theorems.* Nature Physics, 2012. **8**(9): p. 688-694.
22. Jahn, M., et al., *Folding and Domain Interactions of Three Orthologs of Hsp90 Studied by Single-Molecule Force Spectroscopy.* Structure, 2018. **26**(1): p. 96-+.
23. Cecconi, C., et al., *Direct observation of the three-state folding of a single protein molecule.* Science, 2005. **309**(5743): p. 2057-2060.
24. Bechtluft, P., et al., *Direct observation of chaperone-induced changes in a protein folding pathway.* Science, 2007. **318**(5855): p. 1458-1461.
25. Gao, Y., G. Sirinakis, and Y.L. Zhang, *Highly Anisotropic Stability and Folding Kinetics of a Single Coiled Coil Protein under Mechanical Tension.* Journal of the American Chemical Society, 2011. **133**(32): p. 12749-12757.

26. Caldarini, M., et al., *The complex folding behavior of HIV-1-protease monomer revealed by optical-tweezer single-molecule experiments and molecular dynamics simulations.* Biophysical Chemistry, 2014. **195**: p. 32-42.
27. Smith, S.B., Y.J. Cui, and C. Bustamante, *Overstretching B-DNA: The elastic response of individual double-stranded and single-stranded DNA molecules.* Science, 1996. **271**(5250): p. 795-799.
28. Zhang, Y.L., et al., *DNA translocation and loop formation mechanism of chromatin remodeling by SWI/SNF and RSC.* Molecular Cell, 2006. **24**(4): p. 559-568.
29. Mossa, A., et al., *Dynamic force spectroscopy of DNA hairpins: I. Force kinetics and free energy landscapes.* Journal of Statistical Mechanics-Theory and Experiment, 2009: p. 28.
30. Manosas, M., et al., *Dynamic force spectroscopy of DNA hairpins: II. Irreversibility and dissipation.* Journal of Statistical Mechanics-Theory and Experiment, 2009: p. 28.
31. Bongini, L., et al., *Transient kinetics measured with force steps discriminate between double-stranded DNA elongation and melting and define the reaction energetics.* Nucleic Acids Research, 2014. **42**(5): p. 3436-3449.
32. Li, P.T.X., C. Bustamante, and I. Tinoco, *Real-time control of the energy landscape by force directs the folding of RNA molecules.* Proceedings of the National Academy of Sciences of the United States of America, 2007. **104**(17): p. 7039-7044.
33. Ritchie, D.B. and M.T. Woodside, *Probing the structural dynamics of proteins and nucleic acids with optical tweezers.* Current Opinion in Structural Biology, 2015. **34**: p. 43-51.
34. Farre, A., et al., *Stretching single DNA molecules to demonstrate high-force capabilities of holographic optical tweezers.* Journal of Biophotonics, 2010. **3**(4): p. 224-233.
35. Baker, J.E., R.P. Badman, and M.D. Wang, *Nanophotonic trapping: precise manipulation and measurement of biomolecular arrays.* Wiley Interdisciplinary Reviews-Nanomedicine and Nanobiotechnology, 2018. **10**(1): p. 15.
36. Fu, D., et al., *Imaging the intracellular distribution of tyrosine kinase inhibitors in living cells with quantitative hyperspectral stimulated Raman scattering.* Nature Chemistry, 2014. **6**(7): p. 615-623.
37. Enger, J., et al., *Optical tweezers applied to a microfluidic system.* Lab on a Chip, 2004. **4**(3): p. 196-200.

38. Lee, J., et al., *Single beam acoustic trapping.* Applied Physics Letters, 2009. **95**(7): p. 3.
39. Grigorenko, A.N., et al., *Nanometric optical tweezers based on nanostructured substrates.* Nature Photonics, 2008. **2**(6): p. 365-370.
40. Marago, O.M., et al., *Optical trapping and manipulation of nanostructures.* Nature Nanotechnology, 2013. **8**(11): p. 807-819.
41. Chen, Y.F., et al., *Controlled Photonic Manipulation of Proteins and Other Nanomaterials.* Nano Letters, 2012. **12**(3): p. 1633-1637.
42. Shoji, T. and Y. Tsuboi, *Plasmonic Optical Tweezers toward Molecular Manipulation: Tailoring Plasmonic Nanostructure, Light Source, and Resonant Trapping.* Journal of Physical Chemistry Letters, 2014. **5**(17): p. 2957-2967.
43. Juan, M.L., M. Righini, and R. Quidant, *Plasmon nano-optical tweezers.* Nature Photonics, 2011. **5**(6): p. 349-356.
44. Novotny, L., R.X. Bian, and X.S. Xie, *Theory of nanometric optical tweezers.* Physical Review Letters, 1997. **79**(4): p. 645-648.
45. Wang, K., et al., *Trapping and rotating nanoparticles using a plasmonic nano-tweezer with an integrated heat sink.* Nature Communications, 2011. **2**: p. 6.
46. Juan, M.L., et al., *Self-induced back-action optical trapping of dielectric nanoparticles.* Nature Physics, 2009. **5**(12): p. 915-919.
47. Pang, Y.J. and R. Gordon, *Optical Trapping of 12 nm Dielectric Spheres Using Double-Nanoholes in a Gold Film.* Nano Letters, 2011. **11**(9): p. 3763-3767.
48. Zhang, W.H., et al., *Trapping and Sensing 10 nm Metal Nanoparticles Using Plasmonic Dipole Antennas.* Nano Letters, 2010. **10**(3): p. 1006-1011.
49. Righini, M., et al., *Nano-optical Trapping of Rayleigh Particles and Escherichia coli Bacteria with Resonant Optical Antennas.* Nano Letters, 2009. **9**(10): p. 3387-3391.
50. Huang, L., S.J. Maerkl, and O.J.F. Martin, *Integration of plasmonic trapping in a microfluidic environment.* Optics Express, 2009. **17**(8): p. 6018-6024.
51. Pang, Y.J. and R. Gordon, *Optical Trapping of a Single Protein.* Nano Letters, 2012. **12**(1): p. 402-406.
52. Kotnala, A. and R. Gordon, *Double nanohole optical tweezers visualize protein p53 suppressing unzipping of single DNA-hairpins.* Biomedical Optics Express, 2014. **5**(6): p. 1886-1894.
53. Yang, A.H.J., et al., *Optical manipulation of nanoparticles and biomolecules in sub-wavelength slot waveguides.* Nature, 2009. **457**(7225): p. 71-75.

54. Conteduca, D., et al., *Photonic and Plasmonic Nanotweezing of Nano- and Microscale Particles.* Applied Spectroscopy, 2017. **71**(3): p. 367-390.
55. Mandal, S., X. Serey, and D. Erickson, *Nanomanipulation Using Silicon Photonic Crystal Resonators.* Nano Letters, 2010. **10**(1): p. 99-104.
56. Joannopoulos, J.D., P.R. Villeneuve, and S.H. Fan, *Photonic crystals: Putting a new twist on light.* Nature, 1997. **386**(6621): p. 143-149.
57. Yablonovitch, E., *INHIBITED SPONTANEOUS EMISSION IN SOLID-STATE PHYSICS AND ELECTRONICS.* Physical Review Letters, 1987. **58**(20): p. 2059-2062.
58. Yablonovitch, E. and T.J. Gmitter, *PHOTONIC BAND-STRUCTURE - THE FACE-CENTERED-CUBIC CASE.* Journal of the Optical Society of America a-Optics Image Science and Vision, 1990. **7**(9): p. 1792-1800.
59. Lin, S.Y., et al., *Design of nanoslotted photonic crystal waveguide cavities for single nanoparticle trapping and detection.* Optics Letters, 2009. **34**(21): p. 3451-3453.
60. Serey, X., et al., *DNA Transport and Delivery in Thermal Gradients near Optofluidic Resonators.* Physical Review Letters, 2012. **108**(4): p. 5.
61. Jing, P.F., et al., *Photonic Crystal Optical Tweezers with High Efficiency for Live Biological Samples and Viability Characterization.* Scientific Reports, 2016. **6**: p. 7.
62. Krishan, A., *RAPID FLOW CYTOFLUOROMETRIC ANALYSIS OF MAMMALIAN-CELL CYCLE BY PROPIDIUM IODIDE STAINING.* Journal of Cell Biology, 1975. **66**(1): p. 188-193.
63. Keeler, E.G., et al. *MEMS Resonator and Photonic Crystal Integration for Enhanced Cellular Mass Sensing*. in *Optics in the Life Sciences*. 2015. Vancouver: Optical Society of America.
64. Jiang, Y.Q., T. Narushima, and H. Okamoto, *Nonlinear optical effects in trapping nanoparticles with femtosecond pulses.* Nature Physics, 2010. **6**(12): p. 1005-1009.
65. Muramatsu, M., et al., *Picosecond Motional Relaxation of Nanoparticles in Femtosecond Laser Trapping.* Journal of Physical Chemistry C, 2016. **120**(9): p. 5251-5256.
66. Xing, Q.R., et al., *Numerical modeling and theoretical analysis of femtosecond laser tweezers.* Optics and Laser Technology, 2004. **36**(8): p. 635-639.
67. Malmqvist, L. and H.M. Hertz, *Second-harmonic generation in optically trapped nonlinear particles with pulsed lasers.* Applied Optics, 1995. **34**(18): p. 3392-3397.
68. Agate, B., et al., *Femtosecond optical tweezers for in-situ control of two-photon fluorescence.* Optics Express, 2004. **12**(13): p. 3011-3017.

69. Chiang, W.Y., A. Usman, and H. Masuhara, *Femtosecond Pulse-Width Dependent Trapping and Directional Ejection Dynamics of Dielectric Nanoparticles.* Journal of Physical Chemistry C, 2013. **117**(37): p. 19182-19188.
70. Usman, A., W.Y. Chiang, and H. Masuhara, *Femtosecond Trapping Efficiency Enhanced for Nano-sized Silica Spheres*, in *Optical Trapping and Optical Micromanipulation Ix*, K. Dholakia and G.C. Spalding, Editors. 2012, Spie-Int Soc Optical Engineering: Bellingham.
71. Li, Y., Z.Y. Guo, and S.L. Qu, *Living cell manipulation in a microfluidic device by femtosecond optical tweezers.* Optics and Lasers in Engineering, 2014. **55**: p. 150-154.
72. Zhou, M., et al., *Manipulation on human red blood cells with femtosecond optical tweezers.* Chinese Optics Letters, 2008. **6**(12): p. 919-921.
73. Roxworthy, B.J. and K.C. Toussaint, *Femtosecond-Pulsed Plasmonic Nanotweezers.* Scientific Reports, 2012. **2**: p. 6.
74. Shoji, T., et al., *Permanent Fixing or Reversible Trapping and Release of DNA Micropatterns on a Gold Nanostructure Using Continuous-Wave or Femtosecond-Pulsed Near-Infrared Laser Light.* Journal of the American Chemical Society, 2013. **135**(17): p. 6643-6648.
75. Best, R.B., et al., *Pulling direction as a reaction coordinate for the mechanical unfolding of single molecules.* Journal of Physical Chemistry B, 2008. **112**(19): p. 5968-5976.
76. Avdoshenko, S.M. and D.E. Makarov, *Reaction Coordinates and Pathways of Mechanochemical Transformations.* Journal of Physical Chemistry B, 2016. **120**(8): p. 1537-1545.
77. Dame, R.T., M.C. Noom, and G.J.L. Wuite, *Bacterial chromatin organization by H-NS protein unravelled using dual DNA manipulation.* Nature, 2006. **444**(7117): p. 387-390.
78. Inman, J.T., et al., *DNA Y Structure: A Versatile, Multidimensional Single Molecule Assay.* Nano Letters, 2014. **14**(11): p. 6475-6480.
79. Elms, P.J., et al., *The molten globule state is unusually deformable under mechanical force.* Proceedings of the National Academy of Sciences of the United States of America, 2012. **109**(10): p. 3796-3801.
80. Heidarsson, P.O., et al., *A Highly Compliant Protein Native State with a Spontaneous-like Mechanical Unfolding Pathway.* Journal of the American Chemical Society, 2012. **134**(41): p. 17068-17075.

81. Hohlbein, J., et al., *Surfing on a new wave of single-molecule fluorescence methods.* Physical Biology, 2010. **7**(3): p. 22.
82. Hellenkamp, B., et al., *Precision and accuracy of single-molecule FRET measurements-a multi-laboratory benchmark study.* Nature Methods, 2018. **15**(9): p. 669-+.
83. Shabestari, M.H., et al., *Recent Advances in Biological Single-Molecule Applications of Optical Tweezers and Fluorescence Microscopy*, in *Single-Molecule Enzymology: Nanomechanical Manipulation and Hybrid Methods*, M. Spies and Y.R. Chemla, Editors. 2017, Elsevier Academic Press Inc: San Diego. p. 85-119.
84. Chemla, Y.R., *High-Resolution, Hybrid Optical Trapping Methods, and Their Application to Nucleic Acid Processing Proteins.* Biopolymers, 2016. **105**(10): p. 704-714.
85. Cordova, J.C., et al., *Combining single-molecule manipulation and single-molecule detection.* Current Opinion in Structural Biology, 2014. **28**: p. 142-148.
86. van Dijk, M.A., et al., *Combining optical trapping and single-molecule fluorescence spectroscopy: Enhanced photobleaching of fluorophores.* Journal of Physical Chemistry B, 2004. **108**(20): p. 6479-6484.
87. Roy, R., S. Hohng, and T. Ha, *A practical guide to single-molecule FRET.* Nature Methods, 2008. **5**(6): p. 507-516.
88. LeBlanc, S., P. Kulkarni, and K. Weninger, *Single Molecule FRET: A Powerful Tool to Study Intrinsically Disordered Proteins.* Biomolecules, 2018. **8**(4): p. 140.
89. Valeur, B. and M.N. Berberan-Santos, *Molecular fluorescence: principles and applications*. 2012: John Wiley & Sons.
90. Ishii, S., et al., *Estimation of actomyosin active force maintained by tropomyosin and troponin complex under vertical forces in the in vitro motility assay system.* Plos One, 2018. **13**(2): p. 16.
91. Reinemann, D.N., et al., *Collective Force Regulation in Anti-parallel Microtubule Gliding by Dimeric Kif15 Kinesin Motors.* Current Biology, 2017. **27**(18): p. 2810-+.
92. Kudalkar, E.M., et al., *Regulation of outer kinetochore Ndc80 complex-based microtubule attachments by the central kinetochore Mis12/MIND complex.* Proceedings of the National Academy of Sciences of the United States of America, 2015. **112**(41): p. E5583-E5589.

93. Lin, C.-T. and T. Ha, *Probing Single Helicase Dynamics on Long Nucleic Acids Through Fluorescence-Force Measurement*, in *Optical Tweezers*. 2017, Springer. p. 295-316.
94. Brenner, M.D., et al., *Spider Silk Peptide Is a Compact, Linear Nanospring Ideal for Intracellular Tension Sensing.* Nano Letters, 2016. **16**(3): p. 2096-2102.
95. Lee, S. and S. Hohng, *An Optical Trap Combined with Three-Color FRET.* Journal of the American Chemical Society, 2013. **135**(49): p. 18260-18263.
96. Brouwer, I., et al., *Two distinct conformational states define the interaction of human RAD51-ATP with single-stranded DNA.* Embo Journal, 2018. **37**(7): p. 13.
97. Forget, A.L. and S.C. Kowalczykowski, *Single-molecule imaging of DNA pairing by RecA reveals a three-dimensional homology search.* Nature, 2012. **482**(7385): p. 423-U178.
98. van Mameren, J., et al., *A polarized view on DNA under tension.* Journal of Chemical Physics, 2018. **148**(12): p. 9.
99. Whitley, K.D., M.J. Comstock, and Y.R. Chemla, *Ultrashort Nucleic Acid Duplexes Exhibit Long Wormlike Chain Behavior with Force-Dependent Edge Effects.* Physical Review Letters, 2018. **120**(6): p. 6.
100. Ganim, Z. and M. Rief, *Mechanically switching single-molecule fluorescence of GFP by unfolding and refolding.* Proceedings of the National Academy of Sciences of the United States of America, 2017. **114**(42): p. 11052-11056.
101. Duesterberet, V.K., et al., *Observation of long-range tertiary interactions during ligand binding by the TPP riboswitch aptamer.* Elife, 2015. **4**: p. 17.
102. Suksombat, S., et al., *Structural dynamics of E. coli single-stranded DNA binding protein reveal DNA wrapping and unwrapping pathways.* Elife, 2015. **4**: p. 23.
103. Whitley, K.D., M.J. Comstock, and Y.R. Chemla, *High-Resolution Optical Tweezers Combined With Single-Molecule Confocal Microscopy*, in *Single-Molecule Enzymology: Nanomechanical Manipulation and Hybrid Methods*, M. Spies and Y.R. Chemla, Editors. 2017, Elsevier Academic Press Inc: San Diego. p. 137-169.
104. Sirinakis, G., et al., *Combined versatile high-resolution optical tweezers and single-molecule fluorescence microscopy.* Review of Scientific Instruments, 2012. **83**(9): p. 9.
105. Leijnse, N., L.B. Oddershede, and P.M. Bendix, *Helical buckling of actin inside filopodia generates traction.* Proceedings of the National Academy of Sciences of the United States of America, 2015. **112**(1): p. 136-141.

106. Podlipec, R. and J. Strancar, *Cell-Scaffold Adhesion Dynamics Measured in First Seconds Predicts Cell Growth on Days Scale - Optical Tweezers Study*. Acs Applied Materials & Interfaces, 2015. **7**(12): p. 6782-6791.
107. Pang, Y.J., et al., *Optical trapping of individual human immunodeficiency viruses in culture fluid reveals heterogeneity with single-molecule resolution.* Nature Nanotechnology, 2014. **9**(8): p. 624-630.
108. Kaur, G., et al., *Detection of Neisseria meningitidis using surface plasmon resonance based DNA biosensor.* Biosensors & Bioelectronics, 2016. **78**: p. 106-110.
109. Chang, H.W. and J.S. Shih, *Surface acoustic wave immunosensors based on immobilized C60-proteins.* Sensors and Actuators B-Chemical, 2007. **121**(2): p. 522-529.
110. Duhr, S. and D. Braun, *Why molecules move along a temperature gradient.* Proceedings of the National Academy of Sciences of the United States of America, 2006. **103**(52): p. 19678-19682.

The Complex Conformational Dynamics of Neuronal Calcium Sensor-1: A Single Molecule Perspective

Chapter 3

The Complex Conformational Dynamics of Neuronal Calcium Sensor-1: A Single Molecule Perspective

Abstract

The human neuronal calcium sensor-1 (NCS-1) is a multispecific two-domain EF-hand protein expressed predominantly in neurons and is a member of the neuronal calcium sensor (NCS) protein family. Structure-function relationships of NCS-1 have been extensively studied showing that conformational dynamics linked to diverse ion-binding is important to its function. NCS-1 transduces Ca^{2+} changes in neurons and is linked to a wide range of neuronal functions such as regulation of neurotransmitter release, voltage-gated Ca^{2+} channels and neuronal outgrowth. Defective NCS-1 can be deleterious to cells and has been linked to serious neuronal disorders like autism. Here we review recent studies describing at the single molecule level the structural and mechanistic details of the folding and misfolding processes of the non-myristoylated NCS-1. By manipulating one molecule at a time with optical tweezers, the conformational equilibria of the Ca^{2+}-bound, Mg^{2+}-bound and apo states of NCS-1 were investigated revealing a complex folding mechanism underlain by a rugged and multidimensional energy landscape. The molecular rearrangements that NCS-1 undergoes to

transit from one conformation to another and the energetics of these reactions are tightly regulated by the binding of divalent ions (Ca^{2+} and Mg^{2+}) to its EF-hands. At pathologically high Ca^{2+} concentrations the protein sometimes follows non-productive misfolding pathways leading to kinetically trapped and potentially harmful misfolded conformations. We discuss the significance of these misfolding events as well as the role of inter-domain interactions in shaping the energy landscape and ultimately the biological function of NCS-1. The conformational equilibria of NCS-1 are also compared to those of calmodulin (CaM) and differences and similarities in the behaviour of these proteins are rationalized in terms of structural properties.

3.1 Introduction

3.1.1 NCS-1 is a multi-functional, two-domain protein

Calcium ion (Ca^{2+}) signalling is crucial for neurotransmitter release and is intrinsic for neuronal functions. Calcium signalling is mediated by calcium binding proteins that sense changes in cellular concentration of Ca^{2+} ions and respond by interacting with downstream regulatory targets, further cascading the signal. One example of such calcium sensor proteins is the family of neuronal calcium sensors (NCS), which are expressed primarily in neurons and photoreceptor cells [1, 2]. These proteins respond to changes in Ca^{2+} concentration through conformational changes that allow them to bind diverse protein partners [3]. The NCS family has 15 highly-conserved members in mammals and these proteins have numerous functions [4]. Neuronal calcium sensor-1 (NCS-1) is the primordial member of the family and is the most widely expressed. It has been shown to have roles in an array of cellular processes, such as regulation of Ca^{2+}- (N and P/Q type) and K^{+} (Kv4)-channels [5-8], phosphodiesterase activity [9], membrane trafficking [10], and the direct regulation of the dopamine D2 receptor and the GRK2 kinase [11]. A connection between defective NCS-1 and neurodegenerative disorders like schizophrenia, autism and bipolar disorder has also been suggested [11-15]. It was observed that in comparison to healthy individuals, patients suffering from schizophrenia had upregulated levels of NCS-1 in the prefrontal cortex, which may explain their reduced prefrontal cortex activity [11, 15]. Also, NCS-1 has been attributed to the regulation of synaptic activity as it directly interacts with D2 receptors and it is plausible that defective NCS-1 may lead to impairment of cognitive functions and mental retardation [4].

All NCS proteins are composed of ~200 residues organized in a compact and globular structure, have either an N-terminal myristoylation or palmitoylation site [4, 5, 16, 17], and bind calcium through EF-hand motifs. NCS-1 is an all-helical 190 residue protein organized in two ~100 a.a. domains, each containing a pair of EF-hands; the N-domain EF1 and EF2, and the C-domain EF3 and EF4 (Figure 1A) [18]. Due to a conserved Cys/Pro substitution in EF1, NCS-1 is only capable of binding three calcium ions [19, 20], a trait of all NCS family members except for recoverin and KChIP1 who have only two active EF-hands [21, 22]. In NCS-1, EF2 and EF3 are structural sites as they can bind to both Ca^{2+} and Mg^{2+}, whereas EF4 is a regulatory site only binding Ca^{2+} and with lower affinity [19]. A few recent high-resolution structures are

available for NCS-1, which all show excellent agreement regarding the general tertiary structure, the relative orientation of the two domains, and the locations of α-helices [18, 23-25]. An NMR study on NCS-1 suggested that independent movements of the N- and C-domains can occur, which may help accommodating different ligands in the binding pocket, and that the last 15 residues of the protein are disordered yet crucial for conformational stability, undergoing conformational exchange that may regulate ligand binding [18]. The equilibrium unfolding of NCS-1 has been well studied using guanidinium chloride (GdmCl) denaturation and shows that the protein unfolds through two separate unfolding transitions, corresponding to the sequential unfolding of the N- (unfolding at 3.1 M GdmCl with ΔG ~35 KJ mol^{-1}) and C-domain (unfolding at 4.6 M GdmCl with ΔG ~38 KJ mol^{-1}) [18, 19]. While the structure, thermodynamics, and biological functions of NCS-1 have been elucidated in detail with different techniques, the folding and misfolding mechanisms of this protein have long remained elusive. This information gap has recently been bridged by single-molecule optical tweezers studies.

3.1.2 A single molecule perspective on protein folding using direct mechanical manipulation

Protein folding, especially in the case of large multi-domain proteins, is a complex process encompassing many concerted events such as breaking of non-native contacts, formation of native interactions and changes in conformation and dynamics [26-28]. In large multi-domain proteins different domains can fold and unfold via different pathways either independently or dependently and intermediate states can be populated on the way to a native conformation. Their folding and unfolding processes are also dependent on the crosstalk between the domains and on internal friction, brought about by a frustrated search for inter-domain contacts between partially formed domains. Traditional methods such as X-ray crystallography, NMR and optical spectroscopies have been extraordinarily powerful to decipher the structure and folding characteristics of proteins. However, the ensemble nature of the signal provided by such techniques can blur the diversity of folding trajectories and short lived populations, making it difficult to gauge the complicated sequence of events that characterize the folding mechanism of proteins and other biomolecules.

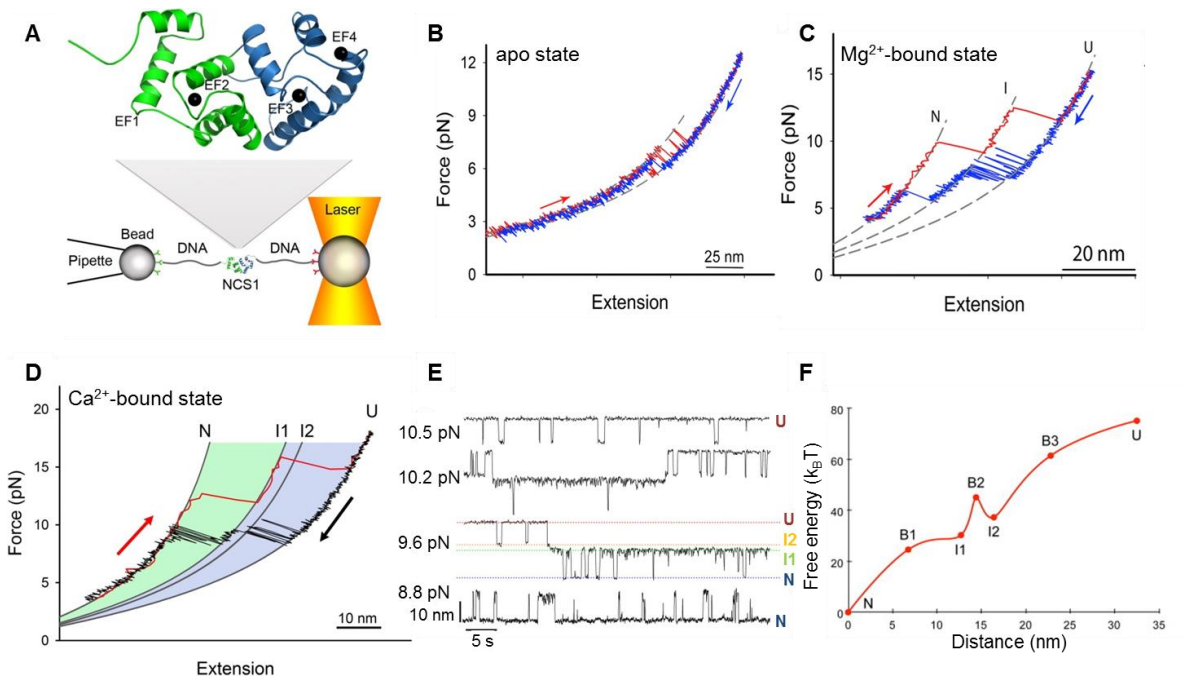

Figure 1: Mechanical manipulation of a single non-myristoylated NCS-1 molecule. A) Schematic representation of the optical tweezers setup. A NCS-1 molecule is tethered to two polystyrene beads by means of molecular handles (~ 500 bp DNA molecules) that function as spacers to avoid unspecific interaction between the tethering surfaces [29]. One bead is held in an optical trap, while the other is held at the end of a pipette by suction. During the experiment the protein is stretched and relaxed by moving the pipette relative to the optical trap, and the applied force and the molecular extension are measured as described in [30]. The inset shows the NMR structure of NCS-1 (PDB code 2LCP), where the C- and N-domains are shown in blue and green, respectively. B) Force vs extension cycle obtained by stretching (red trace) and relaxing (blue trace) NCS-1 in the absence of divalent ions. C) Force vs extension cycle obtained by stretching (red trace) and relaxing (blue trace) NCS-1 in the presence of 10 mM Mg^{2+}. D) Mechanical manipulation of the Ca^{2+}-bound state of NCS-1. During stretching (red trace) the N-domain unfolds at ~ 13 pN and the C-domain at ~ 16 pN. During relaxation (black trace), U folds into N through a four-state process (U > I2 > I1 > N) coordinated by calcium binding. E) Extension vs time traces acquired at different constant forces showing the Ca^{2+}-bound state of NCS-1 fluctuating at equilibrium between N, I1, I2 and U. The population probability of the different states can be modulated by force. Analysis of these experimental data with the Hidden Markov Model allows for the characterization of the energy landscape of the

protein in terms of activation energy barriers, separating the different molecular states, and positions of the transition states along the reaction coordinate [31, 32]. F) Energy landscape of the Ca^{2+}-bound state of NCS-1 at zero force. The transition states of the different folding reactions are indicated with the letter B. The activation barriers separating the different molecular states were calculated using a pre-exponential factor of 1.2×10^{-4} Hz [33]. Panels adapted from [34, 35].

Single molecule force spectroscopy using optical tweezers enables direct mechanical manipulation of individual molecules and the detailed characterization of their conformational equilibria under tension [29, 36-42]. In these experiments, a single molecule is tethered between two polystyrene beads using DNA molecular handles and then is stretched and relaxed by changing the distance between the tethering surfaces (Figure 1A) [43]. Under tension, the unfolding and refolding of a protein is accompanied by changes in the extension of the molecule, giving rise to discontinuities (rips) in the recorded force traces. A molecule can be stretched and relaxed at constant speed [44, 45], or it can be kept at a specific force through a force feedback mechanism and observed to fluctuate between different molecular conformations [35]. A careful analysis of the experimental data and the use of advanced statistical methods allow a detailed characterization of the folding and, possibly, misfolding processes of the molecule and the reconstruction of its energy landscape [46]. An important limitation of optical tweezers to keep in mind is that they describe three-dimensional molecular processes, such as the folding of a protein, along a single reaction coordinate defined by the points of force application, namely the residues to which the DNA handles are attached. As a consequence, during the mechanical manipulation of a molecule, all structural variations that do not produce measurable changes of the molecular extension along the pulling axis are not detected, and hence the energy landscape emerging from these studies is necessarily one-dimensional [47]. However, to circumvent this limitation an increasing number of solutions are emerging. For example, the attachment points of the DNA handles on the protein surface can be changed at will to pull the molecule along various reaction coordinates and assess different regions of its energy landscape [44, 48]. Alternatively, novel instrumentation designs with multiple optical traps can be employed that allow application of force along different pulling axes simultaneously, [49]. Otherwise, it is nowadays possible to use hybrid systems combining optical tweezers with single molecule Förster Resonance Energy Transfer (FRET) where the

additional possibility of monitoring the distance between two or more residues suitably marked with fluorophores allows a multidimensional description of the molecular process under study [50, 51].

3.2 Simple folding mechanism under resting conditions

The cellular environment contains a vast amount of different ions and most EF-hand proteins can bind other divalent ions besides calcium, most prominently Mg^{2+}, which is kept relatively constant at ~5 mM in cells [20, 52]. The Mg^{2+}-bound state of EF hand proteins has many specific roles besides modulating Ca^{2+} binding and its properties are therefore of high interest [19, 53-55]. In the case of NCS-1, the Mg^{2+}-bound state seems to be the primary interacting conformation for many of its targets, such as the dopamine receptor D2 and P14Kb [9, 11] existing in equilibria with the apo and Ca^{2+}-bound states. Elucidating the conformational dynamics of all these states [3] will help us understand better the molecular mechanisms mediating the biological functions of NCS-1.

At resting conditions in the cell, the two dominant forms of NCS-1 are the apo and Mg^{2+}-bound states. In a recent publication,Naqvi et al. used optical tweezers to characterize at the single molecule level the conformational equilibria of these states for the non-myristoylated form of NCS-1 [34]. When they stretched and relaxed individual NCS-1 molecules in the absence of any divalent ions, they obtained force vs extension traces characterized by reversible two-state fluctuations around 6.5 pN that originate from the folding and unfolding of the C-domain (Figure 1B). In fact, the N-domain of the apo form of NCS-1, as shown using deletion variants [34], is unstructured or loosely folded, and under tension it does not give rise to detectable transitions in the recorded traces. In contrast, under the same experimental conditions the C-domain is collapsed in a folded conformation that under tension displays a behaviour that resembles that of molecular structures mainly stabilized by secondary interactions and weak tertiary contacts [29, 56]. Indeed, these data are also consistent with previous NMR studies showing little tertiary contacts in the apo form of NCS-1, and lack of stable globular structure [19, 57].

In the presence of 10 mM Mg^{2+} the behaviour of NCS-1 changes drastically. Both the N- and C-domain acquire compact and mechanically resistant conformations that under tension loose and gain structure as separate units, through fully cooperative and sequential two-state transitions (Figure 1C) [34]. The C-domain is mechanically more resistant than the N-domain and unfolds at higher forces mirroring the observation from equilibrium chemical denaturation experiments [18, 19]. After full mechanical denaturation of the protein and during relaxation of the applied force, the C-domain of NCS-1 is the first to fold, followed by the N-domain folding at lower forces. These sequential folding events are coordinated by Mg^{2+} binding to EF3 and EF2, respectively. The Mg^{2+}-state of NCS-1 thus folds into its native state through a three-state process involving an intermediate state comprising a folded C-domain and an unstructured N-domain with ion occupancy only in EF3. The dimensions of the observed rips in the force vs extension traces reveal more structuring of NCS-1 upon Mg^{2+} binding than previously suggested by NMR studies [19], although the dynamical nature of the folded state is not revealed from the single molecule data.

3.3 Increasing folding complexity under calcium activating conditions

In the presence of activating concentrations of calcium the folding process of non-myristoylated NCS-1 gets considerably more complex [58]. Under these experimental conditions, unfolded NCS-1 molecules fold back into their native states through a strict sequence of events coordinated by calcium binding (Figure 1D). Ca^{2+} first binds to EF3, triggering the collapse of the polypeptide chain (U state) into an on-pathway intermediate state I1; then EF4 binds a calcium ion, to induce the full folding of the C-domain (intermediate state I2). The last calcium ion finally binds to EF2 to fold the N-domain and thus the entire protein reaches its native state (N state). In this folding process, the C-domain always folds first and acts as "internal chaperone" for the correct folding of the N-domain. If the C-domain does not reach its native state, as in the knockout mutant $NCS1^{EF4}$, the N-domain fails to fold correctly. This asymmetrical folding process that always starts with the folding of the C-domain probably reflects the asymmetrical structure of the protein, as further discussed below.

Each folding transition of NCS-1 is associated with a different structural change and energy cost. By monitoring in real time individual NCS-1 molecules fluctuating between

different molecular conformations in constant force experiments, Heidarsson et al. were able to characterize the kinetics and thermodynamics of the folding reactions of non-myristoylated NCS-1 and reconstruct the salient features of its energy landscape (Figure 1E,F) [35]. The results of these studies show how the folding transitions from U to I2 and from I1 to N are associated with large changes in molecular extensions but, at the same time, they are downhill reactions with no activation energy barriers. On the other hand, the transition from the intermediate state I2 to the intermediate state I1, which leads to the complete folding of the C-domain, involves a small compaction of the protein but is a barrier-limited reaction. Thus, folding of the C-domain into its native structure upon calcium binding to EF4 is the rate-limiting step of the entire folding process of NCS-1 at activating concentration of Ca^{2+}. Interestingly, this step is affected by calcium concentration, which can open access to alternative and off-pathway folding trajectories.

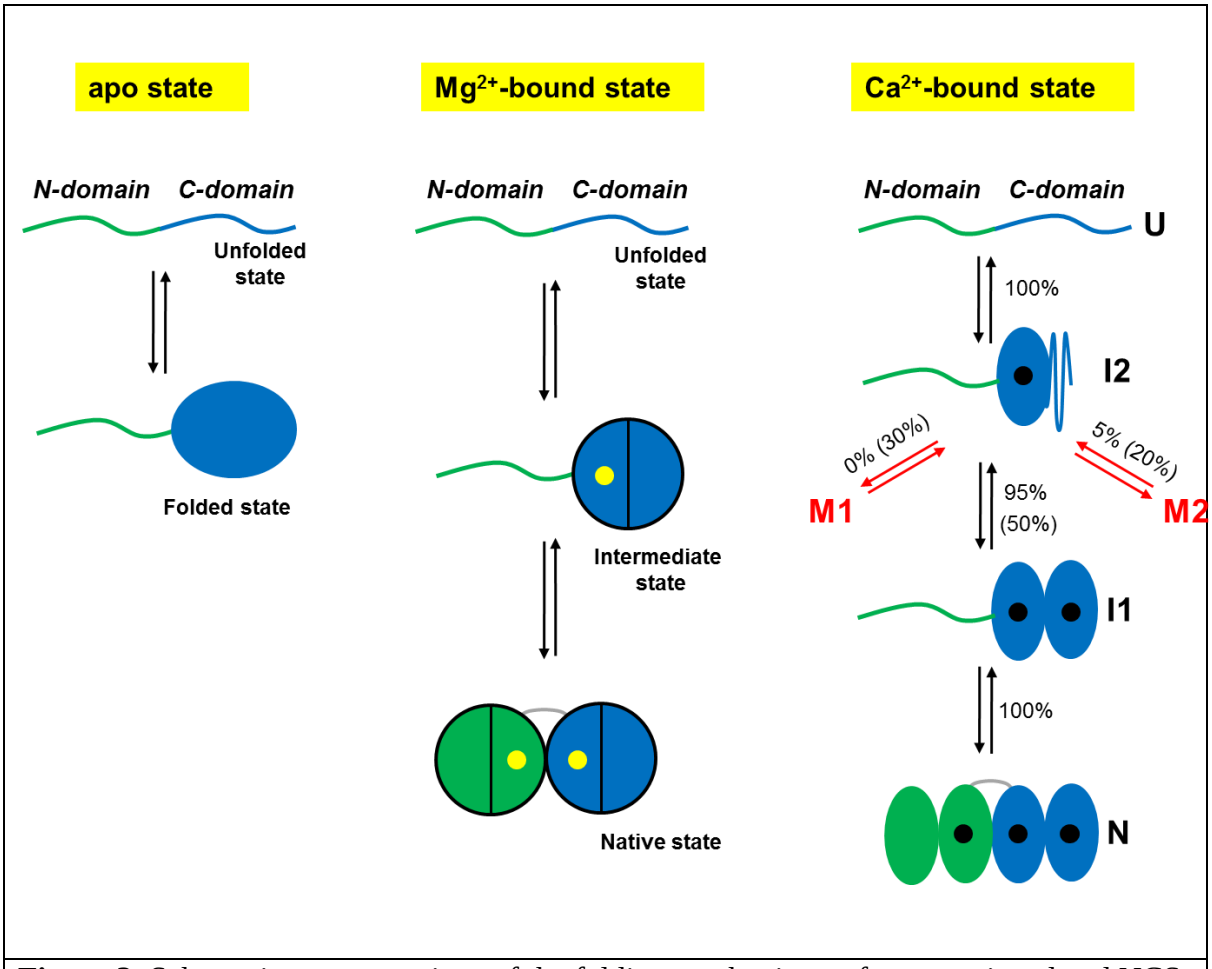

Figure 2: Schematic representations of the folding mechanisms of non-myristoylated NCS-1 in different ionic conditions. In the absence of divalent ions, the C-domain fluctuates between a folded and an unfolded state, while the N-domain remains unstructured or loosely

folded. In the presence of Mg^{2+} (yellow dots), the divalent ions binds first to EF3, triggering the folding of the C-domain, and then to EF2 making the NCS-1 transit into its native state. Only two of the three active EF-hands can bind Mg^{2+}. Under activating Ca^{2+} concentrations, NCS-1 folds into its native state through a four-state process involving the population of the intermediate states I1 and I2. First NCS-1 transits into I2 and then into I1 as Ca^{2+} (black dots) binds to EF3 and EF4, respectively. Finally Ca^{2+} binds to EF2 and the protein reaches N. At high calcium concentration (10 mM), only 1 molecule out of 2 follows this native folding pathway. 50% of the molecules folds into I2 and then takes non-productive pathways leading to misfolded conformations (M1 and M2). In contrast, at physiological calcium concentrations (0,5 uM), only 5% of the molecules misfold. Panels adapted from [34, 58].

3.4 Pathologically high calcium concentrations open access to misfolding pathways

Once an unfolded NCS-1 molecule has collapsed into the on-pathway intermediate state I2, it can either transit into I1 to eventually reach the native state, or take alternative pathways that lead to misfolded states [58]. The probability that the protein takes one pathway or the other depends on the calcium concentration. At physiologically relevant calcium concentration (0.5 μM) only 5% of the NCS-1 molecules misfold, but as the $[Ca^{2+}]$ increase, so does the misfolded population and at $[Ca^{2+}]$ of 10 mM one molecule out of two populates a pathway that leads to non-native structures. Two main misfolded states (M1 and M2) are populated by NCS-1, differing in extension and occupancy probability, with M1 being significantly populated only at high $[Ca^{2+}]$. Figure 2 summarizes the folding and misfolding pathways of NCS-1 under different environmental conditions. Strikingly, misfolding reactions were observed only with wild-type NCS-1. Variants carrying disabled ion-binding sites never populate M1 or M2. These intriguing results suggest that the misfolding reactions observed in [58], stem from specific interactions that take place between properly folded EF hands. Inter-domain crosstalk thus plays a crucial role for the folding and misfolding of NCS-1, determining the final fate of the protein.

3.5 Comparison to the folding network of calmodulin

The folding and misfolding mechanisms of the other NCS family members and of other EF hand calcium binding proteins are still largely uncharacterized and the question remains: is it likely that the same principles of folding and misfolding can be inferred for these similar proteins? Other related proteins have been studied with regards to folding and stability using ensemble methods with varying degrees of details [59, 60]. However, to the best of our knowledge, the only EF hand protein whose conformational equilibria have been characterized in great detail at the single molecule level with optical tweezers is calmodulin (CaM), [46, 61], allowing for a direct comparison with NCS-1.The archetypical calcium binding protein calmodulin is characterized by a symmetrical structure with two almost identical domains, each binding two calcium ions, separated by a long and flexible α helix [62]. The comparison between the folding network of NCS-1 and that of CaM indeed reveals many differences yet some similarities. The folding process of NCS-1 always starts with the U to I2 transition, indicating that only a single pathway is available on its energy landscape to initiate its journey to the native state. In contrast, unfolded CaM can initiate its folding process following three distinct pathways; one leading to an off-pathway intermediate (F_{23}) with the EF hands 2 and 3 mispaired (16% probability), and the other two leading to either the on-pathway intermediate F_{12} (42% probability) or the on-pathway intermediate F_{34} (42 % probability), with either the N- or the C-domain, respectively, fully folded. The folding process of CaM can thus start with equal probability from the N- or the C-domain, while that of NCS-1 always start from the C-domain and always through the same U to I2 transition. For CaM, F_{12} and F_{34} can then both transit into the native state, although with different probabilities as in 50% of the cases F_{12} takes a misfolding pathway leading to the off-pathway intermediate state F_{123}, where EF3 is collapsed onto the folded N-domain in a non-native conformation. The native state of CaM can thus be reached from two distinct intermediate states through two different folding pathways, unlike the native state of NCS-1 that can be accessed only from I1. Moreover, the native unidimensional folding process of NCS-1 is characterized by a bottleneck where the protein can either proceed towards its native state by overcoming the large activation barrier separating I2 from I1 or take misfolding pathways in a calcium dependent manner. No bottleneck characterizes the folding network of CaM where the interconversions between the different molecular states are controlled by similar activation barriers. In addition, despite CaM folding

rates and folding mechanism having been shown to be highly dependent on calcium concentration [61], the population of CaM misfolding states have not yet been demonstrated to display such calcium dependence.

Where do the differences in the folding networks of CaM and NCS-1 originate from? The answer may lie in inter-domain interactions and the coupling free energies that are more developed in NCS-1. Proteins such as CaM have a flexible linker connecting their two domains, allowing a high degree of conformational variation between them and at the same time imposes separation of their folding funnels [52, 63]. For NCS-1, instead, a very short U-shaped linker of four residues [24] considerably limits the orientations of the two domains to face-to-face conformations, and the inter-domain interaction involves evolutionarily conserved residues pointing to a functional relevance of this interface. Additionally, NCS-1 is an asymmetrical protein as its N-domain has one active and one inactive EF hand, resulting in it being thermodynamically less stable than the C-domain [18], very unlike CaM where all EF-hands are active with similar calcium binding affinities [64]. Moreover, NCS-1 carries a C-terminal tail that has an N-domain stabilizing effect [18] and this effect may only become functional, once the C-domain is folded. Thus, the sequential folding observed for NCS-1 could be the result of its intricate structural features and its biological function as a sensor. More studies on related NCS proteins will undoubtedly help clarify these issues. Nevertheless, given the complex folding networks of CaM and NCS-1, and the frequent occurrence of misfolded states in multi-domain proteins [27, 65, 66] we predict that misfolding is likely to occur in similar calcium binding proteins.

3.6 Conclusions and Future perspectives

We have outlined how the Ca^{2+}-bound, Mg^{2+}-bound and apo forms of the non-myristoylated NCS-1 have been investigated at the single molecule level using optical tweezers. We have illustrated the rugged and multistate energy landscape arising from these studies, which underlays the calcium-dependent folding and misfolding trajectories of NCS-1. We have also discussed the importance that the conformational sensitivity of NCS-1 might have for its calcium sensing actions. Finally, we have made comparison to the very similar calcium binding EF hand protein CaM and have highlighted differences and similarities between the folding networks of the two proteins, which are likely to have arisen due to their different structural and functional features across the domains.

For NCS-1, the calcium-dependent modulation of misfolding pathways is highly interesting and suggests an important link between the conformational space, calcium dysregulation, and neurodegeneration. Interestingly, sustained elevated levels of free Ca^{2+} have been associated with aging cells and linked to the development of major neurological diseases such as bipolar disorder and Alzheimer's [67, 68]. In some neurological diseases, such as bipolar disorder and schizophrenia, NCS-1 is up-regulated in the pre-frontal cortex of patients [15]. A compelling hypothesis would be that the upregulation is a response to a loss of protein function caused by calcium-induced misfolding. Studies in cell, focusing directly on the calcium effects on NCS-1 expression levels might reveal whether there indeed is a specific phenotype associated with NCS-1 misfolding, and potentially also of other members of the family.

The behaviour of NCS-1 outlined in this review may also help rationalize how NCS-1 is able to have such promiscuous interactions with over 20 reported binding partners [4] despite a highly folded and globular structure. A certain degree of flexibility must thus be required to accommodate this list of diverse ligands such as dopamine receptors, various ion-channels, glial cell line-derived neurotrophic factor as well as membranes and their constituents. The many conformational states that were uncovered in the papers discussed above may reflect a significant flexibility of NCS-1, which is needed for it to act as a molecular hub [34, 35, 58]. These properties may be even further expanded including its N-terminal myristoylation, which leads to localisation and broader range of interactors. How this lipidic modification changes the molecular landscape of NCS-1 remains to be addressed in detail. The single molecule approach provided by optical tweezers can potentially be used to probe the interaction of NCS-1 with different ligands as well as its modulation by posttranslational modification, and help uncover the connection between conformational states, ligand recognition and disease states. Indeed, the two EF hand proteins for which detailed insight into their single-molecule folding networks exist [46, 58] have revealed that single-molecule approaches are key to their studies and enable the extraction of important insight into structures as well as function and dysfunction.

3.7 References

1. Weiss, J.L., H. Hui, and R.D. Burgoyne, *Neuronal calcium sensor-1 regulation of calcium channels, secretion, and neuronal outgrowth.* Cellular and molecular neurobiology, 2010. **30**(8): p. 1283-1292.
2. Reyes-Bermudez, A., D.J. Miller, and S. Sprungala, *The Neuronal Calcium Sensor Protein Acrocalcin: A Potential Target of Calmodulin Regulation during Development in the Coral Acropora millepora.* Plos One, 2012. **7**(12): p. 8.
3. Burgoyne, R.D. and L.P. Haynes, *Understanding the physiological roles of the neuronal calcium sensor proteins.* Molecular brain, 2012. **5**(1): p. 2.
4. Burgoyne, R.D., *Neuronal calcium sensor proteins: generating diversity in neuronal Ca 2+ signalling.* Nature Reviews Neuroscience, 2007. **8**(3): p. 182.
5. Tsujimoto, T., et al., *Neuronal calcium sensor 1 and activity-dependent facilitation of P/Q-type calcium currents at presynaptic nerve terminals.* Science, 2002. **295**(5563): p. 2276-2279.
6. Weiss, J.L., D.A. Archer, and R.D. Burgoyne, *Neuronal Ca2+ sensor-1/frequenin functions in an autocrine pathway regulating Ca2+ channels in bovine adrenal chromaffin cells.* Journal of Biological Chemistry, 2000. **275**(51): p. 40082-40087.
7. Nakamura, T.Y., et al., *A role for frequenin, a Ca2+-binding protein, as a regulator of Kv4 K+-currents.* Proceedings of the National Academy of Sciences, 2001. **98**(22): p. 12808-12813.
8. Guo, W., et al., *Modulation of Kv4-encoded K+ currents in the mammalian myocardium by neuronal calcium sensor-1.* Journal of Biological Chemistry, 2002. **277**(29): p. 26436-26443.
9. Burgoyne, R.D., et al., *Neuronal Ca2+-sensor proteins: multitalented regulators of neuronal function.* Trends in neurosciences, 2004. **27**(4): p. 203-209.
10. McFerran, B.W., J.L. Weiss, and R.D. Burgoyne, *Neuronal Ca2+ sensor 1 - Characterization of the myristoylated protein, its cellular effects in permeabilized adrenal chromaffin cells, Ca2+-independent membrane association, and interaction with binding proteins, suggesting a role in rapid Ca2+ signal transduction.* Journal of Biological Chemistry, 1999. **274**(42): p. 30258-30265.

11. Kabbani, N., et al., *Interaction with neuronal calcium sensor NCS-1 mediates desensitization of the D2 dopamine receptor.* Journal of Neuroscience, 2002. **22**(19): p. 8476-8486.
12. Handley, M.T.W., et al., *Structural and Functional Deficits in a Neuronal Calcium Sensor-1 Mutant Identified in a Case of Autistic Spectrum Disorder.* Plos One, 2010. **5**(5): p. 14.
13. Pavlowsky, A., et al., *A postsynaptic signaling pathway that may account for the cognitive defect due to IL1RAPL1 mutation.* Current Biology, 2010. **20**(2): p. 103-115.
14. Bai, J., et al., *Abnormalities in the dopamine system in schizophrenia may lie in altered levels of dopamine receptor-interacting proteins.* Biological psychiatry, 2004. **56**(6): p. 427-440.
15. Koh, P.O., et al., *Up-regulation of neuronal calcium sensor-1 (NCS-1) in the prefrontal cortex of schizophrenic and bipolar patients.* Proceedings of the National Academy of Sciences, 2003. **100**(1): p. 313-317.
16. Pongs, O., et al., *FREQUENIN - A NOVEL CALCIUM-BINDING PROTEIN THAT MODULATES SYNAPTIC EFFICACY IN THE DROSOPHILA NERVOUS-SYSTEM.* Neuron, 1993. **11**(1): p. 15-28.
17. Rivosecchi, R., et al., *IMPLICATION OF FREQUENIN IN THE FACILITATION OF TRANSMITTER RELEASE IN DROSOPHILA.* Journal of Physiology-London, 1994. **474**(2): p. 223-232.
18. Heidarsson, P.O., et al., *The C-terminal tail of human neuronal calcium sensor 1 regulates the conformational stability of the Ca2+-activated state.* Journal of molecular biology, 2012. **417**(1-2): p. 51-64.
19. Aravind, P., et al., *Regulatory and structural EF-hand motifs of neuronal calcium sensor-1: Mg2+ modulates Ca2+ binding, Ca2+-induced conformational changes, and equilibrium unfolding transitions.* Journal of molecular biology, 2008. **376**(4): p. 1100-1115.
20. Grabarek, Z., *Insights into modulation of calcium signaling by magnesium in calmodulin, troponin C and related EF-hand proteins.* Biochimica et Biophysica Acta (BBA)-Molecular Cell Research, 2011. **1813**(5): p. 913-921.
21. Zhou, W., et al., *Structural insights into the functional interaction of KChIP1 with Shal-type K+ channels.* Neuron, 2004. **41**(4): p. 573-586.
22. Scannevin, R.H., et al., *Two N-terminal domains of Kv4 K+ channels regulate binding to and modulation by KChIP1.* Neuron, 2004. **41**(4): p. 587-598.

23. Bourne, Y., et al., *Immunocytochemical localization and crystal structure of human frequenin (neuronal calcium sensor 1).* Journal of Biological Chemistry, 2001. **276**(15): p. 11949-11955.
24. Ames, J.B., et al., *Structure and calcium-binding properties of Frq1, a novel calcium sensor in the yeast Saccharomyces cerevisiae.* Biochemistry, 2000. **39**(40): p. 12149-12161.
25. Strahl, T., et al., *Structural insights into activation of phosphatidylinositol 4-kinase (Pik1) by yeast frequenin (Frq1).* Journal of Biological Chemistry, 2007. **282**(42): p. 30949-30959.
26. Batey, S., A.A. Nickson, and J. Clarke, *Studying the folding of multidomain proteins.* HFSP journal, 2008. **2**(6): p. 365-377.
27. Borgia, A., et al., *Transient misfolding dominates multidomain protein folding.* Nature Communications, 2015. **6**: p. 10.
28. Jahn, M., et al., *Folding and assembly of the large molecular machine Hsp90 studied in single-molecule experiments.* Proceedings of the National Academy of Sciences, 2016. **113**(5): p. 1232-1237.
29. Cecconi, C., et al., *Direct observation of the three-state folding of a single protein molecule.* Science, 2005. **309**(5743): p. 2057-2060.
30. Smith, S.B., Y.J. Cui, and C. Bustamante, *Optical-trap force transducer that operates by direct measurement of light momentum*, in *Biophotonics, Pt B*, G. Marriott and I. Parker, Editors. 2003, Elsevier Academic Press Inc: San Diego. p. 134-162.
31. Rabiner, L.R., *A tutorial on hidden markov-models and selected applications in speech recognition.* Proceedings of the IEEE, 1989. **77**(2): p. 257-286.
32. Chodera, J.D., et al., *Bayesian hidden Markov model analysis of single-molecule force spectroscopy: Characterizing kinetics under measurement uncertainty.* arXiv preprint arXiv:1108.1430, 2011.
33. Gebhardt, J.C.M., T. Bornschlogla, and M. Rief, *Full distance-resolved folding energy landscape of one single protein molecule.* Proceedings of the National Academy of Sciences of the United States of America, 2010. **107**(5): p. 2013-2018.
34. Naqvi, M.M., et al., *Single-molecule folding mechanisms of the apo-and Mg2+-bound states of human neuronal calcium sensor-1.* Biophysical journal, 2015. **109**(1): p. 113-123.
35. Heidarsson, P.O., et al., *Single-molecule folding mechanism of an EF-hand neuronal calcium sensor.* Structure, 2013. **21**(10): p. 1812-1821.

36. Shank, E.A., et al., *The folding cooperativity of a protein is controlled by its chain topology.* Nature, 2010. **465**(7298): p. 637.
37. Alemany, A., et al., *Mechanical folding and unfolding of protein barnase at the single-molecule level.* Biophysical journal, 2016. **110**(1): p. 63-74.
38. Yu, H., et al., *Direct observation of multiple misfolding pathways in a single prion protein molecule.* Proceedings of the National Academy of Sciences, 2012. **109**(14): p. 5283-5288.
39. Jahn, M., et al., *Folding and Domain Interactions of Three Orthologs of Hsp90 Studied by Single-Molecule Force Spectroscopy.* Structure, 2018. **26**(1): p. 96-+.
40. Zhang, Y., *Energetics, kinetics, and pathway of SNARE folding and assembly revealed by optical tweezers.* Protein Science, 2017. **26**(7): p. 1252-1265.
41. Xu, A.J. and T.A. Springer, *Mechanisms by which von Willebrand disease mutations destabilize the A2 domain.* Journal of Biological Chemistry, 2013. **288**(9): p. 6317-6324.
42. Wruck, F., et al., *Protein folding mediated by trigger factor and Hsp70: new insights from Single-Molecule approaches.* Journal of molecular biology, 2018. **430**(4): p. 438-449.
43. Heidarsson, P.O., et al., *Conformational dynamics of single protein molecules studied by direct mechanical manipulation.* Advances in protein chemistry and structural biology, 2013. **92**: p. 93-133.
44. Heidarsson, P.t.O., et al., *A highly compliant protein native state with a spontaneous-like mechanical unfolding pathway.* Journal of the American Chemical Society, 2012. **134**(41): p. 17068-17075.
45. Caldarini, M., et al., *The complex folding behavior of HIV-1-protease monomer revealed by optical-tweezer single-molecule experiments and molecular dynamics simulations.* Biophysical Chemistry, 2014. **195**: p. 32-42.
46. Stigler, J., et al., *The complex folding network of single calmodulin molecules.* Science, 2011. **334**(6055): p. 512-516.
47. Avdoshenko, S.M. and D.E. Makarov, *Reaction Coordinates and Pathways of Mechanochemical Transformations.* Journal of Physical Chemistry B, 2016. **120**(8): p. 1537-1545.
48. Elms, P.J., et al., *The molten globule state is unusually deformable under mechanical force.* Proceedings of the National Academy of Sciences of the United States of America, 2012. **109**(10): p. 3796-3801.

49. Dame, R.T., M.C. Noom, and G.J.L. Wuite, *Bacterial chromatin organization by H-NS protein unravelled using dual DNA manipulation.* Nature, 2006. **444**(7117): p. 387-390.
50. Sirinakis, G., et al., *Combined versatile high-resolution optical tweezers and single-molecule fluorescence microscopy.* Review of Scientific Instruments, 2012. **83**(9): p. 9.
51. Lee, S. and S. Hohng, *An Optical Trap Combined with Three-Color FRET.* Journal of the American Chemical Society, 2013. **135**(49): p. 18260-18263.
52. Gifford, J.L., M.P. Walsh, and H.J. Vogel, *Structures and metal-ion-binding properties of the Ca2+-binding helix–loop–helix EF-hand motifs.* Biochemical Journal, 2007. **405**(2): p. 199-221.
53. Zot, H. and J. Potter, *A structural role for the Ca2+-Mg2+ sites on troponin C in the regulation of muscle contraction. Preparation and properties of troponin C depleted myofibrils.* Journal of Biological Chemistry, 1982. **257**(13): p. 7678-7683.
54. Peshenko, I.V. and A.M. Dizhoor, *Ca2+ and Mg2+ binding properties of GCAP-1 evidence that Mg2+-bound form is the physiological activator of photoreceptor guanylyl cyclase.* Journal of Biological Chemistry, 2006. **281**(33): p. 23830-23841.
55. Wingard, J.N., et al., *Structural analysis of Mg2+ and Ca2+ binding to calcium-binding protein 1 (CaBP1), a neuron-specific regulator of calcium channels.* Journal of Biological Chemistry, 2005. **280**(45): p. 37461-37470.
56. Elms, P.J., et al., *The molten globule state is unusually deformable under mechanical force.* Proceedings of the National Academy of Sciences, 2012. **109**(10): p. 3796-3801.
57. Cox, J.A., et al., *Cation binding and conformational changes in VILIP and NCS-1, two neuron-specific calcium-binding proteins.* Journal of Biological Chemistry, 1994. **269**(52): p. 32807-32813.
58. Heidarsson, P.O., et al., *Direct single-molecule observation of calcium-dependent misfolding in human neuronal calcium sensor-1.* Proceedings of the National Academy of Sciences, 2014. **111**(36): p. 13069-13074.
59. Yamniuk, A.P., et al., *Domain stability and metal-induced folding of calcium- and integrin-binding protein 1.* Biochemistry, 2007. **46**(24): p. 7088-7098.
60. Suarez, M.C., et al., *Free-Energy Linkage between Folding and Calcium Binding in EF-Hand Proteins.* Biophysical Journal, 2008. **95**(10): p. 4820-4828.
61. Stigler, J. and M. Rief, *Calcium-dependent folding of single calmodulin molecules.* Proceedings of the National Academy of Sciences, 2012. **109**(44): p. 17814-17819.

62. Chattopadhyaya, R., et al., *CALMODULIN STRUCTURE REFINED AT 1.7 ANGSTROM RESOLUTION.* Journal of Molecular Biology, 1992. **228**(4): p. 1177-1192.
63. Kiran, U., et al., *Intermotif Communication Induces Hierarchical Ca2+ Filling of Caldendrin.* Biochemistry, 2017. **56**(19): p. 2467-2476.
64. Masino, L., S.R. Martin, and P.M. Bayley, *Ligand binding and thermodynamic stability of a multidomain protein, calmodulin.* Protein Science, 2000. **9**(8): p. 1519-1529.
65. Borgia, M.B., et al., *Single-molecule fluorescence reveals sequence-specific misfolding in multidomain proteins.* Nature, 2011. **474**(7353): p. 662-U142.
66. Han, J.H., et al., *The folding and evolution of multidomain proteins.* Nature Reviews Molecular Cell Biology, 2007. **8**(4): p. 319-330.
67. Toescu, E.C. and M. Vreugdenhil, *Calcium and normal brain ageing.* Cell calcium, 2010. **47**(2): p. 158-164.
68. Berridge, M.J., *Calcium signalling remodelling and disease.* Biochemical Society Transactions, 2012. **40**: p. 297-309.

Studying heat shock proteins through single-molecule mechanical manipulation

Chapter 4

Studying heat shock proteins through single-molecule mechanical manipulation

Abstract

Imbalances of cellular proteostasis are linked to aging and human diseases, including neurodegenerative and neuromuscular diseases. Heat Shock Proteins (HSPs) and small Heat Shock Proteins (sHSPs) together form a crucial core of the molecular chaperone family that plays a vital role in maintaining cellular proteostasis by shielding client proteins against aggregation and misfolding. sHSP are thought to act as the first line of defence against protein unfolding/misfolding and have been suggested to act as "sponges" that rapidly sequester these aberrant species for further processing, refolding or degradation, with the assistance of the HSP70 chaperone system. Understanding how these chaperones work at the molecular level will offer unprecedented insights for their manipulation as therapeutic avenues for the treatment of aging and human disease. The evolution in single molecule force spectroscopy techniques, such as Optical Tweezers (OT) and Atomic Force Microscopy (AFM), over the last few decades have made it possible to explore at the single molecule level the structural dynamics of HSPs and sHSPs and to examine the key molecular mechanisms underlying their chaperone activities. In this chapter we describe the working principles of OT and AFM and

the experimental strategies used to employ these techniques to study molecular chaperones. We then describe the results of some of the most relevant single-molecule manipulation studies on HSPs and sHSPs and discuss how these findings suggest a more complex physiological role for these chaperones than previously assumed.

4.1 Introduction

The proper folding of proteins is essential for life [1]. However, protein folding into their native state is constantly challenged by several errors that affect the fidelity in the flow of genetic information from DNA to RNA and, finally, to proteins. These errors can take place during DNA replication or transcription, as well as during translation and they result in the synthesis of mutated and/or truncated polypeptides that cannot fold into their native state, and therefore are unstable and prone to aggregation [2]. If not readily detected by the molecular chaperones and destroyed by the degradation systems, such as the ubiquitin proteasome system (UPS) and autophagy, these aberrant polypeptides or fragments of them can impair protein homeostasis (proteostasis). Loss of proteostasis, in turn, leads to cell dysfunction and toxicity and is considered as an important player in aging and diseases, ranging from cancer to neurodegeneration and myopathies [1, 3].

Molecular chaperones such as the heat shock proteins (HSPs) and the degradation systems together constitute the so-called protein quality control (PQC) system. The PQC surveys the cellular proteome and avoids the accumulation of unfolded/misfolded proteins by assisting the refolding of aberrant peptides into the native state or, when this is not possible, by hiding interactive surfaces on protein aggregates and, finally, by promoting the proteasome or autophagy-mediated clearance of aberrant polypeptides; these concerted actions avoid the irreversible aggregation and accumulation of aberrant polypeptides inside the cells [4-7]. Due to its essential functions in the maintenance of the cellular proteome, it is not surprising that defects and imbalances of the PQC, including HSPs, are associated with the development of neurodegenerative diseases; conversely, boosting the activity of chaperones and degradative machineries has proven to be efficient in delaying disease progression in several cellular and animal models of neurodegenerative diseases [1, 8]. Thus, understanding at the molecular level how the PQC works holds promise for the design of therapeutic strategies against aging and neurodegeneration [9].

In this chapter, we will focus our attention on the experimental attempts that have been made in the past decades to understand at the molecular level how HSPs, in particular the small HSPs, avoid protein misfolding and aggregation with the ultimate goal of finding strategies to exploit their chaperone activity for cell health and fitness. We will put emphasis on the principle and application of single-molecule manipulation using optical tweezers and atomic force microscopy for the study of the chaperone activity of HSPs and small HSPs.

4.2 HSPs and small HSPs

HSPs were discovered more than 40 years ago by Dr. Alfred Tissieres [10]. After their identification in *Drosophila melanogaster*, HSPs were found in archaea, bacteria and eukaryotes. The HSPs identified have been classified according to their molecular weight into families: HSP100, HSP90, HSP70, HSP60, HSP40 and small HSPs, the latter characterized by a molecular weight ranging from 15–30 kDa [7, 11, 12]. In the last decades, the combination of several experimental approaches, ranging from *in vitro* studies with recombinant purified HSPs to gene expression profiling, knockdown and overexpression screening in cells and animal models, such as for example *D. melanogaster* and *C. elegans* allowed us to gain a deeper understanding of the mechanisms of action of HSPs and the identification of the cellular processes that are regulated by HSPs. Advanced mass spectrometry studies that revealed the existence of extensive chaperone–client networks in cells, combined with knockdown/knockout studies, were particularly instrumental in gathering information on the biological processes that are modulated by HSPs both in resting cells and following exposure to stress. Thanks to these studies, it became clear that HSPs regulate, directly or indirectly, nearly all aspects of cell biology in a large variety of organisms, from bacterial cells, to yeast and human cells, but also in plants and mammals [6, 7, 13]. This is because HSPs can bind to many different proteins and regulate protein function and activity by facilitating protein folding, the assembly of multiprotein complexes, as well as interaction of ligands with their targets or receptors, such as in the case of HSP90 [13]. In parallel, thanks to the use of nuclear magnetic resonance spectroscopy, Förster resonance energy transfer (FRET), electron microscopy and crystallography, as well as cross-linking experiments followed by mass spectrometric analysis, we gained detailed knowledge on how HSPs work at the molecular level, as well as on how their conformational changes and their binding affinities to specific clients are regulated. For example, these techniques enabled to describe the conformational transitions of the HSP90 cycle and how specific combination of co-chaperones associate with specific HSP90 conformational states [14]; alternatively, they enabled to demonstrate the cooperation between chaperones such as HSP70 and HSP90 and how, at the molecular level this is stabilized by the binding of the substrate, enabling its transfer from one chaperone to another [15]. Cross-linking experiments followed by mass spectrometry analysis shed light on the mechanisms regulating substrate recognition by the small HSPs that, in contrast to higher molecular weight chaperones such as HSP70 and HSP90, are ATP-independent [16, 17].

The fact that small HSP chaperone activity does not require ATP might become extremely important under conditions of energy deprivation and upon stress conditions, when cells need to prioritize use the energy towards cell stress response/adaptation and survival. The term caloristasis has been coined to complement proteostasis and these are considered as two critical components of cellular metabolic homeostasis [18]. Caloristasis, a concept that emphasizes the integrative regulatory interactions needed to understand cellular energy homeostasis, is discussed in more detail in the chapter herein by Tezgin et al. Against this background, the ATP-independent chaperone functions of small HSPs during periods of depleted cellular energy reserves take on even greater significance.

One essential feature of small HSPs is that their monomers associate to form large oligomers with a dimeric substructure; thus, the homodimers formed via the association of the conserved alpha crystallin domain of small HSPs are considered as the building blocks for the assembly of larger oligomers [19]. The oligomers of small HSPs are thought to act as a reservoir of the chaperone power; in fact, it is the dynamic dissociation of small HSPs into monomers and dimers that governs their binding affinities for the substrates, and therefore their chaperone function [19]. The interaction between small HSPs and their substrates involves several binding sites that are located in the conserved alpha crystallin domain but extend to the less conserved N-terminal region [20]. This would explain how different small HSPs may specifically bind to different substrates (reviewed in [19]). Concerning the chaperone activity of small HSPs, the use of relaxation dispersion and high-pressure nuclear magnetic resonance spectroscopy recently contributed to shed light on the enigmatic mechanism of action of small HSPs. These experiments showed that upon dissociation of the oligomers, the monomers are released and undergo partial unfolding of the conserved alpha-crystallin domain interface; this event seems to be critical to enhance the chaperone activity of small HSPs. Although so far this model has been demonstrated for human Hsp27/HSPB1, considering the high degree of conservation of the alpha-crystallin domain interface between the various small HSPs, it is likely that increased disorder in the small HSP monomers represents a general mechanism that increases their chaperone activity [21].

Although the combination of different techniques allowed us to tremendously improve our understanding of the function of chaperones at the molecular level, the finer mechanisms underlying the structural dynamics and the regulatory actions of HSPs and small HSPs are still partly unresolved. This lack of information is mostly due to the inability of traditional ensemble methods to describe in detail phenomena that are intrinsically highly heterogeneous. The structural dynamics and the functions of proteins, such as HSPs and small HSPs, are ultimately

determined by their conformational equilibria. By diffusing on a rugged energy landscape the structure of a protein fluctuates at equilibrium between a large variety of conformations that collectively define its interactome and thus, its functional profile. Some of these conformations are highly populated and thermodynamically stable, others are transient and less probable; others originates when the protein interacts with its own substrate. Regardless of their origin, structural properties and energetics, any of these conformations might play a key role in the functional cycle of a protein and deserves an accurate characterization. Unfortunately, a detailed description of the structural dynamics of a protein with bulk techniques is a daunting task as these methods provide a signal that is the ensemble average of the contributions of a large and often de-phased population of molecules, where the many different conformational transition pathways and transient molecular states are not resolved. The application of single-molecule manipulation methods, such as optical tweezers and atomic force microscopy, to the study of molecular chaperones has recently opened new avenues of research, allowing us to go beyond the ensemble average and uncover information non accessible to more traditional techniques. In these experiments, individual proteins are tethered between movable surfaces and watched fluctuating at equilibrium between different conformations along a well-defined reaction coordinate, namely the molecular end-to-end distance [22-26]. These studies allow a detailed description of the energy landscapes underlying folding and unfolding transitions and an accurate estimate of the kinetics and thermodynamics of these reactions. Providing non averaged information, these single molecule techniques also permit the identification and characterization of less probable molecular species and a detailed description of the role they play in a protein's functional cycle.

In this book chapter we will illustrate the results of single-molecule manipulation studies aimed at elucidating the structural dynamics and the mechanisms of action of different HSPs and sHSPs.

4.3 Structural, Mechanical and Functional Properties of HSPs

The experimental approach typically used in optical tweezers experiments to mechanically manipulate a single protein is depicted in Figure 1A [27]. The protein is connected to two optically trapped beads by means of DNA molecular handles that act as spacers to avoid non-

specific interactions between the tethering surfaces [28-31]. Each DNA molecule is covalently attached to a cysteine residue of the protein at one end and to a bead (typically made of polystyrene or glass) at the other end through biotin/streptavidin or digoxygenine/antibodies interactions. During the experiments, the protein is stretched and relaxed by varying the distance between the beads while recording the applied force, the molecular extension and the time. The applied force, which acts as denaturant in these experiments, can be varied almost linearly with time (constant-speed experiments) [32-34] or it can be kept constant at a pre-set value through a feedback mechanism (force-constant experiments) [35, 36]. In other cases, the distance between the two optical traps is kept constant and the molecule is watched fluctuating between different molecular states at a constant average force (constant-distance measurements) [37, 38]. Under tension, a denaturation or renaturation event is accompanied by an increase or a decrease in the end-to-end distance of the protein; this because unfolded molecular states are more compliant and thus more extended than folded molecular states. These changes in extension generate detectable discontinuities in the recorded traces that allow us to follow the structural changes of a protein.

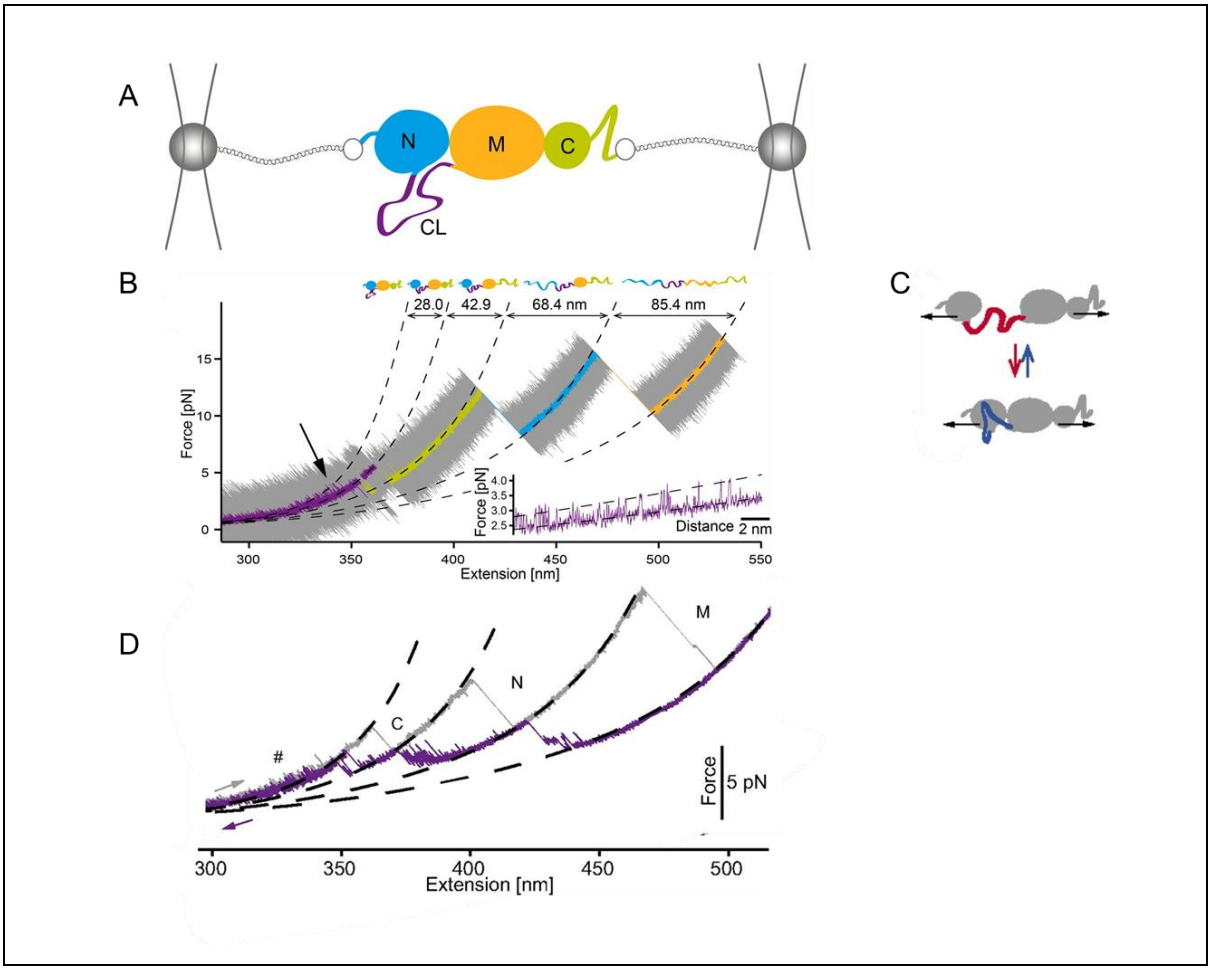

Figure 1: Experimental set-up used to manipulate single Hsp82 monomers with optical tweezers [27, 39, 40]. A) The monomer comprises a N-terminal ATP-binding domain (N, 211 residues), a middle domain (M, 266 residues) responsible for client binding and a C-terminal domain (C, 172 residues) responsible mainly for dimerization. The N- and M-domains are connected to each other by a charged linker (CL), shown in purple. For mechanical manipulation the protein is attached between two glass beads by means of two DNA molecular handles. By varying the position of one of the two traps the force applied on Hsp82 monomer can be varied. B) Stretching trace obtained by pulling on a Hsp82 monomer at constant speed. The original data (20 kHz) were filtered to obtain smooth a trace showing three major transitions (rips) corresponding to the sequential unfolding of the C-, N- and M-domain, respectively. The inset shows fluctuations of Hsp82 monomer at low forces due to hopping of the CL between a compact and an extended conformation, as schematically shown in panel C). D) Stretching (in grey) and relaxation (in purple) cycle acquired by pulling and relaxing a Hsp82 monomer. The relaxation trace shows various fluctuations corresponding to an ensemble of intermediate states. Reprinted with permission from PNAS, [27, 40].

Optical tweezers were employed to decipher structural and dynamic aspects of the chaperone Hsp82 [27, 39], a eukaryote orthologue of HSP90. Hsp82 is a dimer with each monomer comprising three domains (N-, M- and C-domain) connected by linkers (Figure 1A). In particular, the N- and M-domains are connected via a 61-amino acid charged linker (CL) that has so far eluded any structural characterization, suggesting a flexible and disordered conformation for this protein region [41, 42]. When a monomer of Hsp82 is mechanically stretched, it unfolds through three major steps, corresponding to the sequential unfolding of the C-, N- and M-domain respectively (Figure 1B). Interestingly, and importantly, the denaturation of the C domain is preceded at low forces by fluctuations of Hsp82 between two molecular states that differ in length by about 28 nm; this length is very similar to that of CL (purple line and inset in Figure 1B). To better understand the origin of these fluctuations and the role played by CL, mutants were generated in which extended parts of CL were replaced by unstructured glycine-glycine-serine repetitions. No substitution mutants displayed low force fluctuations, suggesting that they originate from reversible folding and unfolding transitions of CL. Performing further experiments with mutants where different protein regions were deleted, the authors showed that indeed CL hops at low forces between a closed and an open conformation, interacting with the N-domain (Figure 1C). When the CL folds, the D domain docks to the N-

domain, and when it opens up, the two domains separate. By analysing the effect of force on the docking-undocking equilibrium, the authors showed that at zero force the molecule spends 75% of the time in the docked state and 25% of the time in the undocked state. What the biological function is of these structural fluctuations at the interface between the N- and C domains is not clear yet; surely, they increase the structural flexibility of the protein and, thus, they might play an important role during the functional cycle of the chaperone.

After its mechanical denaturation, as the applied force is lowered, Hsp82 regains its native structure through a complicated folding process comprising an ensemble of intermediate states (Figure 1D), [40]. One of these partially folded conformations is an on-pathway intermediate state populated by the M-domain, likely corresponding to the so-called smaller alpha/beta/alpha subdomain. All the others are off-pathways (misfolded) intermediate states that both the M- and N-domain populate during their journey to the native state. These misfolding events hinder proper folding, slowing down the productive folding rate constant of Hsp82 by an order of magnitude. The smallest of the three domains instead, the C-domain, folds last through a simple two-state process that involves no detectable intermediate states. These results highlight the complexity of the folding process of a large protein such as Hsp82 and the multitude of conformations that it can populate.

Building on these intriguing results, the folding and unfolding processes of other two HSP90 orthologs, i.e. the bacterial HtpG and the eukaryotic Grp94, were characterized with optical tweezers and compared to Hsp82 [39]. Overall, the structural dynamics of HtpG and Grp94 are similar to that of Hsp82, but some important differences exist. The mechanical denaturation of HtpG and Grp94 also involve three major events corresponding to the sequential unfolding of the C-, N- and M-domain respectively, with similar unfolding forces and changes in contour length to those measured for Hsp82. Similar to Hsp82, during folding these two chaperones populate an ensemble of misfolded states that collectively slow down productive folding. However, some important differences exist in the behaviour of the charged linkers, especially that of Grp94. In fact this linker, unlike that of Hsp82, at zero force does not fluctuate between an open and a closed conformation. Instead, it folds into a compact and thermodynamically stable structure (8.7 k_BT) that under tension unfolds through a distinct transition at ~ 7-8 pN, which immediately precedes the denaturation of the N-domain. Through constant-distance measurements the authors show that at zero force this linker is almost always in its folded state and, thus, the N- and M-domains of Grp94 are always very close to each other with limited rotational freedom. This more rigid N/M domain interface in Grp94 might have functional consequences and might prevent this chaperone from interacting with some

Hsp82 protein clients. Concerning HtpG it should be noticed that its CL is only 7-amino acid long and, so, the conformational freedom of the N- and M-domain of this chaperone is also quite limited compared to that of Hsp82.

In the same vein, Bauer et al investigated the mechanical stability of the Nucleotide Binding Domain (NBD) of the DnaK chaperone from E. coli, a bacterial homologue of human HSP70, in the presence and in the absence of ATP (Figure 2), [43]. The NBD of DnaK is primarily sub-divided into two lobes, termed lobe I and lobe II, connected together by a C-terminal helix. Each lobe is composed of two sub-domains – Ia, Ib for lobe I and IIa, IIb for lobe II. Upon mechanical manipulation and in the absence of ATP, the NBD of DnaK denatures into a completely unfolded polypeptide chain by populating two short lived intermediate states, named Iapo1 and Iapo2 (Figure 2B and C). By selectively varying the lengths of the different subdomains of NBD through loop insertions, the authors showed that the first unfolding event corresponds to the unravelling of the C-terminal helix and the concomitant separation of lobe I from lobe II, leading to Iapo1. As stretching proceeds, the first lobe I unfolds, generating Iapo2, followed by the denaturation of lobe II that completes NBD denaturation. In the presence of ATP, the unfolding pathway of NBD changes dramatically, as lobe II becomes mechanically more stable and the lobe-lobe interactions are stabilized. In fact, under tension, the holo-NBD unfolds by populating three intermediates states that all differ from those observed with the apo-form. The first unfolding event, leading to the intermediate state Iholo1, originates from the unravelling of the C-terminal helix that, in this case, does not induce the concomitant separation of the two lobes, which instead split at higher extensions through a transition that generates the intermediate state Iholo2. As stretching proceeds, firstly lobe II unfolds (leading to Iholo3), and then lobe I unfolds, completing the mechanical denaturation of the protein. Nucleotide binding thus reverses the mechanical hierarchy between the two lobes of NBD, making lobe II the most mechanically resistant. This is not so surprising if we consider that most of the NBD residues interacting with ATP belong to lobe II (13 total) and only a few residues belong to lobe I [44]. Moreover, ATP binding strengthens the interaction between the two domains that in the holo-form remain connected after the denaturation of the C-terminal helix; their splitting requires further pulling. In summary, the results of this study provide unique insights into the structural and energetic changes that nucleotide binding can induce in a heat shock protein and provide hints on how a signal can get transmitted through a protein structure.

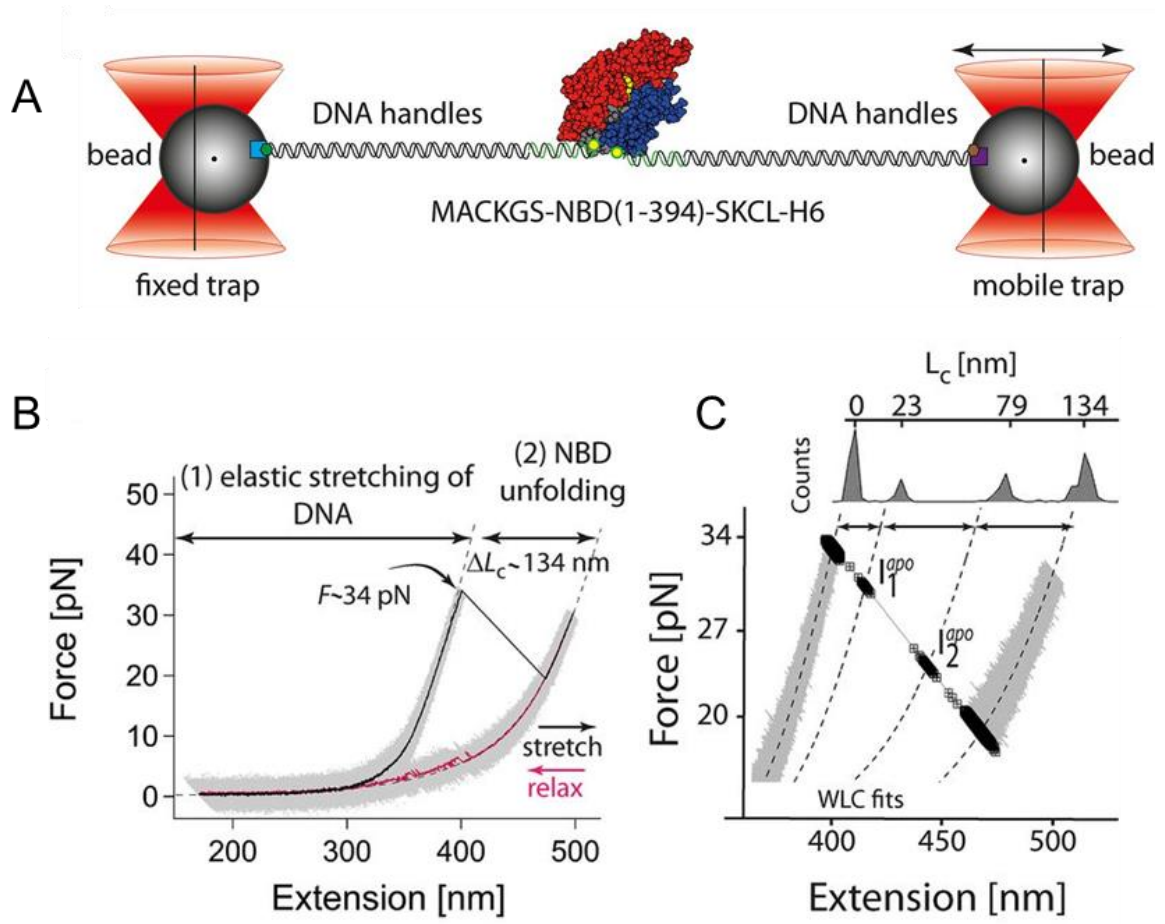

Figure 2: Mechanical manipulation of DnaK NBD in the absence of ATP [43]. As the applied force is increased, the apo form of NBD unfolds at ~ 35 pN, panel B), through a process involving two short lived intermediate states, Iapo1and Iapo2, panel C). Reprinted with permission from PNAS, [43].

In a follow-up study, Bauer and co-authors elucidated the folding mechanism of the NBD of E. coli DnaK [45]. Through single-molecule optical tweezers experiments, the authors show that, upon relaxation of the applied force, a denatured NBD molecule refolds into its native structure through a hierarchical multistep process. This multistep process involves, the sequential folding of subdomain IIb, then of whole lobeII and, eventually, of lobeI. Through a careful analysis of the recorded traces, the authors show that along the NBD folding pathway, the fully folded lobeII represents an obligatory on-pathway intermediate state that acts as an internal chaperone for the folding of lobeI; if lobeII does not reach its native state, lobe I folding

fails. While lobe I cannot fold independently, lobeII can fold into a stable protein even in isolation, displaying nucleotide binding ability and native-like folding behaviour. To better understand the role played by lobeII in the driving of the folding process of E. coli NBD, the authors pulled on the yeast mitochondrial NBD that, unlike its prokaryotic counterpart, does not fold *in vitro* unless it is helped by dedicated chaperones. They showed that replacement of the yeast lobeII with the E. coli lobeII rescues the folding-incompetent yeast NBP, which now can fold effectively even in the absence of chaperones. The results described in [45] clearly show the importance of lobeII for the folding and nucleotide binding of the E. coli NBP and shed light on the molecular basis of the different folding behaviours displayed by the various members of the sugar kinase family.

Optical tweezers assays are also well suited to discern the functional activity of chaperone proteins *in vitro* at the single molecule level. The experimental approach that has so far been adopted for these studies is illustrated in Figure 3. A homotetramer of Maltose Binding Protein from E.coli (4MBP) has been identified as a viable and versatile substrate for these experiments [46-48]; this because MBP has a strong propensity to aggregate *in vitro* and is a client to a wide variety of chaperones, including e.g. SecB, GroEL and the yeast small HSP Hsp42 [46, 49]. The homotetrameric structure mimics a condition of molecular crowding, where neighbouring domains can interact with each other and aggregate into aberrant molecular structures. In these experiments, a single 4MBP is subject to sequential stretching-relaxation cycles, where the force is increased to denature the molecule and then decreased to allow refolding. During refolding the neighbouring MBP domains interact with each other and give rise to aggregates that in the subsequent stretching trace generate transitions of variable size and unfolding forces. Figure 3A shows the first stretching-relaxation cycle for a 4MBP [50]. The stretching trace show discontinuities at 8-9 pN (first blue dot), due to unfolding of mechanically weak helical segments, followed by four unfolding peaks, in a force range between 15 and 30 pN; the latter correspond to the sequential denaturation of the core structure of each MBP domain (subsequent 4 blue dots). This native-like unfolding pattern is visible only in the first stretching trace, as the subsequent stretching traces show non reproducible discontinuities that correspond to the mechanical denaturation of aggregates of variable size and mechanical resistance. Rarely, in ~ 10% of cases, a MBD domain avoids aggregation and folds into its native state giving rise to a native-like unfolding transition in the subsequent stretching trace. The folding and aggregation processes of individual 4MBPs can be studied in the absence or in the presence of a HSP, and the corresponding results can then be compared to decipher the molecular mechanisms underlying the chaperone activity.

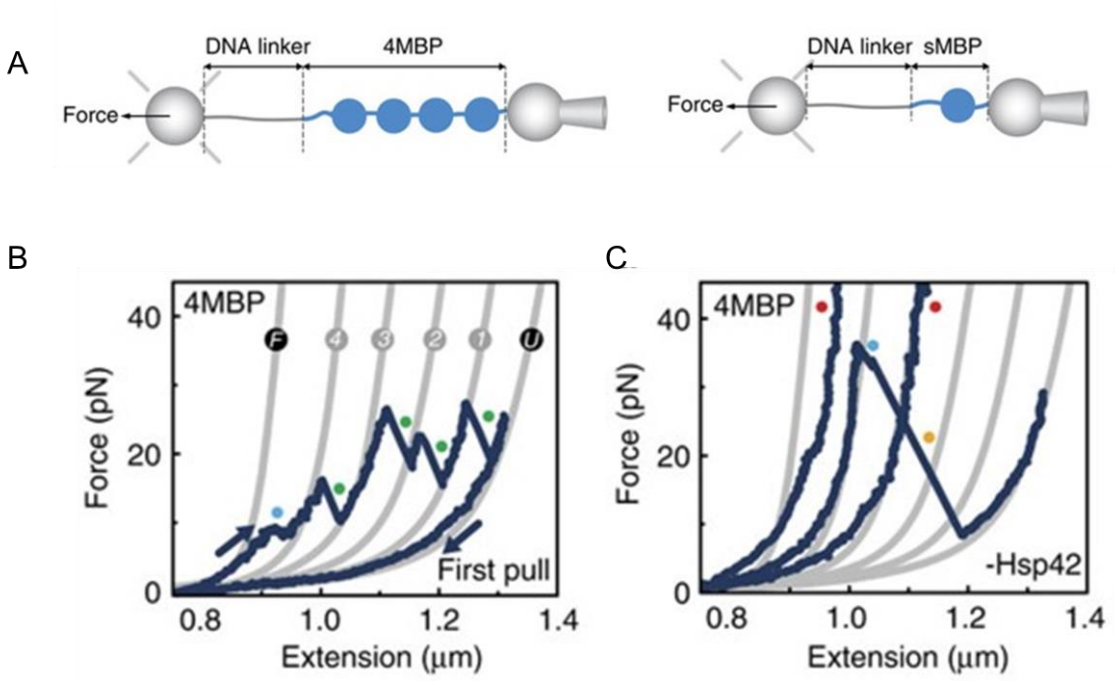

Figure 3: Experimental set up to probe the functional activity of chaperone proteins [50]. (A) Four MBP molecules connected end to end and the single MBP molecule are tethered in between two beads via a DNA linker. One bead is kept in a stationary spot by a micro-pipette while the other bead is trapped in the optical trap allowing for the induction of denaturation in the MBP molecule and measurement of applied force. (B) First unfolding and refolding cycle of the MBP homotetramer. The grey lines represent the WLC fitting of the unfolding rips. The first observed unfolding at low forces (F to 4) represents the untangling of the alpha helical structures from the MBP core. This is followed by four distinct rips (4 to 3, 3 to 2, 2 to 1 and 1 to U) corresponding to the unfolding of the core of each MBP molecule with U representing the completely unstructured homotetramer. The 4MBP molecule is then relaxed by gradually reducing the applied force (last blue line) giving the molecule a chance to fold back in their native states. (C) Subsequent pulling cycles in the absence of chaperone showing aggregated structures unfolding at higher forces (blue dot) or not unfolding at all (red dots). Adapted with permission from [50] via Creative Commons Attribution 4.0 International License.

This experimental approach was employed by Mashaghi et al. to investigate the chaperone mechanism of the bacterial Hsp70 homologue DnaK [48]. In [48], the authors show

that when 4MBP is pulled in the presence of the DnaK chaperone system (DnaK, DnaJ, GrpE, ADP), the homotetramer displays far less tendency for aggregation than in the absence of the chaperone. Rather, an increased presence of unfolding events corresponding to the denaturation of single MBP cores and minor aggregates was observed. These results indicate a strong holdase action of DnaK, as well as its propensity to promote native folding, which is in line with previous data obtained from bulk assays [51-53]. To decipher the underlying chaperone mechanisms, the authors simplified the experimental assay and characterized the effect of DnaK on the folding process of single MBP domains (sMBP). The results of these experiments show that DnaK binds both to denatured polypeptide chains, preventing protein refolding, and to partially folded native-like protein structures, stabilizing them mechanically. OT studies can be performed using the full-length protein or truncated versions of it, allowing us to study the functions performed by various parts of the chaperone. In addition to the nucleotide binding domain described above, DnaK comprises a substrate binding domain (SBD)) containing an α-helical subdomain that acts as a lid and a β sheet subdomain that accommodates the peptide binding pocket [54]. To shed light on the roles played by the lid and the peptide binding pocket, experiments similar to those described above were performed using a truncated lid variant, DnaK (2–538), and a binding groove mutant, DnaK (V436F). The lid-truncated variant could bind to an unfolded sMBP and prevent its refolding, but could not stabilize folded structures. By contrast, the groove-mutated variant was unable to hinder refolding of sMBP, but managed to stabilize (although weakly) near-native conformations. These data indicate that while the groove plays a key role in the DnaK-substrate interaction, the lid is necessary for the stabilization of folded structures. In light of these results, the authors surmised that DnaK counters aggregation by binding not only to extended peptides but also to partially folded, near-native conformations, stabilizing them. They also extended upon the canonical model of DnaK action by suggesting that DnaK can help guide partially folded structures to native conformations by limiting inter-domain interactions, staying bound to them until they are close to a native conformation.

The structural and functional properties of proteins can also be studied with atomic force microscopy. An atomic force microscope is typically used to image the topography of a sample. However, it can also be employed for other purposes, for example to measure molecular forces. In this mode of operation, called “force spectroscopy”, single molecules or pairs of interacting molecules are stretched between an AFM tip and a substrate and the forces generated by their elongation measured at pN level (Figure 4A) [55]. Specifically, the mechanical properties of proteins are usually studied by pulling on a polyprotein, a molecule

made of a linear array of a globular domain, which is stretched between a flat surface, typically made of gold, and a silicon nitrite AFM tip [56-61]. The need for polymeric proteins in these experiments comes from the necessity of keeping the tethering surfaces far enough from each other in order to avoid short-range tip-surface interactions. As the tip is pulled away from the surface, the tension along the polymer increases and the single domains start unfolding sequentially, producing a characteristic saw tooth-like pattern in the force-extension curves, where each peak corresponds to the unfolding of one domain (Figure 4B). A careful analysis of the recorded trace allows us to characterize the unfolding pathway of the stretched protein in terms of different parameters, including: i) unfolding forces of tertiary and secondary structures, ii) unfolding activation barriers and their position along the reaction coordinate, iii) presence of intermediate states and estimation of their structural features.

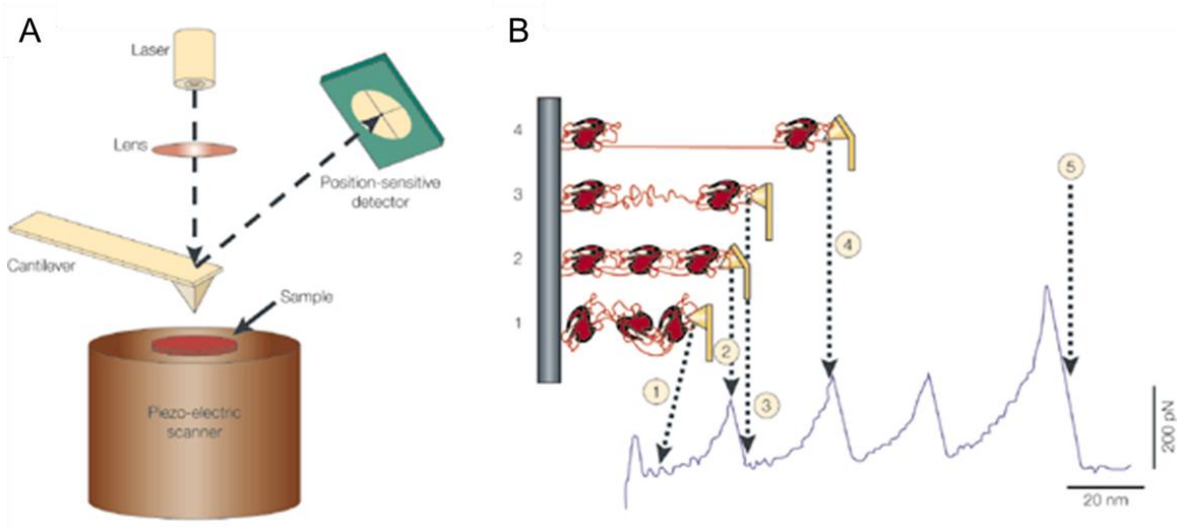

Figure 4: Mechanical manipulation of a polyprotein with an atomic force microscope [55]. A) Schematic representation of an atomic force microscope. The sample is mounted on a piezo-electric scanner that can change the position of the sample relative to the AFM tip, which is integrated at the end of a flexible cantilever. The force applied on the tip is measured by monitoring the deflection of the cantilever through an "optical lever" made of a laser and a position-sensitive detector. B) Mechanical denaturation of a polyprotein. As the distance between the tip and the surface increases (from state 1 to state 2), the molecule extends and generates a restoring force that bends the cantilever. At a certain point one domain stochastically unfolds generating an increase of the molecule contour length that makes the cantilever relax and the force drop (state 3). As the stretching of the polymer continues the

force raises again until another domain unfolds generating another drop in force. At the end of the mechanical denaturation of the polymer the corresponding stretching trace will be characterized by a saw tooth-like pattern where each peak corresponds to the denaturation of one domain. Reprinted with permission from Springer Nature Customer Service Centre GmbH : Springer Nature, Nature Reviews Molecular Cell Biology [55], Copyright 2000.

Atomic Force Microscopy was employed by Nunes et al. to study the chaperone activities of DnaJ and DnaK [62]. The authors used a octomer of I27 domains (8xI27) as a substrate for these experiments since 8xI27 is prone to misfolding and aggregation when manipulated with an AFM tip (Figure 5A) [63, 64]. In these studies a single I27 octomer is subject to multiple stretching-relaxation cycles in which first the polymer is stretched and mechanically denatured, then the applied tension is decreased to low force values for 5 seconds to allow refolding and, finally, the polymer is stretched and denatured again (Figure 5B). During the 5 second relaxation time, a denatured I27 domain can fold into its native state, misfold into an aberrant structure or remain unfolded. Each of these three possible conformations can be easily recognized in the subsequent stretching trace (Figure 5C), thereby allowing for a statistical analysis of the refolding process of I27 (Figure 6).

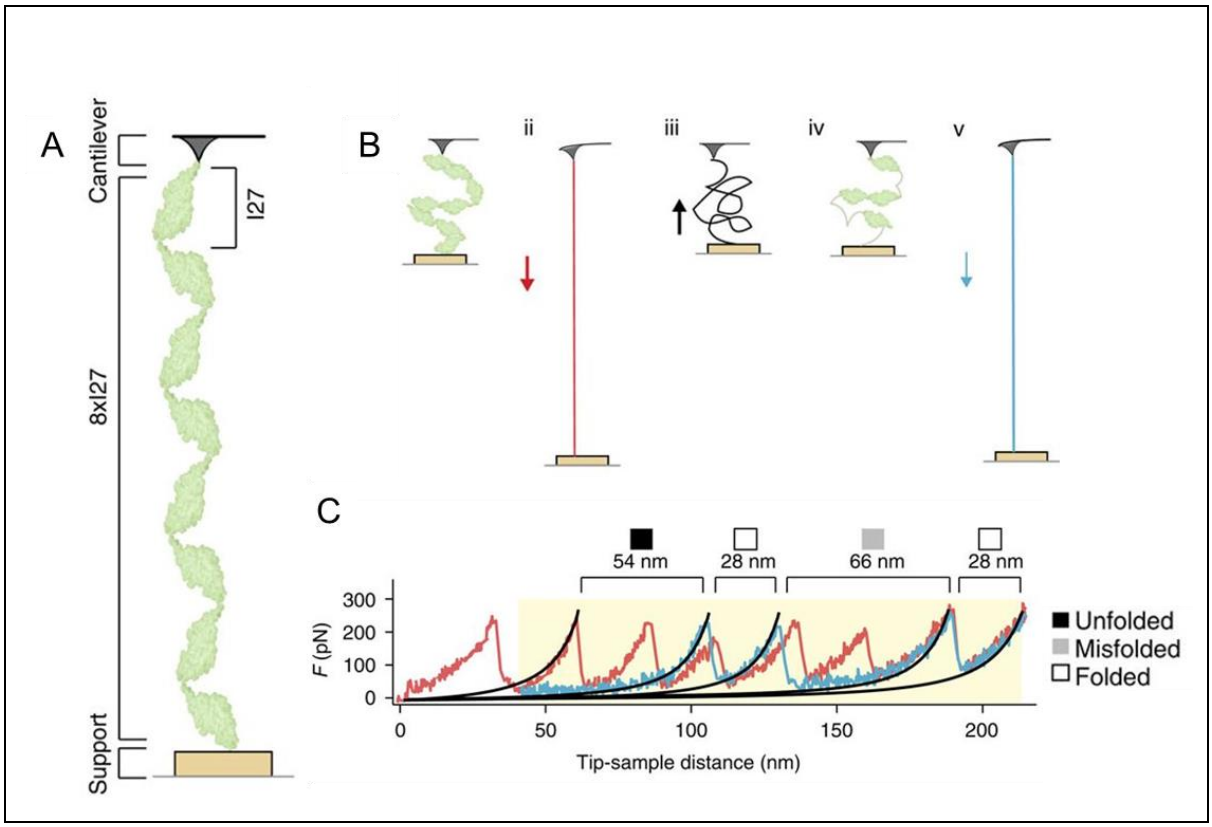

Figure 5: Mechanical manipulation of a I27 octomer (8xI27), [62]. A) A I27 octomer is attached between an AFM tip and a gold surface. B) Schematic of the experimental strategy used to study the refolding process of mechanically denatured I27 domains. The I27 octomer is first stretched and mechanically denatured by moving the gold surface away from the tip (I and ii). Then, the surface is approached back towards the tip to lower the applied tension and allow refolding (iii and iv). Finally, the polymer is mechanically unfolded again to probe the refolding process of the denatured I27 domains (v). C) The first stretching trace, showing a characteristic saw tooth-like pattern corresponding to the mechanical denaturation of I27 native states, is shown in red. The second stretching trace (panel v in B), acquired after force relaxation, is instead shown in blue and presents different types of transitions corresponding to: i) stretching of unfolded I27 domains (filled square), denaturation of I27 native states (empty square) and denaturation of I27 misfolded states (grey square). Reprinted with permission from Springer Nature Customer Service Centre GmbH : Springer Nature, Nature Communications [62], Copyright 2015.

In the absence of a chaperone, ~ 54% of I27 domains misfold, ~ 21% fold into their native state and the rest remain unfolded. In the presence of DnaJ, these percentages change. In fact, denatured I27 domains misfold less (~ 40%) and transit into their native states more often (~ 35%), while the fraction of unfolded conformers remains the same. These data reveal that DnaJ, under these experimental conditions, presents an unexpected foldase activity. If we consider that DnaJ binds to denatured polypeptide chains and that its presence does not change the size of the misfolded states observed in the stretching traces, it seems unlikely that it interacts directly with misfolded states facilitating their direct conversion into native states. Instead, the hypothesis that after binding to denatured I27 domains DnaJ limits their conformational space, guiding them preferentially towards their native states seems more likely. In cells, DanJ cooperates with DnaK. It is thus possible to extend the study from one single chaperone to chaperone complexes. When DnaJ and DnaK are both present in a 1:2 molar ratio, the folding behaviour of I27 is affected even more: under these conditions almost no proteins misfold (~ 1%), and the rest either transit into the native state (~ 65%) or remain unfolded (~ 34%). Thus, compared to the no chaperone condition, the chaperone pair DnaJ/DnaK, through synergic mechanisms, stabilizes significantly both the native and the

unfolded states, thereby hindering misfolding and aggregation of the substrate protein (Figure 6).

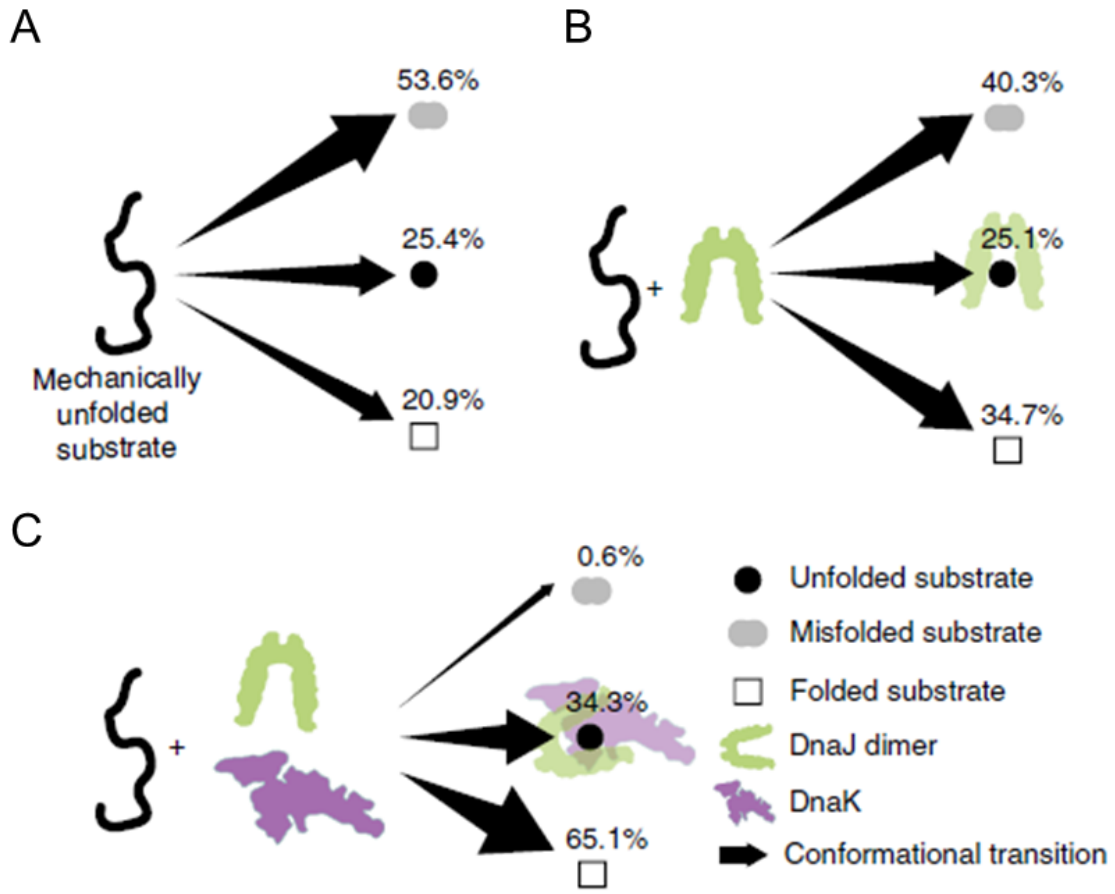

Figure 6: Refolding process of a denatured I27 domain upon relaxation of the applied force, under different experimental conditions [62]. A) In the absence of chaperones, the unfolded domain mostly misfolds. B) In the presence of DnaJ the I27 domain misfolds less and transits into its native state more often, while the probability of remaining unfolded does not change. C) In the presence of DnaJ and DnaK (1:2 molar ratio) the I27 domain folds into its native state most of the time, or alternatively remains unfolded. Misfolding is almost abolished. Reprinted with permission from Springer Nature Customer Service Centre GmbH : Springer Nature, Nature Communications [62], Copyright 2015.

4.4 Structural, Mechanical and Functional Properties of small HSPs

Small HSPs are characterized by their ability to dynamically change their structure and oligomerization state, which has been reported to influence their chaperone activity [19, 65-67]. As a consequence, experimental techniques such as optical tweezers and atomic force microscopy that allow us to monitor in real time the conformational changes that a molecule undergoes spontaneously or as a consequence of the interaction with its own substrate, are particularly indicated for the study of these chaperones.

Expanding upon their previous optical tweezers studies on DnaK, the group of Prof. Tans characterized the chaperone action of the small heat shock protein HSP42 [50]. Strong holdase, as well as some foldase action for HSP42 was reported by analyzing its impact on 4MBP. The authors noticed that large and mechanically resistant aggregates of MBP disappeared in the presence of HSP42. Instead, they observed an appreciable increase in the number of native-like core unfolding events, along with transitions corresponding to the denaturation of small and weakly aggregated structures. From these results, the authors hypothesized that HSP42 hinders non-native interactions in 4MBP by forming a complex with near-natively folded MBP structures, and shielding them from aggregation partners; alternatively, but not mutually exclusive, HSP42 disrupts large aggregated structure and allows the protein to fold back in its native conformation, or to aggregate weakly. To learn more about the molecular mechanism underlying its chaperone action, the authors characterized the effect of HSP42 on single MBP domains (sMBP). These studies revealed that HSP42 does not interact with the native state, nor with the denatured state of sMBP (the substrate protein), but its presence increases the probability of observing native-like core unfolding. These unfolding events, however, as in the case of 4MBP, occurred at lower forces than in the absence of HSP42 and hence correspond to the denaturation of native-like molecular structures that are less stable than the native state. These results prompted the authors to conclude that HSP42 carries out its chaperone activity by binding to partially folded, close to native conformations and prevent them from aggregating any further. It can then propel these bound structures towards their native conformations by hindering non-native interactions. It is also possible that this chaperone actively discourages aggregation by guiding the folding protein in a less mechanically stable native-like state, which is not available to the MBP protein in the absence

of HSP42. This will require that HSP42 alters the energy landscape of the target protein during the folding state. Although no conclusive evidence is provided for this hypothesis, further single-molecule studies of HSP42 could help us better understanding the molecular mechanisms that mediate the biological function of this chaperone. These data paint a more complicated mechanism of action for small HSPs, which extends well-beyond small HSPs acting as "sponges" that promiscuously bind to heterogeneous substrates to avoid their aggregation. Although they are considered as "holdases", a term that implies a rather passive function, these data suggest that small HSPs may actively favour protein folding in an ATP-independent manner. Future studies using OT and extending the characterization to different small HSPs from several species should unravel this hypothesis and may provide surprising data that can potentially change the way the scientific community looks at small HSPs.

Atomic force microscopy was employed by Bertz et al. to characterize the mechanical stability of the α-crystallin domain dimer of the small heat shock protein Hsp16.5, from the hyperthermophilic archaeon Methanocaldococcus jannaschii [68]. The α-crystallin domain dimer represents the building block of the three-dimensional structure of Hsp16.5, comprising 24 subunits arranged into a spherical homo-oligomer. Bertz et al. characterized the disassembly and unfolding of the α-crystallin domain dimer through both single-molecule force spectroscopy and fluorescence bulk experiments, where they monitored GdmCl induced equilibrium unfolding transitions. The results of these latter studies indicate that the disassembly and assembly processes of the dimer are strictly coupled to the unfolding and refolding of the monomers, so that, through an all-or-none process, the system goes directly from a structured dimer to denatured polypeptide chains and vice versa, with no population of intermediate folded monomeric species. Single-molecule manipulation studies provided different information. A first series of experiments were performed by pulling on a molecular construct where the C terminus of each 16.5α was connected to a molecular handle comprising three filamin domains (ddFLN3–5) [69] and three titin domains (I27–29) [70]. These domains can easily be distinguished one from another in a force-extension curve by both their contour lengths and their unfolding forces, with the ddFLN3–5 unfolding below 120 pN and I27–29 unfolding at ~ 230 pN. A typical stretching trace recorded in these experiments is characterized by a sawtooth-like pattern, corresponding to the sequential unfolding of filamin domains, followed by a final force peak at ~ 180 pN, which was interpreted as the rupture force of the dimer that dissociates before force could unfold the titin domains. The interpretation of these data was corroborated by the results of similar experiments in which force was applied to different molecular constructs, where the two 16.5α monomers are flanked by three ubiquitin

domains, acting as handles for mechanical manipulation, and are connected to each other through an ubiquitin trimer linker that prevents dissociation of the stretched molecular construct upon disassembly of the dimer. The resulting force-extension curves showed the characteristic sawtooth-like unfolding signature of the ubiquitin domains interrupted by a longer unfolding event, which produces an increment in contour length that is consistent with that expected for the complete unfolding of the 16.5α dimer. A closer inspection of the recorded traces shows that the longer unfolding event in reality is a three-step transition process, where two intermediate states are populated. The first transition takes place at a force (183 ± 4 pN) that is quite similar to that of the final force peak observed in the abovementioned experiments, and produces an increment in contour length (9.2 ± 0.4 nm) that corresponds well to that expected for the dissociation of the 16.5α dimer. The second and third transitions generate increments in contour length that are consistent with the sequential denaturation of the two isolated α monomers. Thus, these results indicate that a 16.5α dimer can be split into two stable fully folded monomers, which subsequently can unfold independently of each other. These findings are in contrast to those emerging from chemical unfolding bulk experiments that suggest that no folded monomeric intermediates are populated during dimer disassembly. This may appear surprising, but in reality, discrepancies between chemical and mechanical denaturation has already been reported [71]. Surely, the force spectroscopy data collected by Bertz et al. demonstrate the efficacy of single-molecule manipulation studies in spotting and characterizing molecular species that are difficult to detect with ensemble methods. On the basis of the data illustrated in this study, we can hypothesize that assembly of the three-dimensional structure of Hsp16.5 begins with the folding of polypeptide chains into stable monomeric species that later associate into stable dimers that eventually assemble into the final oligomeric conformation.

4.5 Conclusions

Recently, optical tweezers and atomic force microscopy have been successfully applied to the study of structural and functional properties of molecular chaperones. Some of the most significant experimental results obtained with HSPs and sHSPs using these techniques are illustrated in this chapter. Optical tweezers have been effectively employed to decipher the intricacy of the multistate conformational dynamics of Hsp82, HtpG and Grp94, revealing an

ensemble of on- and off-pathways intermediate states that these chaperones populate during their journey towards the native state [27, 39, 40]. Particular attention was paid to the characterization of the structural dynamics of the charged linker (CL) connecting the N- and M-domains of these chaperones. The results of these studies show that the CL of Hsp82, unlike that of HtpG and Grp94, fluctuates at equilibrium between a closed and an open conformation, providing a structural flexibility to Hsp82 that might play a key role during its interaction with the client proteins. Using a similar experimental strategy, Bauer and co-authors characterized in great detailed the unfolding and refolding pathways of the Nucleotide Binding Domain (NBD) of DnaK chaperone, assessing also the effect of nucleotide binding to the energy landscape of the chaperone [43]. These studies reveal a mechanical hierarchy between NBD structural lobes that is reversed in the presence of ATP, and disclose the role played by lobe II in the driving of the productive folding process of NBD. OT studies were also applied to decipher the mechanism of action of the small heat shock protein HSP42, revealing an unexpected foldase activity that the chaperone seems to carry out by binding to partially folded close to native conformations of the substrate, rather than to its unfolded state [45]. Similarly, AFM was used to study the structural and functional properties of different chaperones. In particular AFM was employed to characterize the mechanical properties of the α-crystallin domain dimer of the small heat shock protein Hsp16.5, revealing that it can be split into two stable fully folded monomers, in contrast to what suggested by chemical denaturation bulk studies [68]. Moreover, through AFM force spectroscopy the molecular mechanisms underlying the chaperone activities of DnaJ and DnaK were explored in great detail [62].

While excellent details have been extracted through the application of these techniques to the study of biomolecules, OT and AFM are to a certain extent limited in their approach by the fact that they probe a molecular process along a single reaction coordinate, which is determined by the points of force application [24]. As a consequence, any structural transition of the molecule under examination that does not produce an appreciable change in molecular extension along the pulling axis is not detected in these experiments. One way to move past this hurdle is to perform multiple pulling assays with varied attachment points to extract structural dynamics information across different reactions coordinates [32, 72]. Also, in case of Optical Tweezers, multi-trap systems are now available, which can overcome the single dimensional probing limit [73]. Alternatively, novel hybrid approaches of combining fluorescence based imaging techniques with single molecule manipulation methods can be employed to provide a multidimensional picture of the molecular processes under study [74, 75].

In conclusion, key aspects of the structural and functional properties of HSPs and small HSPs have been revealed recently through single molecule manipulation experiments. However, this field of research is still in its infancy and great room for improvement exists both for the instrumentation and for the methods used to prepare biological samples. It is therefore reasonable to assume that these types of experiments will produce even more surprising and relevant discoveries in the near future.

Finally, the comparison at the single molecule level of the function of wild-type small HSPs with their disease-causing mutation counterparts may illuminate on how they affect their functionality, via a gain or loss-of-function. This knowledge will be essential for the design of any potential therapeutic approach for the treatment of neuromuscular diseases, myopathies, cardiomyopathies and congenital cataract that have been so far associated with mutations in human genes encoding for small HSPs, such as e.g. HSPB1, HSPB3, HSPB4, HSPB5 and HSPB8 [76-78].

4.6 References

1. Klaips, C.L., G.G. Jayaraj, and F.U. Hartl, *Pathways of cellular proteostasis in aging and disease.* J Cell Biol, 2018. **217**(1): p. 51-63.
2. Kapur, M. and S.L. Ackerman, *mRNA translation gone awry: translation fidelity and neurological disease.* Trends in Genetics, 2018. **34**(3): p. 218-231.
3. Shibata, Y. and R.I. Morimoto, *How the nucleus copes with proteotoxic stress.* Current Biology, 2014. **24**(10): p. R463-R474.
4. Chen, B., et al., *Cellular strategies of protein quality control.* Cold Spring Harbor perspectives in biology, 2011. **3**(8): p. a004374.
5. Balchin, D., M. Hayer-Hartl, and F.U. Hartl, *In vivo aspects of protein folding and quality control.* Science, 2016. **353**(6294): p. aac4354.
6. Bukau, B., J. Weissman, and A. Horwich, *Molecular chaperones and protein quality control.* Cell, 2006. **125**(3): p. 443-451.
7. Hartl, F.U., A. Bracher, and M. Hayer-Hartl, *Molecular chaperones in protein folding and proteostasis.* Nature, 2011. **475**(7356): p. 324.
8. Labbadia, J. and R.I. Morimoto, *The biology of proteostasis in aging and disease.* Annual review of biochemistry, 2015. **84**: p. 435-464.
9. Hipp, M.S., P. Kasturi, and F.U. Hartl, *The proteostasis network and its decline in ageing.* Nature Reviews Molecular Cell Biology, 2019: p. 1.
10. Tissiéres, A., H.K. Mitchell, and U.M. Tracy, *Protein synthesis in salivary glands of Drosophila melanogaster: relation to chromosome puffs.* Journal of molecular biology, 1974. **84**(3): p. 389-398.
11. Bult, C.J., et al., *Complete genome sequence of the methanogenic archaeon, Methanococcus jannaschii.* Science, 1996. **273**(5278): p. 1058-1073.
12. Caspers, G.-J., J.A. Leunissen, and W.W. de Jong, *The expanding small heat-shock protein family, and structure predictions of the conserved "α-crystallin domain".* Journal of molecular evolution, 1995. **40**(3): p. 238-248.
13. Schopf, F.H., M.M. Biebl, and J. Buchner, *The HSP90 chaperone machinery.* Nature reviews Molecular cell biology, 2017. **18**(6): p. 345.

14. Hessling, M., K. Richter, and J. Buchner, *Dissection of the ATP-induced conformational cycle of the molecular chaperone Hsp90.* Nature structural & molecular biology, 2009. **16**(3): p. 287.
15. Genest, O., et al., *Hsp70 and Hsp90 of E. coli directly interact for collaboration in protein remodeling.* Journal of molecular biology, 2015. **427**(24): p. 3877-3889.
16. Kappé, G., et al., *The human genome encodes 10 α-crystallin–related small heat shock proteins: HspB1–10.* Cell stress & chaperones, 2003. **8**(1): p. 53.
17. de Jong, W.W., J.A. Leunissen, and C. Voorter, *Evolution of the alpha-crystallin/small heat-shock protein family.* Molecular biology and evolution, 1993. **10**(1): p. 103-126.
18. Bonorino, C., et al., *The VIII International Congress on Stress Proteins in Biology and Medicine: täynnä henkeä.* Cell Stress and Chaperones, 2018. **23**(2): p. 171-177.
19. Haslbeck, M., S. Weinkauf, and J. Buchner, *Small heat shock proteins: Simplicity meets complexity.* Journal of Biological Chemistry, 2019. **294**(6): p. 2121-2132.
20. van Montfort, R.L., et al., *Crystal structure and assembly of a eukaryotic small heat shock protein.* Nature Structural & Molecular Biology, 2001. **8**(12): p. 1025.
21. Alderson, T.R., et al., *Local unfolding of the HSP27 monomer regulates chaperone activity.* Nature communications, 2019. **10**(1): p. 1068.
22. Cecconi, C., et al., *Direct observation of the three-state folding of a single protein molecule.* Science, 2005. **309**(5743): p. 2057-2060.
23. Stigler, J., et al., *The complex folding network of single calmodulin molecules.* Science, 2011. **334**(6055): p. 512-516.
24. Choudhary, D., et al., *Bio-molecular applications of recent developments in optical tweezers.* Biomolecules, 2019. **9**(1): p. 23.
25. Bertz, M., A. Kunfermann, and M. Rief, *Navigating the folding energy landscape of green fluorescent protein.* Angewandte Chemie International Edition, 2008. **47**(43): p. 8192-8195.
26. Ritchie, D.B. and M.T. Woodside, *Probing the structural dynamics of proteins and nucleic acids with optical tweezers.* Current opinion in structural biology, 2015. **34**: p. 43-51.
27. Jahn, M., et al., *The charged linker of the molecular chaperone Hsp90 modulates domain contacts and biological function.* Proceedings of the National Academy of Sciences, 2014. **111**(50): p. 17881-17886.

28. Cecconi, C., et al., *Protein-DNA chimeras for single molecule mechanical folding studies with the optical tweezers.* European Biophysics Journal, 2008. **37**(6): p. 729-738.
29. Cecconi, C., et al., *DNA molecular handles for single-molecule protein-folding studies by optical tweezers*, in *DNA Nanotechnology*. 2011, Springer. p. 255-271.
30. Pfitzner, E., et al., *Rigid DNA beams for high-resolution single-molecule mechanics.* Angewandte Chemie International Edition, 2013. **52**(30): p. 7766-7771.
31. Wen, J.-D., et al., *Force unfolding kinetics of RNA using optical tweezers. I. Effects of experimental variables on measured results.* Biophysical journal, 2007. **92**(9): p. 2996-3009.
32. Heidarsson, P.t.O., et al., *A highly compliant protein native state with a spontaneous-like mechanical unfolding pathway.* Journal of the American Chemical Society, 2012. **134**(41): p. 17068-17075.
33. Caldarini, M., et al., *The complex folding behavior of HIV-1-protease monomer revealed by optical-tweezer single-molecule experiments and molecular dynamics simulations.* Biophysical chemistry, 2014. **195**: p. 32-42.
34. Mandal, S.S., et al., *Nanomechanics of the substrate binding domain of Hsp70 determine its allosteric ATP-induced conformational change.* Proceedings of the National Academy of Sciences, 2017. **114**(23): p. 6040-6045.
35. Heidarsson, P.O., et al., *Single-molecule folding mechanism of an EF-hand neuronal calcium sensor.* Structure, 2013. **21**(10): p. 1812-1821.
36. Shank, E.A., et al., *The folding cooperativity of a protein is controlled by its chain topology.* Nature, 2010. **465**(7298): p. 637.
37. Gao, Y., G. Sirinakis, and Y. Zhang, *Highly anisotropic stability and folding kinetics of a single coiled coil protein under mechanical tension.* Journal of the American Chemical Society, 2011. **133**(32): p. 12749-12757.
38. Neupane, K., et al., *Direct observation of transition paths during the folding of proteins and nucleic acids.* Science, 2016. **352**(6282): p. 239-242.
39. Jahn, M., et al., *Folding and domain interactions of three orthologs of Hsp90 studied by single-molecule force spectroscopy.* Structure, 2018. **26**(1): p. 96-105. e4.
40. Jahn, M., et al., *Folding and assembly of the large molecular machine Hsp90 studied in single-molecule experiments.* Proceedings of the National Academy of Sciences, 2016. **113**(5): p. 1232-1237.

41. Ali, M.M., et al., *Crystal structure of an Hsp90–nucleotide–p23/Sba1 closed chaperone complex.* Nature, 2006. **440**(7087): p. 1013.
42. Hainzl, O., et al., *The charged linker region is an important regulator of Hsp90 function.* Journal of Biological Chemistry, 2009. **284**(34): p. 22559-22567.
43. Bauer, D., et al., *Nucleotides regulate the mechanical hierarchy between subdomains of the nucleotide binding domain of the Hsp70 chaperone DnaK.* Proceedings of the National Academy of Sciences, 2015. **112**(33): p. 10389-10394.
44. Kityk, R., et al., *Structure and dynamics of the ATP-bound open conformation of Hsp70 chaperones.* Molecular cell, 2012. **48**(6): p. 863-874.
45. Bauer, D., et al., *A folding nucleus and minimal ATP binding domain of Hsp70 identified by single-molecule force spectroscopy.* Proceedings of the National Academy of Sciences, 2018. **115**(18): p. 4666-4671.
46. Bechtluft, P., et al., *Direct observation of chaperone-induced changes in a protein folding pathway.* Science, 2007. **318**(5855): p. 1458-1461.
47. Mashaghi, A., et al., *Reshaping of the conformational search of a protein by the chaperone trigger factor.* Nature, 2013. **500**(7460): p. 98.
48. Mashaghi, A., et al., *Alternative modes of client binding enable functional plasticity of Hsp70.* Nature, 2016. **539**(7629): p. 448.
49. Scholz, C., et al., *Autocatalytic folding of the folding catalyst FKBP12.* Journal of Biological Chemistry, 1996. **271**(22): p. 12703-12707.
50. Ungelenk, S., et al., *Small heat shock proteins sequester misfolding proteins in near-native conformation for cellular protection and efficient refolding.* Nature communications, 2016. **7**: p. 13673.
51. Skowyra, D., C. Georgopoulos, and M. Zylicz, *The E. coli dnaK gene product, the hsp70 homolog, can reactivate heat-inactivated RNA polymerase in an ATP hydrolysis-dependent manner.* Cell, 1990. **62**(5): p. 939-944.
52. Schröder, H., et al., *DnaK, DnaJ and GrpE form a cellular chaperone machinery capable of repairing heat-induced protein damage.* The EMBO journal, 1993. **12**(11): p. 4137-4144.
53. Szabo, A., et al., *The ATP hydrolysis-dependent reaction cycle of the Escherichia coli Hsp70 system DnaK, DnaJ, and GrpE.* Proceedings of the National Academy of Sciences, 1994. **91**(22): p. 10345-10349.
54. Mayer, M.P., et al., *Multistep mechanism of substrate binding determines chaperone activity of Hsp70.* Nature Structural & Molecular Biology, 2000. **7**(7): p. 586.

55. Bustamante, C., J.C. Macosko, and G.J. Wuite, *Grabbing the cat by the tail: manipulating molecules one by one.* Nature Reviews Molecular Cell Biology, 2000. **1**(2): p. 130.
56. Rief, M., et al., *Reversible unfolding of individual titin immunoglobulin domains by AFM.* science, 1997. **276**(5315): p. 1109-1112.
57. Carrion-Vazquez, M., et al., *Mechanical and chemical unfolding of a single protein: a comparison.* Proceedings of the National Academy of Sciences, 1999. **96**(7): p. 3694-3699.
58. Yang, G., et al., *Solid-state synthesis and mechanical unfolding of polymers of T4 lysozyme.* Proceedings of the National Academy of Sciences, 2000. **97**(1): p. 139-144.
59. Dietz, H. and M. Rief, *Exploring the energy landscape of GFP by single-molecule mechanical experiments.* Proceedings of the National Academy of Sciences, 2004. **101**(46): p. 16192-16197.
60. Sandal, M., et al., *Conformational equilibria in monomeric α-synuclein at the single-molecule level.* PLoS biology, 2008. **6**(1): p. e6.
61. Perales-Calvo, J., et al., *The force-dependent mechanism of DnaK-mediated mechanical folding.* Science Advances, 2018. **4**(2): p. eaaq0243.
62. Nunes, J.M., et al., *Action of the Hsp70 chaperone system observed with single proteins.* Nature communications, 2015. **6**: p. 6307.
63. Borgia, M.B., et al., *Single-molecule fluorescence reveals sequence-specific misfolding in multidomain proteins.* Nature, 2011. **474**(7353): p. 662.
64. Wright, C.F., et al., *The importance of sequence diversity in the aggregation and evolution of proteins.* Nature, 2005. **438**(7069): p. 878.
65. Delbecq, S.P. and R.E. Klevit, *One size does not fit all: the oligomeric states of αB crystallin.* FEBS letters, 2013. **587**(8): p. 1073-1080.
66. Ito, H., et al., *Phosphorylation of αB-crystallin in response to various types of stress.* Journal of Biological Chemistry, 1997. **272**(47): p. 29934-29941.
67. Peschek, J., et al., *Regulated structural transitions unleash the chaperone activity of αB-crystallin.* Proceedings of the National Academy of Sciences, 2013. **110**(40): p. E3780-E3789.
68. Bertz, M., et al., *Structural and mechanical hierarchies in the α-crystallin domain dimer of the hyperthermophilic small heat shock protein Hsp16. 5.* Journal of molecular biology, 2010. **400**(5): p. 1046-1056.

69. Schwaiger, I., et al., *A mechanical unfolding intermediate in an actin-crosslinking protein.* Nature structural & molecular biology, 2004. **11**(1): p. 81.
70. Li, H., et al., *Reverse engineering of the giant muscle protein titin.* Nature, 2002. **418**(6901): p. 998.
71. Bertz, M. and M. Rief, *Mechanical unfoldons as building blocks of maltose-binding protein.* Journal of molecular biology, 2008. **378**(2): p. 447-458.
72. Elms, P.J., et al., *The molten globule state is unusually deformable under mechanical force.* Proceedings of the National Academy of Sciences, 2012. **109**(10): p. 3796-3801.
73. Dame, R.T., M.C. Noom, and G.J. Wuite, *Bacterial chromatin organization by H-NS protein unravelled using dual DNA manipulation.* Nature, 2006. **444**(7117): p. 387.
74. Sirinakis, G., et al., *Combined versatile high-resolution optical tweezers and single-molecule fluorescence microscopy.* Review of Scientific Instruments, 2012. **83**(9): p. 093708.
75. Lee, S. and S. Hohng, *An optical trap combined with three-color FRET.* Journal of the American Chemical Society, 2013. **135**(49): p. 18260-18263.
76. Benndorf, R., et al., *Neuropathy-and myopathy-associated mutations in human small heat shock proteins: characteristics and evolutionary history of the mutation sites.* Mutation Research/Reviews in Mutation Research, 2014. **761**: p. 15-30.
77. Boncoraglio, A., M. Minoia, and S. Carra, *The family of mammalian small heat shock proteins (HSPBs): implications in protein deposit diseases and motor neuropathies.* The international journal of biochemistry & cell biology, 2012. **44**(10): p. 1657-1669.
78. Dierick, I., et al., *Small heat shock proteins in inherited peripheral neuropathies.* Annals of medicine, 2005. **37**(6): p. 413-422.

Single-molecule studies of the molecular mechanisms underlying the chaperone activity of HSPB8

Chapter 5

Single-molecule studies of the molecular mechanisms underlying the chaperone activity of HSPB8

Abstract

Molecular chaperone are key contributors to the Protein Quality Control (PQC) in maintaining proteostasis in cellular atmosphere. In the present study we investigate *in vitro* the effect of small heat shock protein molecular chaperone HSPB8 on the re-folding and aggregation processes of the maltose binding protein (MBP) using optical tweezers. Optical tweezers assays were performed on two forms of Maltose Binding Protein, namely 4MBP (homotetramer of MBP) and sMBP (single MBP) in the presence or absence of wild type HSPB8 and mutant HSPB8-K141E. We observe a strong holdase activity for wild type HSPB8 on the other hand a lack of such holdase action was seen for the mutant K141E. Moreover, and importantly our results reveal an unexpected and hereto unknown foldase activity of HSPB8.

5.1 Introduction

Molecular chaperone such as Heat Shock Proteins (HSP) assist in maintaining proteostasis in cellular atmosphere under stressful conditions [1]. They perform this action by discouraging protein aggregation (holdase function) and by helping proteins in their search for native conformations (foldase function) [2-6]. A recent member of HSP family is HSPB8, a small heat shock protein, expressed in striated and smooth muscles [7, 8]. HSPB8, primarily has been understood to act as a holdase chaperone and its upregulation can help curb motoneurons disease (MDs) such as amyotrophic lateral sclerosis (ALS) and spinal and bulbar muscular atrophy (SBMA) [9-11]. Additionally, mutation in HSPB8, namely HSPB8-K141E and HSPB8-K1141N, are expected to induce destabilization in the chaperone structure and activity. They have been linked to motor neuropathies such as Charcot-Marie-Tooth neuropathy type 2L (CMT2L) [12, 13]. While significant progress have been made in understanding the structural, functional and conformational changes involved in the chaperone action of HSPB8, a molecular–level insight in its functional profile is still lacking [7, 9, 14, 15].

As discussed in chapter 4, recently single molecule techniques such as optical tweezers and AFM have been employed to decipher the functional activity of molecular chaperones at single molecule level [16-21]. These techniques add the advantage of going beyond the averaging effects observed in traditional methods and explore the functional and structural profile of biomolecules individually. Optical tweezers enable the direct manipulation of individual biomolecules to study their folding and unfolding dynamics and map the energy landscape involved in these transitions [22-29]. Additionally, they allow for the detection of partial and metastable events and interactions accruing at molecular level, which may get lost in traditional setups such as X-ray crystallography, NMR and optical spectroscopies due to ensemble nature of the signal in such systems.

Here we will explore the functional profile of wild type HSPB8 and its mutated version HSPB8-K141E by employing an optical tweezers set up to study their impact on the unfolding, refolding and aggregation induced in Maltose Binding Protein (MBP). These experimental assays are very similar to other optical tweezer assays, which have been employed to study molecular chaperones allowing us to juxtapose the behavior of HSPB8 with other chaperones and gauge the similarities and differences observed [16-18, 20]. MBP constructs for the

experiment were produced by Mario J Avellaneda in the lap of Prof. S Tans, FOM institute, AMOLF and HSPB8 was produced by Laura Mediani and Simon Alberti at Max Planck Institute of Molecular Cell Biology and Genetics, Pfotenhauerstr.

5.2 Experimental approach

As elaborated upon in the previous chapter Optical Tweezer assays have been employed to probe and study at the single molecule level the functional profile of chaperones such as, SecB, HSP70, HSP42 and Trigger Factor chaperone [16-18, 20]. A similar approach was adopted to perform the aforementioned study, i.e. to discern the impact of HSPB8 on the aggregation, folding and misfolding of suitable substrate protein. Maltose Binding Protein (MBP) from *Escherichia coli*, which is a client protein to a vast range of molecular chaperones including HSPB8, was identified as the substrate for these experiments [16, 30]. As discussed previously, because of non-native intramolecular interactions MBP molecules have a high tendency to form aggregated structures and hamper their folding yields *in vitro*. This indisposition to readily form aggregated structures make MBP ideal substrate candidate to explore the functional profile of HSPB8. An additional advantage that stems from selecting MBP for these Optical Tweezer assays is the behavior of HSPB8 can be relatively easily compared and contrasted with similar studies performed on other molecular chaperones using MBP as a substrate partner.

The Optical tweezer assay was performed by tethering the substrate molecule, flanked on both sides by 500 bp DNA handles, in between two polystyrene beads, Figure 1. The polystyrene bead that binds to the digoxigenin end of the DNA handles is trapped in a dual beam optical trap while the other bead, which binds to the biotin end of DNA handles, is held by a micropipette. The dual beam optical tweezer set up was employed to pull on two different forms of MBP, Figure 1. a) A homotetrameric MBP construct produced by connecting four MBP molecules end-to-end. This construct, termed 4MBP, in particular is designed to induce aggregation during the pulling experiments. It imitates the condition of molecular crowding and allows the MBP molecules to interact non-natively resulting in aggregated protein structures. b) A single MBP molecule, termed sMBP, which allows for the evaluation of the folding and unfolding trajectories of the single protein molecule in an aggregation free

atmosphere. The pulling experiment on both MBP constructs was performed in HMK buffer (Hepes 50 mM, KCl 100 mM, MgCl2 5 mM, sodium azide 1 %, pH=7.5) to provide conducive environment for protein folding.

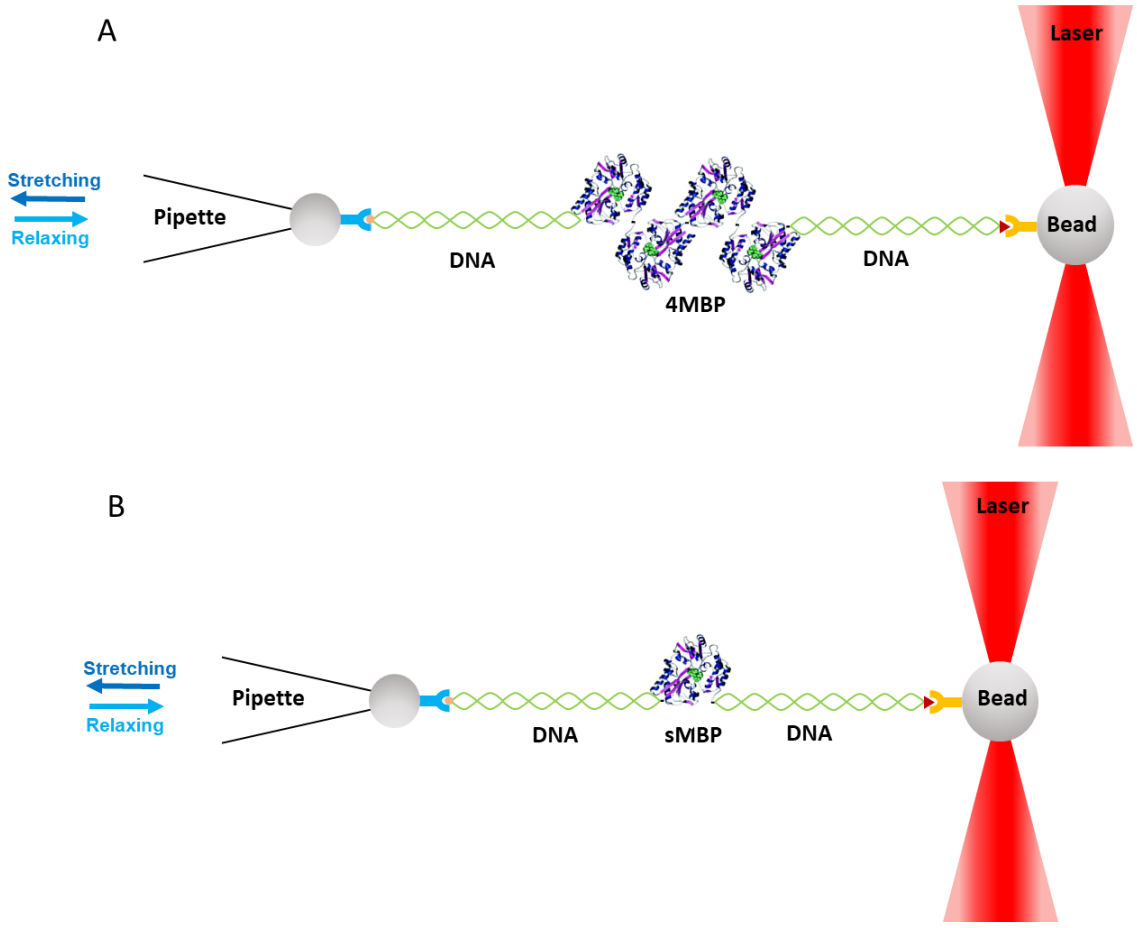

Figure 1: Optical tweezer experiment: schematic representation (not to size). The substrate is manipulated between two beads by means of 500 bp DNA handles. Both the experiments are carried out in a pulling buffer environment, which is later replaced by a buffer containing 5 uM concentration of molecular chaperone to perform tweezing experiment in presence of chaperone. A) MBP homotetramer with four MBP molecules connected end to end sandwiched between two beads, B) single MBP molecule tethered between two beads.

The experiments were carried out in two phases. In the initial phase the substrates were put through multiple cycles of mechanical denaturation (to completely unfold the substrate

protein) followed by refolding cycle (applied force was slowly reduce to 0 pN) and force-extension curves for the same were derived. 5 seconds of waiting time at 0 pN was punctuated between relaxation and next pulling cycle to give the denatured substrate ample time to go back in its native conformation. The initial phase of the optical tweezers assays were performed with a goal to characterise the behaviour of both 4MBP and MBP molecules in terms of the induced aggregation and their unfolding and refolding capabilities. The second phase of the experiment entailed the same pulling assays performed in a chaperone rich environment. First the pulling assay was performed on both substrates in the presence of wild type HSPB8 (5 uM concentration) and then similar experiments in the presence of the mutant HSPB8-K141E (5 uM concentration) with a goal to discern the impact of the two molecular chaperones at single molecule level.

5.3 Results

5.3.1 Pulling on 4MBP

Denaturation force is applied on the 4MBP molecule by moving the pipette at a constant force away from the trap. Once the pulling assay on 4MBP construct commences, very small consecutive rips are first observed in the pulling trace of the Force-Extension plot (Figure 2A) at around 14 pN. These small rips can be attributed to the untangling of the external α-helical structures from the core native MBP structures. On further pulling these small rips are followed by four substantial rips in the pulling trace (~28 pN), each corresponding to the complete unfolding of the native core of individual MBP molecules. The pulling is allowed to continue a little more to make sure that the construct is completely unstructured and then the applied force is reduced gradually to allow the unstructured peptide chain a chance to go back in a structured conformation. The refolding trace is smooth and a plateau is observed at very low force representing the hydrophobic collapse of the unstructured polypeptide chain. This initial pulling and refolding step combined is termed as the first pulling cycle.

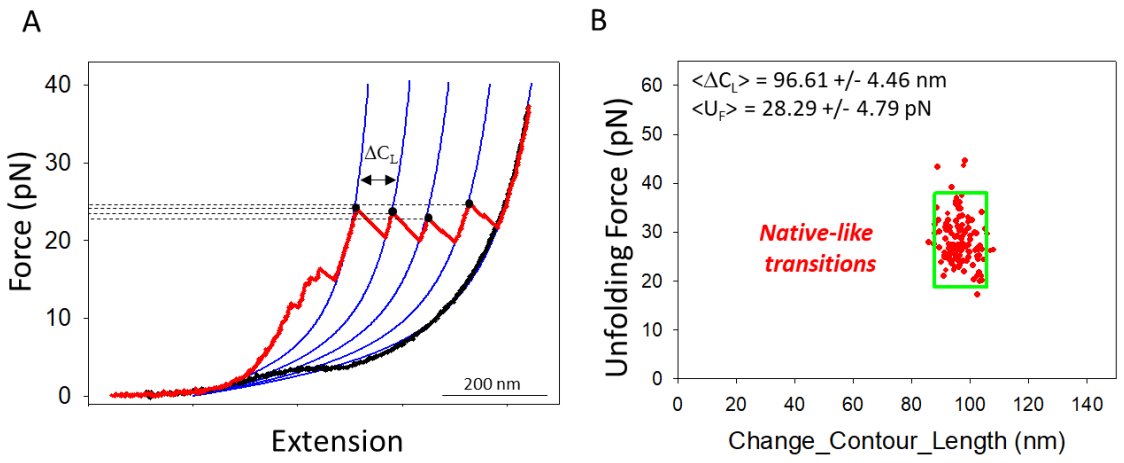

Figure 2: A) A typical first pulling cycle of the 4MBP construct at constant velocity showing first the untangling of α-helices followed by the consecutive unfolding of four MBP cores (red trace). This is followed by a refolding trace (black) of the completely unstructured polypeptide chain where the plateau at the base represents the hydrophobic collapse of the unstructured 4MBP construct. The blue line represent the worm-like chain (WLC) fits that discerns the behavior of stretched DNA handles as well as unfolded protein and calculates the contour length (CL) change for each transition. B) Scatter plot of the each MBP unfolding event from the first cycle of 32 4MBP molecules. Each red dot corresponds to the contour length change and unfolding force for each transition. The green line represents the native unfolding range constructed from these events.

Worm-like Chain (WLC) fitting was employed to measure the change in contour length (C_L) corresponding to the rips observed in the pulling traces of the force-extension graph. An average contour length of 96.61 nm was seen for the observed rip at high forces, which is in line with the expected length increase for the complete unfolding of the MBP core. Consequently, the four rips observed in the first pulling trace were designated as native-unfolding events. The first pulling cycle from 32 4MBP constructs was used to calculate the average contour length (C_L = 96.61 nm) and average unfolding force (U_F = 28.29 pN) for native unfolding of the individual MBP molecules in the 4MBP construct. A native unfolding range (average +/- twice the standard deviation) was procured from the distribution of the native unfolding of the MBP molecules (Figure 1B). The native range acts as a guideline to determine the occurrence of native or native-like transition in the consecutive cycles. Simply put, a

transition in the consecutive pulling cycles would be characterized as a native-like transition if it falls in the native range, i.e. has a contour length between 87.69 nm - 105.53 nm and occurs at an unfolding force between 18.71 pN – 38.87 pN.

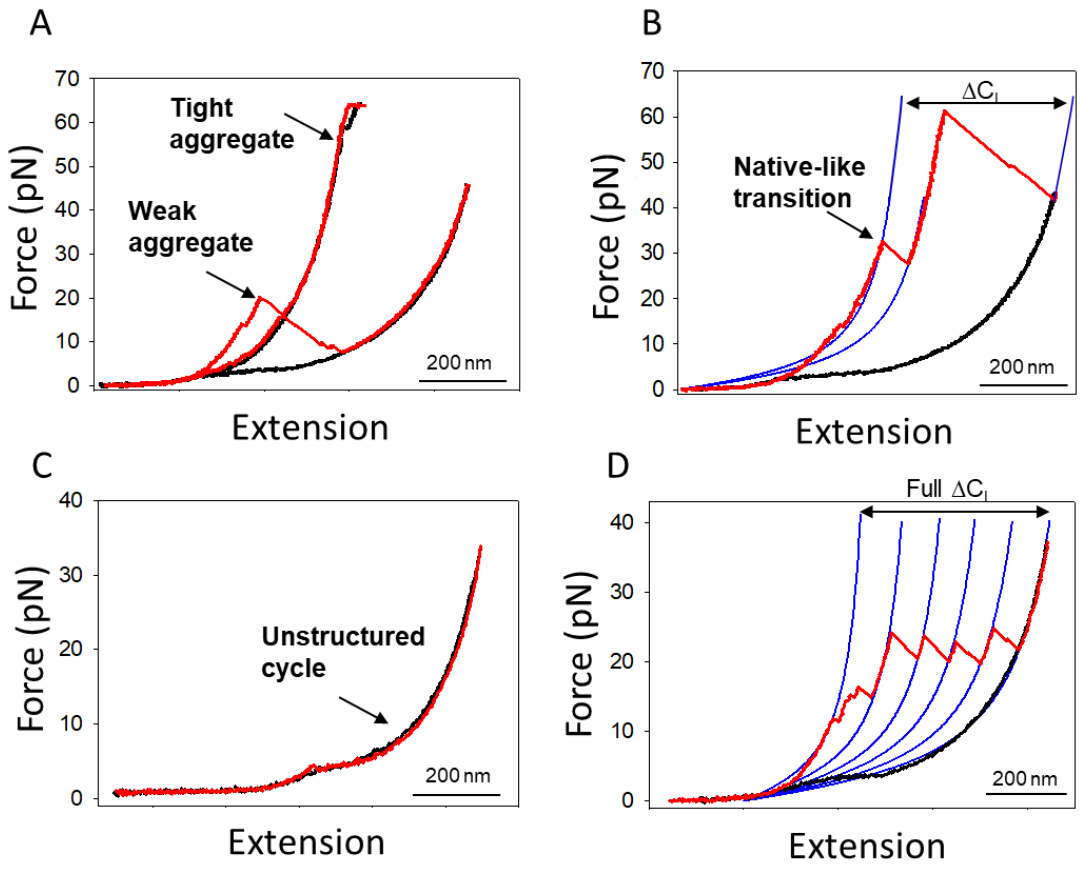

Figure 3: A) Subsequent pulling cycles showing a tight aggregation and a week aggregation. B) A pulling cycle containing a native-like transition and week aggregation. WLC fitting (blue line) is employed to measure the contour length of the complete pulling trace. C) An unstructured pulling cycle. D) WLC fitting (blue line) is used to measure the full contour length of the first pulling cycle. 32 first pulling cycles were used to calculate the average full contour length of the 4MBP construct.

The unstructured 4MBP construct was allowed to rest at 0 pN for 5 seconds after the first pulling cycles (after every cycle too). Intriguingly, the 4 nice native unfolding events from the first pulling cycle go completely missing in any of the subsequent pulling cycles, instead a wide range of alternative transitions were observed. The most observed transitions were

characterized by their large contour length (larger than one MBP core C_L) and with varying unfolding force ranging from very high (>50 pN) to low (<18 pN). In some pulling cycles, unfolding transitions were completely absent event for forces as high as 65 pN. Such transitions boasting a large contour length can be attributed to the unfolding of aggregated protein structures. As expected the unstructured MBP molecules interact non-natively amongst each other giving rise to this observed aggregation. The transitions with large contour lengths were termed as weak aggregations while the pulling cycles in which the aggregated protein did not unfold were termed tight aggregation. Additionally, some pulling cycles also contained transitions in the native unfolding range along with aggregated transitions, indicating that one of the MBP molecules in the 4MBP construct refolded to its native or close to native conformations while the other MBP molecules interacted among themselves to give rise to aggregation. A few pulling cycles also showcased a rare event in which no structuring was observed in the polypeptide chain and it remained completely unstructured. Such cycles were christened as unstructured cycles.

28 % of consecutive pulling cycles (6 molecules, N = 274) went into a tightly aggregated state while 2 % of the total consecutive pulling cycles remained completely unstructured. In order to better quantify the structuring in the substrate molecule after the first pulling cycle, the observed structuring in each subsequent pulling cycle was compared with that seen in the first pulling cycle. This was done by measuring the total contour length of each subsequent cycle and comparing it with the average of the full contour length (~505.17 nm) observed in the first pulling cycle for the MBP construct (Figure 3D). On an average ~ 82 % of the 4MBP molecule was found to have gone into some sort of structured state (weak aggregation, tight aggregation or native + aggregation) and the rest remained unstructured. Additionally we observed that there was 5.43 % chance that one of the MBP molecules were able to refold into their native or native-like conformation per cycle.

5.3.2 Pulling on 4MBP in presence of wild type HSPB8

After characterizing the behavior of 4MBP molecule, similar pulling assays were performed on the 4MBP molecule in presence of wild type HSPB8. The first pulling cycle for the 4MBP

construct did not change in the presence of the molecular chaperone as the untangling of α-helical structures was observed followed by the 4 distinct unfolding events corresponding to each MBP molecule similar to no chaperone condition (Figure 4A). While the first cycle remains anonymous to the presence of HSPB, it is in the subsequent pulling cycle where HSPB8 manifests its action. While the range of different observed transitions remains the same, i.e. week aggregation, tight aggregation, native + aggregation and unstructured, presence of HSPB8 seemingly alters there frequency of occurrence. Only 1 % of the subsequent pulling cycles went into tightly aggregated state. On the other hand, 22 % of the subsequent pulling cycles (5 molecules, N =157) remained completely unstructured. While weekly aggregated structures persist in these assays, it is quite clear that they are less robust (low average unfolding force) and less structured (low average contour length) in comparison to their counterparts in previous pulling assays on 4MBP alone, Figure 3B. On a closer examination, it was seen that on an average only ~ 54 % of the 4MBP molecule forms some sort of structured conformation in the presence of HSPB8. This number is quite significant as almost half of the 4MBP construct remains unstructured. Furthermore, the probability that one of the MBP molecules can refold into a native or native-like conformation per cycle rises to 8.12 %.

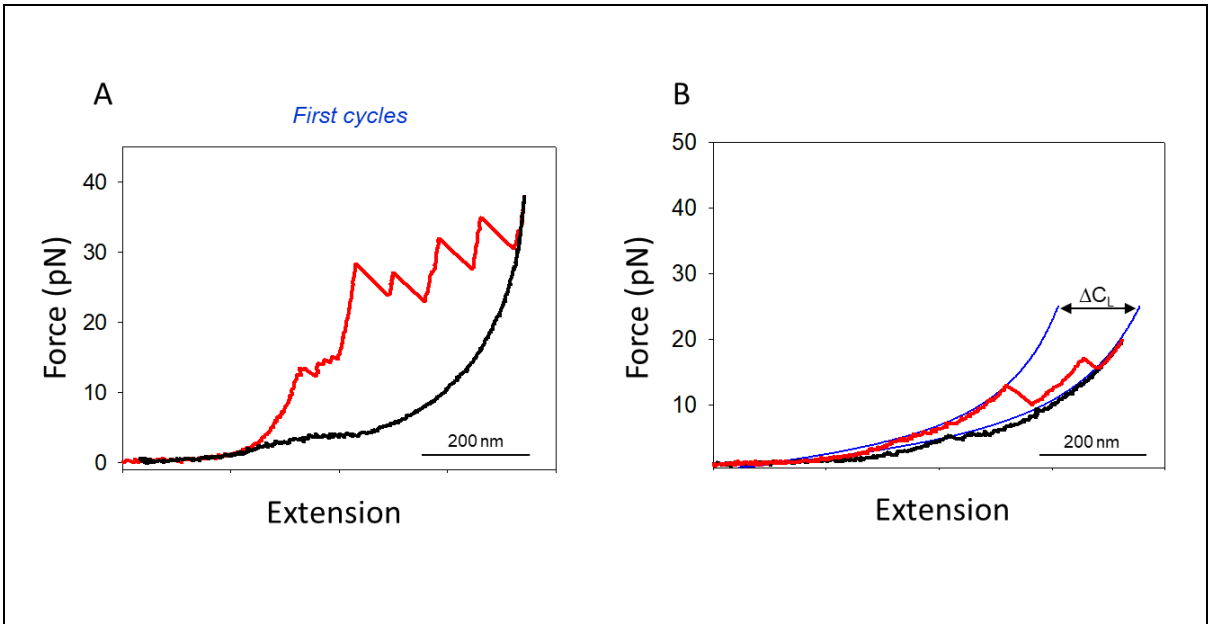

Figure 4: A) First pulling cycle of the 4MBP construct in the presence of wild type HSPB8. B) A subsequent pulling cycle showing a weekly aggregated structure. Such structures break at comparatively weaker forces and constitute less part of the substrate molecule.

5.3.3 Pulling on 4MBP in the presence of mutant HSPB8-K141E

Optical tweezer assays were then performed on 4MBP construct in the presence of a mutated version of HSPB8, namely HSPB8-K141E. The presence of K141E mutated chaperone did not alter the first pulling cycle of the 4MBP construct while a variation in the behavior of the substrate molecule was observed in the subsequent pulling cycles. Similar to no chaperone condition, completely unstructured cycles only comprised 2 % of the total subsequent pulling cycles (7 molecules, N = 222) in the presence of mutated chaperone, but unlike the no chaperone condition the amount of tightly aggregated cycles went down to ~ 7 %. Though less tight aggregation was observed in this case, the induced aggregation resembled the no chaperone condition with seemingly large parts of the 4MBP construct participating in the aggregated structures. This fact can be quantified in the structural analysis of the subsequent pulling cycles wherein on an average 70 % of the 4MBP construct was found to form structural conformations in the presence of K141E mutation. Despite the relatively high amount of induced aggregation in this case the amount of native events observed per cycle per MBP molecule were more similar to the one seen in the presence of HSPB8, with the probability of that one of the MBP domains to fold into a native or native like conformation per cycle found to be 8.9 %.

5.3.4 Pulling on sMBP

Optical tweezer assays were then performed on the sMBP molecule in an aggregation free scenario. Similar to 4MBP construct, on the application of pulling force in the first pulling cycle a small rip is observed initially at ~ 15 pN resulting from the unraveling of the α helical structures followed by a the complete unfolding of the native MBP core at ~ 23 pN (Figure 5A). Similar to 4MBP, a small hydrophobic collapse was observed at low force during the relaxation curve and in between the relaxation and pulling cycle the unstructured sMBP molecule was allowed to rest for 5 seconds at 0 pN. However, the native folding range constructed for the 4MBP molecule cannot be used in the case of sMBP as pulling on a single molecule is different from pulling on a homotetramer. Hence, 43 pulling cycles with α-helix

unfolding rip (signifying that the protein has completely refolded in such a case) were selected to construct a new native folding range. From these 43 cycles, the average Contour length (C_L) for native unfolding of the MBP molecule was found to be 106.3 nm and the average unfolding force (U_F) was found to be 23.04 pN. Taking these average values and extending them over two standard deviations the native range for sMBP molecule was designed to be between 91.20 nm - 121.40 nm for C_L and in between 39.71 pN - 6.43 pN for U_F (Figure 5B).

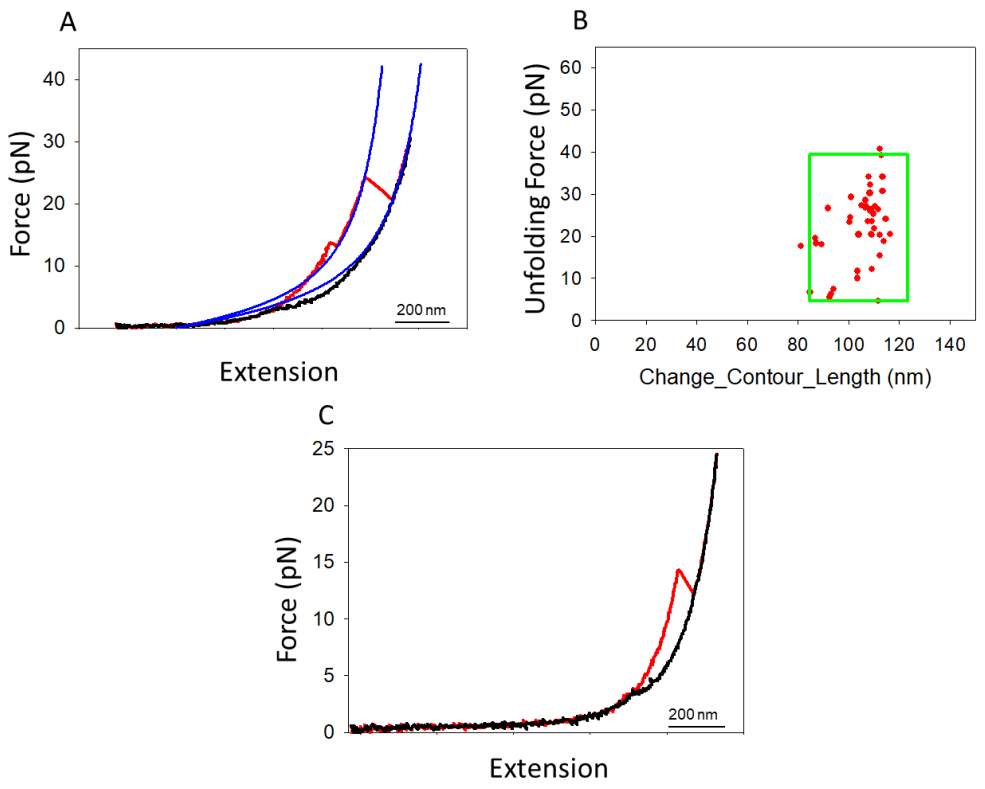

Figure 5: A) Typical first pulling cycle for sMBP molecule showing the untangling of α-helical structure followed by unfolding of MBP core (red trace) and the relaxation trace (black) contacting the hydrophobic collapse of the unstructured chain at low force. Blue trace represent the WLC fitting. B) Scatter plot of the unfolding transitions with the cycles containing α-helix unfolding rips (N = 35). The red dots represent the C_L and U_F corresponding to each transition. The green box corresponds to the native folding range. C) A typical non-native transition.

In the subsequent pulling cycles on sMBP molecule, three different types of transitions were observed – transitions in the native unfolding range, transitions outside the native

unfolding range and pulling cycles with no observed transition. The first of these is simple to understand and signifies that the unstructured peptide has folded back to its native or native-like conformation in this case. 29.53 % of transitions per cycle were found to fall in the native range marking the fact that there is a ~ 30 % probability for the sMBP molecule to fold back into its native conformation. The transitions outside the native range can be understood in terms of unfolding of partially folded native conformers or misfolded states arising from intramolecular non-native interactions. Additionally, 36.78 % of total subsequent pulling cycles (5 molecules, N = 194) were completely unstructured where the protein is not able to fold into any type of structural conformation.

5.3.5 Pulling on sMBP in the presence of HSPB8

After characterizing the behavior of sMBP molecule, similar assays were performed in the presence of HSPB8 (5 uM concentration). Behavior of the first pulling cycle in the presence of HSPB8 remained unaltered when compared to no chaperone condition and similarly impalpable impact was observed on the unstructured cycles with 33.64 % of total subsequent pulling cycles (6 molecules, N = 213) were found to be unstructured. More fascinating results were seen for native or native like transitions with the percentage of subsequent pulling cycles with native like transitions (falling in the native range) rising to 46.72 % in the presence of HSPB8.

5.3.6 Pulling on sMBP in the presence of mutant HSPB8-K141E

Finally, pulling assays were performed on sMBP in the presences of mutated HSPB8. As seen previously the first pulling cycle of sMBP molecule was not affected by the presence of K141E mutant. In addition, the amount of unstructured cycles were more or less consistent with previous two pulling experiments with an observed value of 38.22 % of total subsequent pulling cycles (7 molecules, N = 215) remaining unstructured. Contrasting results to no chaperone condition were again observed in terms of the native like folding transitions with 48.22 % of all observed transition falling in the native unfolding range.

5.4 Discussion

The results obtained from the optical tweezer assays discussed above paint a clear and fascinating picture of HSPB8's functional profile. The identical nature of the first pulling cycle of the two MBP constructs in both the presence and absence of chaperone indicate that HSPB8 (wild type and mutant) does not promote or hinder the unfolding of native MBP molecules and rather shows no interactions with the natively folded protein conformations. This neutral behaviour is short lived and considerable difference in the behaviour of the MBP molecule is noted in the stretching curves post the first pulling cycle. A strong anti-aggregation action of the wild type HSPB8 is reflected in the fact that the large number of cycles with tightly aggregated structures (~ 29 %) in the absence of chaperone go mostly missing (~1 %) in the presence of wild type HSPB8. Furthermore, a strong holdase action of the wild type HSPB8 can be deduced from the stark decrease in the average structural fraction per cycle (82 % to 53 %, figure 5) for the 4MBP construct as well as from the increase in the amount of unstructured cycles (from 1.8 % to 22 %) in the presence of HSPB8. The nature of holdase activity observed for HSPB8 is also quite different from the one reported for SecB, a molecular chaperone with strong holdase action [16]. In similar assays, Bechtluft et al found that SecB binds only to the extended peptides and prevents the formation of any tertiary structures while in the case of HSPB8 we find that it performs its holdase action in a more moderate manner. The perceived holdase action of HSPB8 can be understood by two possible mechanisms. It can interact with and then breaks the aggregated proteins structures. Hence while tightly aggregated structures go missing in the presence of chaperone some aggregation is still present. Alternatively, it might hinders aggregation by selectively binding to the unstructured peptide as well as to the weakly structured protein conformers, thus preventing non-native interactions. The evidence for this possible mechanism stems from the increased amount of unstructured pulling cycles in the presence of HSPB8.

Inversely, the holdase activity is significantly reduced in the case of the mutant HSPB8-K141E. On one hand, the number of observed tight aggregations is reduced (~7 %) in the presence of K141E but on the other hand, the average structural fraction per cycle is found to be 70 %, which is not far away from the behaviour seen in the no chaperone condition (Figure 6). So, while the mutant K141E is able to fight the formation of tightly aggregated structures to some extent, its overall holdase actions is not as robust as the one seen for wild type HSPB8

and large chunks of the 4MBP construct are able to aggregate weekly. The observed holdase activity for wild type HSPB8 and the reduced holdase action for its mutated form are consistent with the results obtained from bulk assays. Another interesting point to note here is that the observed unstructured cycles in the presence of mutant K141E mirror the scenario in no chaperone condition. Therefore, if the holdase action of wild type HSPB8 partly depends on its ability to selectivity bind to the unstructured polypeptide chain, this selectivity is lost due to the mutation and can be one possible reason for the reduced holdase activity.

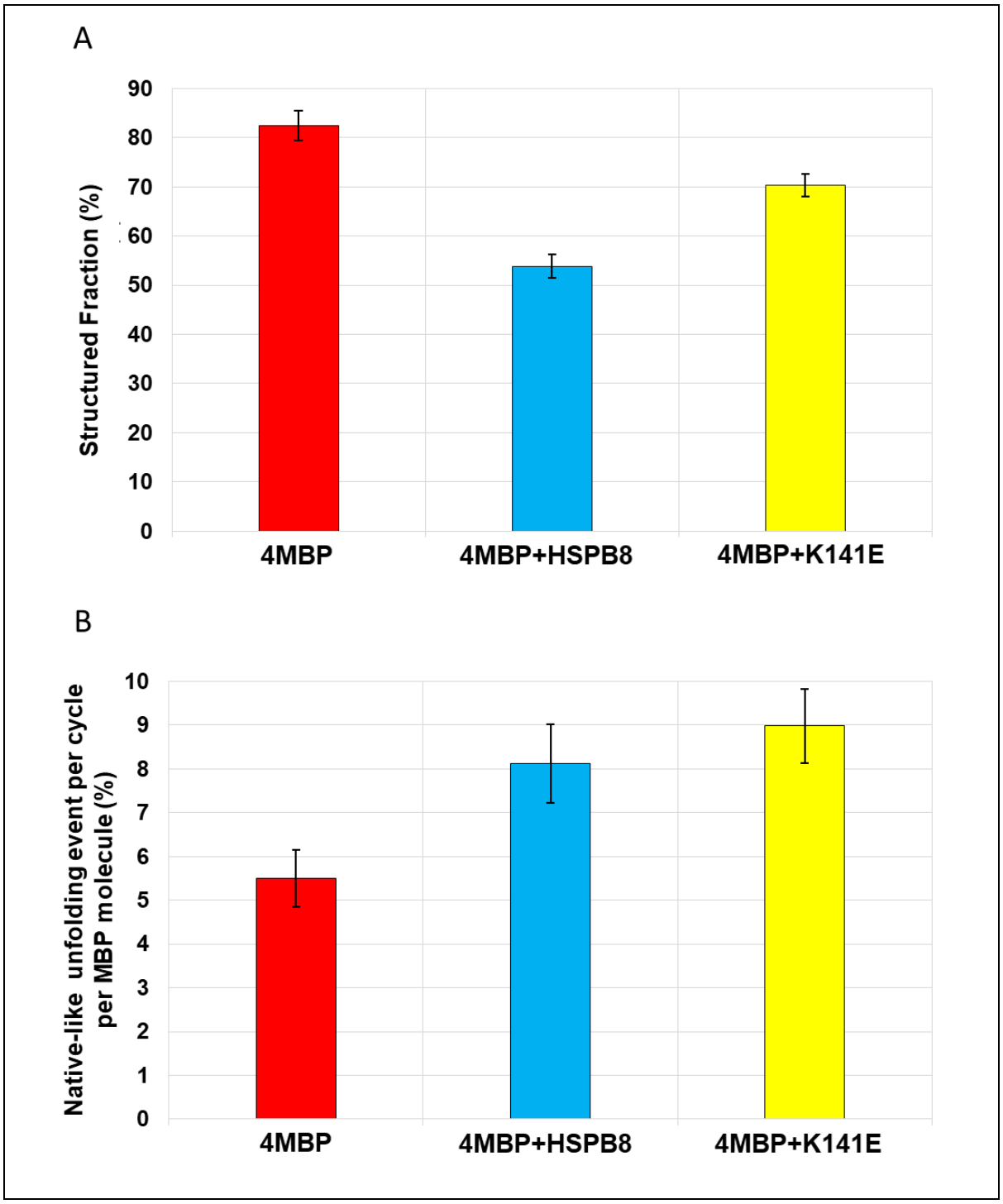

Figure 6: A) Average structural fraction observed per cycle for 4MBP (Red), in presence of wild type HSPB8 (Blue) and in the presence of mutant K141E (Yellow). B) Probability of observing native-like folding for a MBP molecule per cycle in all three scenario.

In addition to the anti-aggregation behaviour of HSPB8, the optical tweezers assays performed on the MBP homotetramer also revealed that both wild type and mutated version of HSPB8 seemingly prefer the native-like refolding of the unstructured MBP peptides. The probability that one of the MBP molecules fold back into their native or native like conformation per pulling cycle was found to be 5.43 % in no chaperone scenario (figure 6B). This value rose to 8.12 % in the presence of wild type HSPB8 and to 8.97 % in the presence of K141E. This increase is even more significant, specifically in the case of wild type HSPB8, when we consider the reduced structural fraction in the presence of chaperone. In other word, while part of 4MBP construct that interacts to form structured conformations decreases in the presence of chaperone (almost half in the case of HSPB8), the probability of native or native-like folding increases within this reduced structured part. A simple explanation can be that native refolding rate increases as a by-product of the holdase activity of wild type HSPB8, i.e. less available aggregating partners for the MBP molecules due to the holdase activity and hence the MBP molecule is more likely to fold back in its native conformation. However, this does not explain why native-like folding probability is even higher for the mutant K141E where the holdase activity is significantly reduced. Optical tweezers assays were performed on the sMBP molecule to study among other things also whether the functional profile of HSPB8 possess a foldase activity or that the increased native folding observed for 4MBP is purely incidental.

4MBP assays quite clearly reveal that chaperone-protein interactions occur in such a manner that the molecular chaperone, in this case HSPB8, alters the behaviour of the substrate molecule in the subsequent pulling cycles. However not many details regarding the nature of this chaperone-protein interaction can be drawn from the 4MBP optical tweezer assays. This is where the sMBP assays, which allow us to monitor the behaviour of a single molecule in aggregation free atmosphere, become more useful. Such assays can aide us in deciphering exactly how and at which step of the folding-unfolding process the molecular chaperones interact with the substrate protein. In similar vein, a clear indication regarding the interaction of HSPB8 with the unstructured polypeptide chains was observed in the sMBP assays. The percentage of unstructured cycles in the subsequent pulling cycles for sMBP molecule in all three scenarios was found to be very similar (Figure 7A). If the holdase function of wild type

HSPB8 partially transpire because it binds to the unstructured MBP peptides and hence prevents non-native interactions, then it logically follows that we should also observe a rise in the amount of the induced unstructuring in the presence of wild type HSPB8. Inversely, not only do we find that the amount of unstructured cycles remain similar in all cases, rather on closer examination we find a marginal drop in the case of HSPB8 (33.64 %) when compared to no chaperone scenario (36.78 %). These data suggest that HSPB8 in all probability does not stabilise unstructured peptides by binding to them unlike other molecular chaperones such as SecB and DnaJ [16, 18].

The most fascinating insight in the functional activity of HSPB8 was discovered when looking at the impact of both wild type and mutant HSPB8 on the native-like refolding of single MBP molecule. In the absence of chaperone, the sMBP molecule refolded into its native or native-like conformation ∼29 % of the time in the subsequent pulling cycles. Now if we consider the idea that HSPB8 acts solely as a holdase chaperone and the observed increase in the native-like folding for the MBP molecule in the 4MBP construct is simply a by-product of the holdase action of HSPB8. Then in the case of sMBP molecule where aggregating partners are absent, a reasonable assumption can be made that the amount of native-like refolding should remain consistent or even decrease as the holdase function might provide a hindrance to the native-like refolding of MBP core. Interestingly and unexpectedly, a sharp increase in the native-like folding was noted for both wild type HSPB8 (∼ 47 %) and K141E mutant (∼ 49 %) (Figure 7B). These results coupled with the increase in the native-like folding observed for 4MBP construct advocates the presence of a foldase action alongside the principal holdase activity in the functional profile of HSPB8.

Additionally, the native refolding observed in the presence of HSPB8 is very dissimilar to the one observed for another small heat shock protein chaperone HSP42 [20]. In the case of HSP42, it was seen that it reduces the unfolding force (from 24 pN to 15 pN) required to unfold the native MBP structures. Such drastic drop in the unfolding forces for the MBP core was not present in the case of HSPB8 as average unfolding force for native like transitions was noted to be ∼21 pN in the case of both the wild type and mutant chaperone in comparison to it being ∼23 pN in the no chaperone scenario. This behaviour is also very different to the stabilization action reported for HSP70 [18]. Mashaghi et al reported that HSP70 binds to and stabilizes the partially folded and near native like MBP structures in such a manner that these structures fail to unfold even at higher forces (> 40 pN). Unlike HSP70, the native or native like MBP core structures unfold at almost the same force in both the presence and absence of HSPB8.

Additionally, the amount of partially folded transitions, which can be described as the on-pathway metastable MPB structures, decrease from 33.69 % in the absence of chaperone to 19.64 % in the presence of HSPB8. In addition, while there is a small increase in the unfolding forces for the non-native transitions in the presence of chaperone (from ~ 12 pN to ~ 15 pN); it is nowhere comparable to the strong stabilisation reported in the case of HSP70.

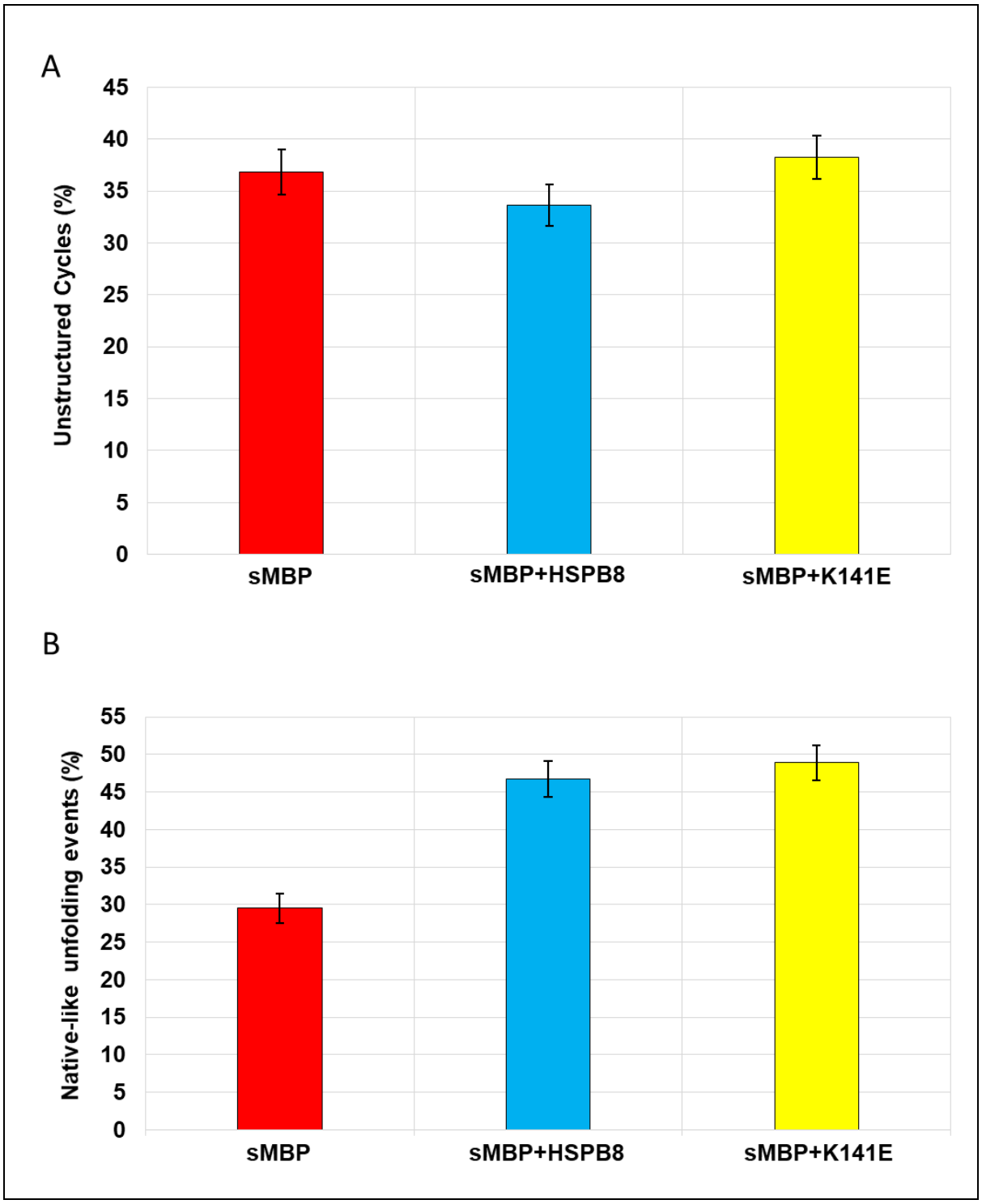

Figure 7: A) Total unstructuring observed for sMBP molecule in the absence of any chaperone (red), in presence of wild type HSPB8 (blue) and in presence of K141E (yellow). B) Native unfolding events observed in subsequent pulling cycles for all three scenario.

A sharp decrease in the non-native transitions in the presence of both wild type HSPB8 and K141E mutant fuel a simple hypothesis that HSPB8 performs its foldase activity to a certain extent by specifically interacting with the partially folded structures that enables such structures to further fold in its native structure. We can also infer that such protein chaperone interactions are short lived as no palpable deviation in the average unfolding force for both non-native and native like transitions is present. These interactions can be as simple as masking certain misfolding prone sections or hydrophobic parts long enough to prevent initial non-native contact and restrict the available conformational space to a native like route. It can then detach from the near natively folded protein structure, allowing it to progress in its folding cycle towards a native conformation. This foldase activity though is in service of the overall holdase action performed by HSPB8, it transpires independently of the principal holdase activity of HSPB8. The evidence for this separation between the holdase and foldase functions of HSPB8 can be seen in the effects of mutant K141E. As illustrated before, the holdase activity of K141E is largely diminished but still it is able to perform its foldase function just as efficiently if not marginally better than the wild type HSPB8. Along the same line on comparing the observed non-native transitions for both wild type (19.64 %) and mutant (~ 13 %), a small decrease is noted. This marginal decrease can be understood in terms of the foldase and holdase activity of HSPB8 being active at the same time/working together in one case and only one being dominant in another. In the case of HSPB8, the foldase function enables it to assist the substrate molecule in its refolding towards a native conformation while the holdase action entails that it prevents less natively folded or even misfolded species from further non-native interactions. Hence, the slightly increased number of non-native transitions when compared to K141E can be explained as a result of its holdase activity. Though separate, the two functions are not mutually exclusive in the grand scheme and work together to inform the chaperone activity of HSPB8.

Overall, our results reveal some probable mechanisms underlying the functional activity of HSPB8. The active discouragement of aggregation seen for HSPB8 can be explained in terms of the combination of two possible actions. Firstly, HSPB8 recognizes and interrupts

non-native intra-molecular interactions hence breaking the large aggregated structures into small aggregates and unstructured peptide segments. It additionally also masks the misfolding prone exposed parts of partially folded protein structures and prevents them from interacting non-natively with other partially folded or misfolded proteins. This masking action can be particularly more fascinating as by actively discouraging non-native inter and intra molecular interactions it increases the energy barrier that partially folded structures should cross to transition towards aggregations. Rather, it restricts the possible conformational space available to partially folded structures and hence performs its foldase action by facilitating the transition of the partially folded states into natively folded structures. While K141E is able to retain this masking action and is able to act as an efficient foldase chaperone, it is probably not able to break aggregated structures and hence has a poor chaperone activity.

In order to probe the functional dynamics of HSPB8 further, it will be informative to observe how its functional profile evolves in the presence of BAG23 with which it actively interacts to form chaperone complex. Additionally, it can be interesting to counter the lack of holdase action of mutant K141E by either introducing a pharmacological chaperone or by boosting other ATP driven chaperone such as HSP70 or HSP90. Similar assays can also be performed using truncated versions of HSPB8 to identify exactly which element of HSPB8 are involved in holdase function and which are responsible for foldase function.

5.5 Conclusions

The effects of HSPB8 on the unfolding, refolding and aggregation induced in substrate proteins were investigate at single molecule level using optical tweezers and an intricate picture of its functional profile was uncovered. Our experiments reveal that HSPB8 acts actively against protein aggregation and possess a strong holdase action. This holdase action is greatly diminished in K141E mutant of HSPB8. HSPB8-K141E has been linked to various human neuronal disorders and the reduction in its holdase activity can be a primary cause for its dysfunction. We also note that in all probability the mechanism of holdase function seen for HSPB8 does not entail it interacting with or stabilising the unstructured substrate peptide chain. Rather it discourages aggregation by disrupting non-native contacts and quarantining the

weekly aggregated or misfolded structures. In addition to the strong holdase activity, we also discovered an unexpected foldase action in both wild type HSPB8 and K141E mutant. The foldase function in all probability is a result of short-lived chaperone-protein interactions and exists independently of the holdase attributes of HSPB8. The results of these optical tweezers assays inform a more involved chaperone activity for HSPB8 than thought before, where its holdase and foldase action work at tandem to assist substrate proteins in their frustrated search for native conformation.

5.6 References

1. Hartl, F.U., A. Bracher, and M. Hayer-Hartl, *Molecular chaperones in protein folding and proteostasis.* Nature, 2011. **475**(7356): p. 324.
2. Haslbeck, M., et al., *Some like it hot: the structure and function of small heat-shock proteins.* Nature structural & molecular biology, 2005. **12**(10): p. 842.
3. Skowyra, D., C. Georgopoulos, and M. Zylicz, *The E. coli dnaK gene product, the hsp70 homolog, can reactivate heat-inactivated RNA polymerase in an ATP hydrolysis-dependent manner.* Cell, 1990. **62**(5): p. 939-944.
4. Sharma, S., et al., *Monitoring protein conformation along the pathway of chaperonin-assisted folding.* Cell, 2008. **133**(1): p. 142-153.
5. Thirumalai, D. and G.H. Lorimer, *Chaperonin-mediated protein folding.* Annual review of biophysics and biomolecular structure, 2001. **30**(1): p. 245-269.
6. Kim, Y.E., et al., *Molecular chaperone functions in protein folding and proteostasis.* Annual review of biochemistry, 2013. **82**: p. 323-355.
7. Rusmini, P., et al., *The role of the heat shock protein B8 (HSPB8) in motoneuron diseases.* Frontiers in molecular neuroscience, 2017. **10**: p. 176.
8. Benndorf, R., et al., *HSP22, a new member of the small heat shock protein superfamily, interacts with mimic of phosphorylated HSP27 (3DHSP27).* Journal of Biological Chemistry, 2001. **276**(29): p. 26753-26761.
9. Carra, S., et al., *HspB8, a small heat shock protein mutated in human neuromuscular disorders, has in vivo chaperone activity in cultured cells.* Human molecular genetics, 2005. **14**(12): p. 1659-1669.
10. Crippa, V., et al., *The small heat shock protein B8 (HspB8) promotes autophagic removal of misfolded proteins involved in amyotrophic lateral sclerosis (ALS).* Human molecular genetics, 2010. **19**(17): p. 3440-3456.
11. Rusmini, P., et al., *Clearance of the mutant androgen receptor in motoneuronal models of spinal and bulbar muscular atrophy.* Neurobiology of aging, 2013. **34**(11): p. 2585-2603.
12. Irobi, J., et al., *Mutant HSPB8 causes motor neuron-specific neurite degeneration.* Human molecular genetics, 2010. **19**(16): p. 3254-3265.

13. Fontaine, J.-M., et al., *Abnormal small heat shock protein interactions involving neuropathy-associated HSP22 (HSPB8) mutants.* The FASEB journal, 2006. **20**(12): p. 2168-2170.
14. Carra, S., S.J. Seguin, and J. Landry, *HspB8 and Bag3: a new chaperone complex targeting misfolded proteins to macroautophagy.* Autophagy, 2008. **4**(2): p. 237-239.
15. Kim, M.V., A.S. Seit-Nebi, and N.B. Gusev, *The problem of protein kinase activity of small heat shock protein Hsp22 (H11 or HspB8).* Biochemical and biophysical research communications, 2004. **325**(3): p. 649-652.
16. Bechtluft, P., et al., *Direct observation of chaperone-induced changes in a protein folding pathway.* Science, 2007. **318**(5855): p. 1458-1461.
17. Mashaghi, A., et al., *Reshaping of the conformational search of a protein by the chaperone trigger factor.* Nature, 2013. **500**(7460): p. 98.
18. Mashaghi, A., et al., *Alternative modes of client binding enable functional plasticity of Hsp70.* Nature, 2016. **539**(7629): p. 448.
19. Nunes, J.M., et al., *Action of the Hsp70 chaperone system observed with single proteins.* Nature communications, 2015. **6**: p. 6307.
20. Ungelenk, S., et al., *Small heat shock proteins sequester misfolding proteins in near-native conformation for cellular protection and efficient refolding.* Nature communications, 2016. **7**: p. 13673.
21. Bertz, M., et al., *Structural and mechanical hierarchies in the α-crystallin domain dimer of the hyperthermophilic small heat shock protein Hsp16. 5.* Journal of molecular biology, 2010. **400**(5): p. 1046-1056.
22. Cecconi, C., et al., *Direct observation of the three-state folding of a single protein molecule.* Science, 2005. **309**(5743): p. 2057-2060.
23. Shank, E.A., et al., *The folding cooperativity of a protein is controlled by its chain topology.* Nature, 2010. **465**(7298): p. 637.
24. Yu, H., et al., *Direct observation of multiple misfolding pathways in a single prion protein molecule.* Proceedings of the National Academy of Sciences, 2012.
25. Xu, A.J. and T.A. Springer, *Mechanisms by which von Willebrand disease mutations destabilize the A2 domain.* Journal of Biological Chemistry, 2013. **288**(9): p. 6317-6324.
26. Alemany, A., et al., *Mechanical folding and unfolding of protein barnase at the single-molecule level.* Biophysical journal, 2016. **110**(1): p. 63-74.

27. Zhang, Y., *Energetics, kinetics, and pathway of SNARE folding and assembly revealed by optical tweezers.* Protein Science, 2017. **26**(7): p. 1252-1265.
28. Jahn, M., et al., *Folding and Domain Interactions of Three Orthologs of Hsp90 Studied by Single-Molecule Force Spectroscopy.* Structure, 2018. **26**(1): p. 96-105. e4.
29. Wruck, F., et al., *Protein folding mediated by trigger factor and Hsp70: new insights from Single-Molecule approaches.* Journal of molecular biology, 2018. **430**(4): p. 438-449.
30. Mashaghi, A., et al., *Chaperone action at the single-molecule level.* Chemical reviews, 2013. **114**(1): p. 660-676.

Conclusion

Like any compelling story, the narrative of the present thesis revolves around its primary protagonist optical tweezers (OT) and the multifaceted roles played by OT in biomolecular research. The thesis elaborates upon the single molecule approach taken by OT assays to study the structural dynamics and functional profile of protein molecules and access the evolving trends in the optical tweezer technology.

Expanding on these evolving trends, the thesis describes the key instrumental features and biological applications of four specific versions of OT set ups namely, Plasmonic Optical Tweezers (POT), Photonic Crystal Optical Tweezers (PhC OT), Femtosecond Optical Tweezers (Fs OT) and Optical Tweezers combined with various fluorescence techniques. These instrumental developments have been spurred by a desire to improve upon the limitations of conventional optical trapping. The aforementioned techniques have paved the path for new avenues in optical trapping such as efficient optical manipulation in rayleigh regime, more dynamic control in optical manipulation at nano and sub-nano scale and simultaneous exploration of the structural, conformational as well as stoichiometric changes involved in biomolecular processes at single molecule level. Additionally, with further instrumentation improvements, specifically eyeing robust application on biological samples, these new trends hold great promise for future.

OT assays can prove to be excellent tools to study protein folding. Emphasising on this aspect, results from single molecule optical tweezer experiments on non-myristoylated NCS–1 (Neuronal Calcium Sensor – 1) which reveal a rugged and multistate energy landscape for NCS–1 were discussed comprehensively and the folding, misfolding and unfolding dynamics of Ca^{+2} – bound, Mg^{+2} – bound and apo form of NCS–1 were compared. OT assays exhibit that NCS–1 possess a unidirectional and multistate folding pathway in comparison to structurally similar protein CaM (Calmodulin) where three distinct folding pathways are available. Evidently, single molecule approach is instrumental in probing the structure, function and dysfunction of EF hand containing calcium sensor proteins and similar studies should further be carried out on other members of calcium sensor family.

Heat shock proteins (HSP) are molecular chaperones that actively protect proteostasis in cellular atmosphere in stressful conditions. This thesis sheds light on the single molecule

studies aimed at deciphering the structural and functional properties of HSPs and small HSPs. Complex structural dynamic of HSP82, Htpg, Grp94, DnaK and HSP 16.5 as well as functional profile underlying the functional activity of HSP70 and HSP42 were discussed.

Finally, the results obtained from OT assays aimed at deciphering the functional activity of HSPB8, a small HSP chaperone, were described. It was revealed that similar to results obtained from bulk assays HSPB8 possess a strong holdase action. Additionally and surprisingly, it was also discovered that to go along with its perceived holdase function HSPB8 also displays a significant foldase activity. In contrast, the mutated version HSPB8-K141E, which has been linked muscular neuropathies, was found to have similar foldase function but its holdase action is severely reduced.